MEASUREMENT OF RADIATION-INDUCED DNA DOUBLE STRAND BREAKS IN YEAST BY PULSED FIELD GEL ELECTROPHORESIS

BY

SAMUEL EFFIONG IKPEME B.SC.(HONS), M.SC.

A Thesis submitted to the Post-Graduate School, Ahmadu Bello University, in partial fulfilment of the requirements for the award of the degree of Doctor of Philosophy (Physics)

Department of Physics

Faculty of Science

Ahmadu Bello University

ZARIA - NIGERIA

MAY 1995

DECLARATION

I hereby declare that:

(i) the report presented in this thesis is the result of my original research

(ii) this thesis has not been submitted to any other instuition or body for an award of a degree other than Ahmadu Bello Unviversity; and

(iii) all inclusions from works other than this have been duly referenced and acknowledged.

Samuel Effiong Ikpeme

25/05/95

Date

CERTIFICATION

This Thesis entitled "MEASUREMENT OF RADIATION-INDUCED DNA DOUBLE-STRAND BREAKS IN YEAST BY PULSED FIELD GEL ELECTROPHORESIS" by Samuel Effiong Ikpeme meets the regulations governing the award of the degree of Ph.D. Physics of Ahmadu Bello University and is approved for its contribution to knowledge and literary presentation.

.....
Professor J. Kiefer
Chairman, Supervisory Comittee
Strahlenzentrum, Institüt für Biophysik
Justus Liebig Universität, Giessen, Germany

4/10/95
Date

.....
Dr. B. W. Jimba
Member, Supervisory Committee
Department of Physics
Ahmadu Bello University, Zaria

17-Oct 95
Date

.....
Professor S. B. Ojo
Head, Department of Physics
Ahmadu Bello University, Zaria

04/03/96
Date

.....
Dean, Postgraduate School
Ahmadu Bello University, Zaria

10/7/96
Date

DEDICATION

Dedicated to my mother, Mrs. Rose Ekpri Ikpeme, who laboured for me, my wife Maria and daughter Rosemary,who stood by me, the GWB and the God of my Heart who makes all things possible.

ACKNOWLEDGEMENT

My thankful acknowledgement goes to the *German Academic Exchange Service* (DAAD) for the 3-year fellowship which made it possible for me to carry out this research work in the group B3 laboratories at the Biophysics Institute, University of Giessen, Federal Republic of Germany. My gratitude also goes to the *Nigerian Defence Academy, Kaduna* for granting me a study leave to enable me undertake the research work. The support provided by the *Gesellchaft für Schwereionenforschung (GSI)* is gratefully acknowledged. Also, in the course of the investigation, laboratory facilities of the *Gesellschaft für Strahlen- und Umweltforchung (GSF) Frankfurt, Germany* were made available to me by the Director, Dr. (Mrs) Frankenberg-Schwager; I therefore remain indebted to her.

My profound thanks to Professor J. Kiefer who secured the DAAD-fellowship for me and, as my supervisor in Giessen, guided me with helpful suggestions and criticisms throughout the duration of the research work. Other members of the B3 research group in *Strahlenzentrum, Giessen* deserve being mentioned in this regard; they include Dr. E. Schneider who helped to arrange my experiments at GSI, Darmstadt, Frau Beate Barth, Helga Schneider, both of *Strahlenzentrum Giessen*, as well as Frau R. Harbich of *GSF, Frankfurt* who provided technical assistance to me. Mention should also be made of Dr. Herman Straaten, Dr. Michael Kost, Dr. Hans-Dieter Pross and Mr. Mathias Brendamour who helped with the computing aspect of the work. I cannot forget to thank Dr. Marcus Löbrich, my friend and colleague, who helped me with useful suggestions and hints at various stages of the work. In the actual performance of the experiments, I remain obliged to Dr Gunther Lenz of *GSI, Darmstadt* who helped with the heavy ion irradiations and Dr. Horst Weintraut of Strahlenzentrum, Giessen who operated the video cameras.

On the home front, I wish to register my indebtedness to Professor J. Adetunji, who as Head of Physics Department, *Ahmadu Bello University, Zaria*, was instrumental

in securing the DAAD fellowship for me. I would also like to mention with thanks, Dr. E. J. Uwah, my former Head of Department at NDA, Kaduna, who provided the initial encouragement and inspiration.

I cannot fail to mention Dr. T. C. Akpa and Dr. B. W. Jimba who prove-read the thesis and made many useful suggestions; their meticulous approach is deeply appreciated. Dr. I. Osazuwa deserves also to be mentioned in this regard; he was always available for consultation and, in fact, went beyond the duties of his office as departmental post-graduate coordinator to ensure that this work is successfully concluded. Mention must be made, too, of Dr. N. Agu, present *Head of Physics Department, NDA*, Kaduna and Col. Mbeh, *Former Director of Military Training, NDA*, Kaduna who were very supportive of my efforts. I would also like to use this medium to pay a small tribute to the following, Chief M. Akpabio, Mrs. E. Abia-Okon, Messrs T. K. O. Okpapi, E. Eggahson, F. Bakare, E. Ezenekwe, C. Ayeni and other members of Morning Light Temple, Kaduna as well as my brother Arc. E. Ekanem-Kofi, for the material, moral and spiritual support they gave me and my family throughout the duration of the research.

I would also like to thank Mrs. Kiefer and Mrs Kraft for making my stay in Giessen comfortable and enjoyable. Mrs Kiefer made a point of inviting me and my family to her house every Christmas and Easter throughout my stay in Germany and on such occasions would entertain us lavishly; she also tried in many other ways to make us feel at home in Germany.

Lastly, but most importantly, my most profound gratitude goes to my wife, Maria and daughter, Rosemary, who have stood by me through thick and thin, supported and encouraged me in more ways than one towards the successful completion of this work.

ABSTRACT

DSB (double strand break) induction in the diploid yeast, *Saccharomyces cerevisiae*, was measured by the PFGE (Pulsed Field Gel Electrophoresis) technique after the cells had been exposed on membrane filters to a variety of energetic heavy ions with values of linear energy transfer (LET) ranging from about 100 to 11500 KeV/µm, ^{241}Am alpha particles and 80-kV X-rays. After irradiation, the cells were lysed and the DNA purified. The samples were then placed in 1 % agarose gels electrophoresed in a CHEF-DR II system. After electrophoresis, the gels were stained with ethidium bromide, placed on a UV-transilluminator and photographed with a computer-coupled digitizing camera. The pictures obtained were then processed with the help of a specially developed computer software which allows for the correction of the camera's shading effect and background fluorescence. The software was used to quantify the ethidium bromide-induced fluorescence after subtracting background fluorescence and the camera's "shading" effect. Fluorescence intensity for the band with the lowest electrophoretic mobility was found to decrease exponentially with dose. Based on the known size of the native DNA molecules, (DSB) production cross-sections (QDSB) were calculated. Linearity between the induced DSB and fluence was found in all cases. The DSB cross-section increases until it reaches a plateau value of about 1.05 xlO^{-8} cm^2 at about 10^3 - $4xl0^3$ keV/µm. This could be due to the limited probability of an ion to produce DSB as long as effects by delta electrons in the so-called "penumbra" are negligible so that only interactions in or very close to the track centre contribute significantly. Inside this LET region, the relative biological effectiveness for DSB induction (RBE_{DSB}) (relative to unfiltered 80 kV X-rays) decreases from about 2 down to 0.5. With higher LET values (beginning from about $2xl0^3$ keV/µm), Q_{DSB} rises above the plateau. A comparison of the derived DSB production cross-sections with the corresponding cross-section for inactivation shows that a close relationship exists between the two end-points.

TABLE OF CONTENTS

CHAPTER		Page
	Title Page	i
	Declaration	ii
	Certification	iii
	Dedication	iv
	Acknowledgements	v
	Abstract	vii
	Table of Contents	viii
	List of Tables	xii
	List of Figures	xiii
	List of Appendices	xv
	List of Abbreviations	xvi
1.0	GENERAL INTRODUCTION	1
1.1	Rationale for Radiation Studies	1
1.1.1	Structure of the DNA	2
1.1.2	Suitability of yeast for DNA DSB measurements	6
1.2	An Overview of Previous Studies	8
1.3	The Present Work	10
2.0	THEORETICAL BACKGROUND	13
2.1	Introduction	13
2.2	Interaction of Radiation with Matter	13
2.2.1	Electromagnetic radiation	16
2.2.2	Interaction of Particulate Radiation with Matter	19

2.3	Nature and interaction of Radiation with Biological systems	22
2.3.1	Alpha particles	22
2.3.2	Absorption of photons	24
2.4	Deposition of Energy by Energetic Ions	27
2.4.1	Effective charge	32
2.4.2	Energy loss, LET and RBE	34
2.4.3	Distribution of energy deposition events	37
2.5	Ion Sources and Physical Properties	41
2.5.1	Track structure	41
2.5.2	Track entities of energetic electrons	45
2.5.3	Target size and cross-sections	46
2.5.4	Radiation quality	47
2.5.5	Microdosimetry	49
2.5.6	Energy density	51
2.6	Targets in Biological cells	54
2.6.1	Chemical changes induced ionizing radiation	56
2.6.2	Formation of radicals	57
2.6.3	Radiation chemistry of water	58
2.6.4	Routes to damage production	61
2.7	Lesions Induced by Ionizing Radiation, their Measurement and Repair	62
2.7.1	Techniques for double strand break measurements	67
2.7.2	The electrophoretic technique	68
2.7.3	Detecting the DNA migration	71

2.7.4	DNA migration pattern in pulsed field gel separations	71
2.7.5	Shift of DNA between the four zones	73
2.7.6	The parameters governing PFGE separations	73
2.7.7	Unusual migration characteristics of DNA in PFGE	74
2.7.8	Theoretical models	74
2.8	Measurement of Radiation Dose	77
3.0	MATERIALS AND METHODS	80
3.1	Yeast Strain	80
3.2	Irradiation Conditions	80
3.2.1	X-ray and alpha irradiation	80
3.2.2	Heavy ion irradiation	82
3.2.3	DNA preparation and gel electrophoresis	88
3.2.4	System and processing	89
3.2.5	Recording gel picture	90
3.2.6	Corrections and evaluations	92
3.3	Reagents and Buffers	97
4.0	RESULTS	100
4.1	Size Separation of yeast DNA	100
4.2	Gel Fluorescence as a Function of DNA Content	100
4.3	Correction of the Electrophoretic Gels	103
4.4	Quantification of the Band Fluorescence	106
4.5	DSB induction by 80 kV X-rays and 3.5 MeV alphas	106
4.6	DSB Repair	111
4.6.1	Survival after X-irradiation	111

4.6.2 DSB-repair kinetics after X-irradiation....111

4.7 Heavy Ion Effects....114

4.71 Inactivation....111

4.72 DSB induction....118

4.7.3 DSB induction as a function of LET....122

5.0 DISCUSSION....124

5.1 Separation of Yeast Chromosomes....124

5.2 DSB Measurement by PFGE....124

5.3 DSB-Repair Kinetics....126

5.4 LET-Dependence and RBE for DSB-induction....129

5.5 Conclusions....134

References....136

Appendix....150

List of Tables

Page

Table 1.1: Haploid DNA content and chromosome number of a variety of organisms...5

Table 1.2 A summary of DSB measurements for yeast and mammalian cells for sparsely ionizing radiation....9

Table 1.3: DSB measurements for heavy ions....11

Table 2.1: Particulate radiations used in radiobiological studies....19

Table 2.2: Chain of events leading to radiation injury....23

Table 2.3: Track average LET values for various radiations....39

Table 2.4: Initial and final yields of water radiolysis products for low LET radiation..59

Table 3.1: Physical parameters of the heavy ions 98

Table 3.2: Heavy ion inactivation cross sections....114

Table 3.3: Heavy ion DSB cross-sections....118

List of Figures

Page

Figure 1.1: Primary structure of the DNA and the major types of radiation damage.....3

Figure 1.2: Comparison of survival curves of mammalian and yeast cells.....7

Figure 2.1: Relative distribution events for high and low LET radiation.....14

Figure 2.2: Tracks of low LET γ-rays and high LET particles through a cell nucleus....15

Figure 2.3: Reduction of X- or γ-ray intensity with absorber thickness.....26

Figure 2.4: Range of heavy ions in water according to Northcliffe and Schilling 28

Figure 2.5: Stopping power as a function of ion specific energy 30

Figure 2.6: Linear energy transfer of different ions in carbon.....31

Figure 2.7: Relative biological effectiveness (RBE) as a function of LET.....33

Figure 2.8: Penumbra radii according to different beam models as a function of energy.....43

Figure 2.9: Lesions induced in cellular DNA by ionizing radiation.....53

Figure 2.10: Excision repair mechanism for DNA single strand breaks.....64

Figure 2.11: A proposed scheme for DSB repair by recombination in yeast 66

Figure 2.12: The four zones of DNA resolution.....72

Figure 2.13: Bag model - the different DNA configurations as it passes through a gel..76

Figure 3.1: The biological working station at GSI, Darmstadt, Germany.....83

Figure 3.2: Sample preparation for PFGE: a schematic representation.....84

Figure 3.3: The CHEF-DR II drive module.....85

Figure 3.4: Wiring of the CHEF-DR II system.....86

Figure 3.5: Voltage clamping by the CHEF-DR II system.....87

Figure 3.6: The video imaging system 91

Figure 3.7: Schematic diagram showing the gel processing procedure.....94

Figure 4.1: Separation pattern of the Bio-rad length standard performed in a 1% gel...99

Figure 4.2: Ethidium bromide fluorescence as a function of DNA content.....101

Figure 4.3: An uncorrected gel picture of yeast DNA after electrophoresis.....102

Figure 4.4: The gel picture (figure 4.3) after all the corrections 104

Figure 4.5: Intensity distribution across the gel before and after the corrections.....105

Figure 4.6: Relative fluorescence for yeast (211*B) cells after 80 kV X-rays irradiation.....108

Figure 4.7: Relative fluorescence for yeast (211*B) cell after α- particles irradiation.109

Figure 4.8: Yeast (rad 53-4) survival during incubation in phosphate buffer.....110

Figure 4.9: Liquid holding recovery survival curves for yeast (rad 53-4) cells.....112

Figure 4.10: Relative fluorescence curves for rad 53-4 yeast cells after X-irradiation and incubation in phosphate buffer.....113

Figure 4.11: Survival curves for yeast (211*B) after low LET heavy ion irradiation...115

Figure 4.12: Survival curves for yeast 211*B after medium LET heavy ion irradiatio.116

Figure 4.13: Survival curves for yeast 211*B after high LET heavy ion irradiation.....117

Figure 4.14: Relative fluorescence curves corresponding to the ions in figure (411)...119

Figure 4.15: Relative fluorescence curves corresponding to the ions in figure (4.12)..120

Figure 4.16: Relative fluorescence curves corresponding to the ions in figure (4.13)..121

Figure 4.17: DSB production cross-section as a function of LET.....123

Figure 5.1: Comparison of PFGE (this work) with sedimentation data (Akpa *et al.* 1993) and elution (Weber and Flentje 1993).....128

Figure 5.2: Parallelism between cross-section for initial DSB and inactivation.....131

Figure 5.3: RBE for DSB production as a function of LET.....133

List of Appendices

Page

Appendix A: A Summary of DSB measurements in yeast and mammalian cells for sparsely ionizing radiation.....150

Appendix B: Summary of DSB measurements for heavy ions.....152

Appendix C: Survival data for yeast (rad 54-3) after X-ray irradiation and incubation in phosphate buffer.....154

List of Abbreviations

Am.....Americium

BEVALAC.....Billion Electron Volts linear accelerator (Heavy ion accelarator at Berkerley, California)

BEVATRON.....Billion electron volts synchrotron

DNA.....Deoxrybonucleic Acid

Bp.....Base pairs

DPC.....DNA - protein cross-links

DSB.....Double Strand Breaks

FIGE.....Field Inversion Gel Electrophoresis

GSF.....*Gesellschaft für Strahlen- und Umweltforchung*

GSI.....*Gesellchaft für Schwereionenforschung*

Gy.....Gray

HILAC.....Heavy Ion Linear Accelerator

LET.....Linear Energy Transfer

mM.....MiliMolar

nm.....Nanometer

OFAGE.....Orthogonal Field Alternation Gel Electrophoresis

PFGE.....Pulsed Field Gel Electrophoresis

RBE.....Radiobiological effectiveness

RNA.....Ribosenucleic Acid

SDS.....Sodium Dedecyl Sulphate

SSB.....Single Strand Breaks

TAFE.....Transverse Alternating Field Gel Electrophoresis

TBE.....Tris Borate

TLD.....Thermoluminescent Dosimeters

UNILAC.....Universal Linear Accelerator

CHAPTER ONE

1.0 GENERAL INTRODUCTION

1.1 Rationale for radiation studies

Interest in the biological action of accelerated charged particles has greatly increased in recent years particularly because of their potential usefulness for understanding and treatment of cancer. Another reason for this heightened interest is in connection with manned space flights. It is known that heavy charged particles constitute an important part of the cosmic space radiation field, hence an understanding of their biological action is not only of fundamental interest but also a necessary prerequisite for a rational approach to the problems of radiation in space (Kiefer, 1988). With the enhanced expertise in accelerator design, it has become practical to investigate the radiobiological actions of these ions in the laboratory. Yet another motivation is in connection with the fact that biologically relevant delta electrons are produced by the primary ions as a continuous track having a well defined diameter and ionization density inside the track. The diameter of the track is determined by the maximum range of the delta electrons and depends on the velocity of the ion, independent of the atomic number, while the ionization density is determined by the energy loss of the particle which depends on the square of the atomic number. Thus by an appropriate choice of ion mass and energy, it is possible to change both parameters independently and study the resulting biological action. Hence, the damaged area in a cell and the intensity of damage can be varied independently, which is not possible with electromagnetic radiation. Historically speaking, the first particle experiments used lighter ions. The construction of the synchrotrons at Princeton and Berkeley (Grunder *et al.*, 1971; White *et al.*, 1971) first permitted examination of the biological effects of heavy ions with atomic numbers (z)

between 6 and 18 at higher energies than were previously available. The first particle experiments used lighter ions like deuterons and helium ions; in 1975, the BEVALAC, an extension of the BEVATRON, using a heavy ion linear accelerator (HILAC) as an injector went into operation at Berkeley, USA (Ghiorso *et al.*, 1973). At about the same time the UNILAC in Darmstadt, Germany, was completed (Angert and Schmelzer, 1977). Since that time, all heavy ions from helium to uranium are available (Kraft, 1987).

1.1.1 Structure of the DNA

An understanding of the behaviour of nucleic acids under the action of radiation necessitates a knowledge of those physio-chemical properties which govern its structure. The compounds DNA and RNA are classified as nucleic acids. Fundamental building blocks of both DNA and RNA are the bases, purines and pyrimidines (figure 1.1). The purines are adenine and guanine; the pyrimidines are thymine, cytosine and uracil. As figure 1.1 shows, the only difference between adenine and guanine lies in the peripheral groups; the heterocyclic groups are the same. The same principle holds for the pyrimidines.

The second set of building blocks are the five-carbon sugars, ribose and deoxyribose (deoxyribose does not have an oxygen at the 2' position). Compounds made of a combination of a base and a sugar are known as nucleosides and if, in addition, a phosphate is present on the sugar, the compound becomes known as a nucleotide. The nucleotides are linked together by phosphate groups. This linkage forms the so-called phosphodiester backbone of the DNA molecule. The information carried by the DNA molecule is a result of the sequence of the bases (Darymple *et al.* 1973).

According to the model initially proposed by Watson and Crick (Darymple and Baker, 1973), a DNA molecule consists of two anti-parallel polynucleotide chains

arranged in the form of a double helix (figure 1.1). The radius of the double helix is about 10 Å; a distance of 3.4 Å separates the base pairs. A complete turn requires 34 Å. The phosphodiester backbones of the strands are oriented to the `outside' while the bases are projected `inside'. The sequence of the bases in the two strands is complementary in nature; that is, an adenine (A) moiety in one strand opposes a thymine (T) moiety in the other. In a similar manner a guanine moiety opposes a cytosine moiety. Although, by definition, the number of adenine moieties must be equal to the number of thymine moieties (A=T), and the number of guanine moieties must equal the number of cytosine moieties (G=C), the relative amounts (ratios) of A+T and G+C varies greatly in DNA from different sources. In fact, an increased amount of G+C has been related to an increased radiosensitivity (Darymple and Baker, 1973). A double-stranded segment of DNA is shown along with the structures of the four bases. Hydrogen bonding between the bases of the two strands are illustrated by a dotted line. The major types of radiation injury to the DNA are shown.

More refined X-ray diffraction studies of oriented fibres have shown, however, that DNA fibres can exist in three double-stranded helical structures: the A-DNA, the B-DNA, and the C-DNA. The B-DNA is generally considered the native form, while the C-DNA is closely related to the B-DNA. In all secondary structures of DNA, the two helices are right-handed and the chains are held together by H-bonds between complementary bases. However, the pitch of the helix and the number of bases per turn vary. Also the plane defined by the base pairs is perpendicular to the helix axis only in B-DNA. In A-DNA, the normal of the base pairs is tilted by 20 degrees to the helix axis.

DNA does not occur only as long double-stranded linear rods of restricted flexibility. In viruses and bacteteriophages single-stranded DNA is found. Tertiary structures such as

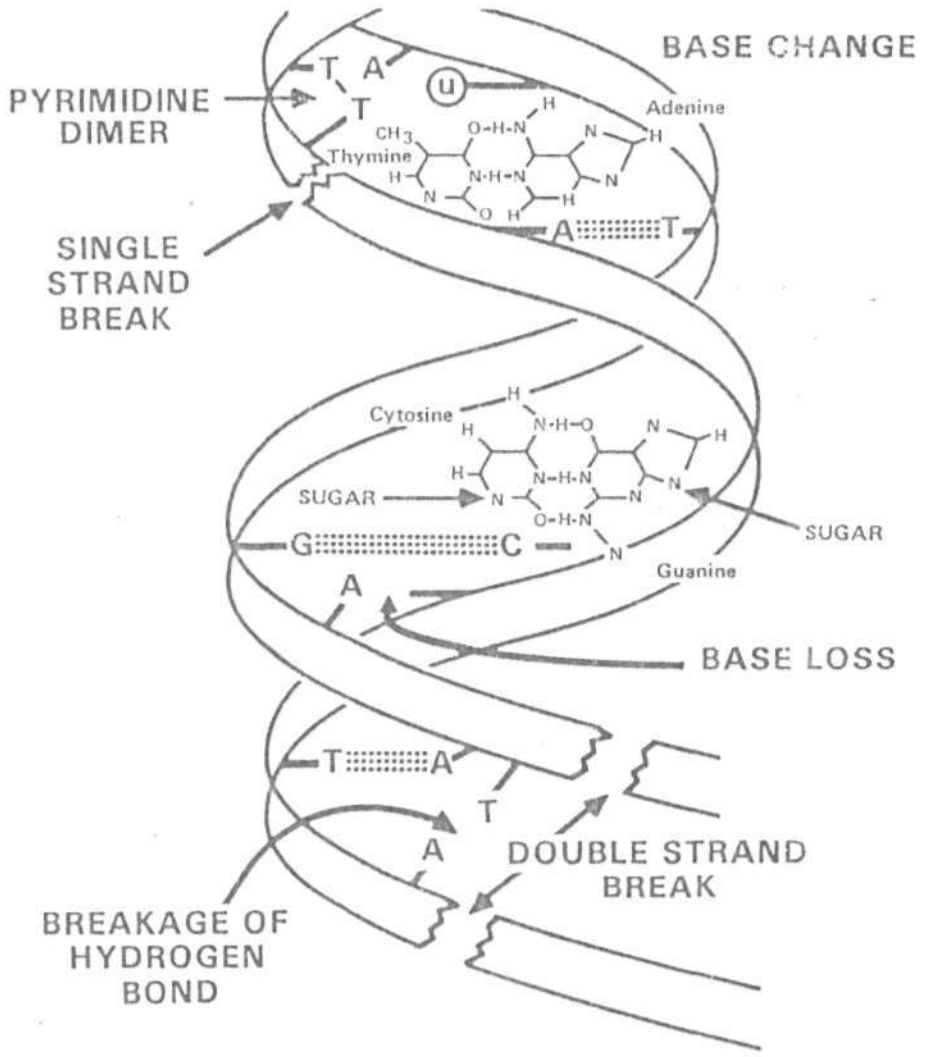


Figure 1.1: Primary structure of the DNA and the major types ofradiation damage

Source: Walden and Farzaneh (1990)

supercoiled and open-cyclic molecules are obtained when double-stranded DNA is isolated in an undegraded form. In the supercoiled structure, the

Table 1.1: Haploid DNA content and chromosome number of a variety of organisms (After Coggle, 1983)

Organism	Haploid DNA content (Picograms)	(Base pairs)	Haploid chromosome number
Simian virus 40	0.000006	5.3×10^3	1
Herplex simplex virus	0.00017	151×10^3	1
E. coli	0.005	4.5×10^6	1
Saccharomyces cerevisiae	0.025	22.5×10^6	17
Drosophilia melanogaster	0.17	1.5×10^8	4
Sea urchin	0.45	4.1×10^8	20
Gallus domesticus	0.7	6.3×10^8	39
Mus musculus	3.0	2.7×10^9	20
Homo sapiens	2.7	2.4×10^9	23
Hella cells human cell culture (aneuploid)	8.5	7.7×10^9	70-164
Xenopus laevis (toad)	4.2	3.8×10^9	18
Triturus cristatus (newt)	35.0	31.5×10^9	12
Zea mays (corn)	7.8	7.0×10^9	10

double-stranded DNA chain is covalently closed and twisted into a superhelix. The DNA is the largest known biologic molecule. The molecular weight of the DNA of bacteria and bacteriophages generally falls between $2x10^6$ and 10^{12} Daltons. The molecular weight of mammalian DNA, however, may be a great deal larger (estimates of 10^{10} and 10^{12} Daltons have been proposed). Watson and Crick suggested that the genetic information in the cell nucleus is held in the DNA molecules in the form of a linear sequence of bases-genes. The information is in the form of a four letter alphabet (the four bases), the 'words' of the code

are of three letters each. Each triplet of adjacent bases, in the messenger RNA (mRNA), codes for a particular amino acid. A specific sequence of bases corresponds therefore to a specific linear sequence of amino acids, that is, to a specific protein molecule. Table 1.1 lists the haploid DNA content and chromosome number of a variety of organisms used in radiobiological studies.

1.1.2 Suitability of yeast for DNA DSB measurements

The unicellular yeast *Saccharomyces cerevisiae* has contributed significantly to the understanding of the role of DSB in irradiated eukaryotic cells. It has proved to be especially suitable for the study of induction and rejoining of DSB at biologically relevant radiation doses (Frankenberg-Schwager and Frankenberg 1990).

Radiation-sensitive yeast mutants exist for which rejoining of DSB is not detectable. These mutants are very valuable in assessing the biological relevance of DSB. In contrast, all the radiation-sensitive mammalian cell mutants so far isolated are able to rejoin DSB, at least to a certain extent (Kemp *et al.* 1984) or at a certain stage of the cycle (Giaccia *et al.* 1985).

Figure 1.2 shows a comparison of survival curves of mammalian and yeast cells. The surviving fraction is plotted versus the number of radiation-induced DSB per cell. Similar radiation resistance is observed for HeLa (Duncan and Nias 1977), mouse leukaemia L1210 (Duncan and Nias 1977) and yeast *Saccharomyces cerevisiae* cells. The CHO mutant xrs-7 which is partially deficient in DSB repair shows reduced radioresistance (Jeggo 1985). Extreme radiosensitivity (about one DSB per cell per lethal event) is found for the yeast mutant rad54-3, which is completely deficient in DSB-repair at 36^{o}C. A

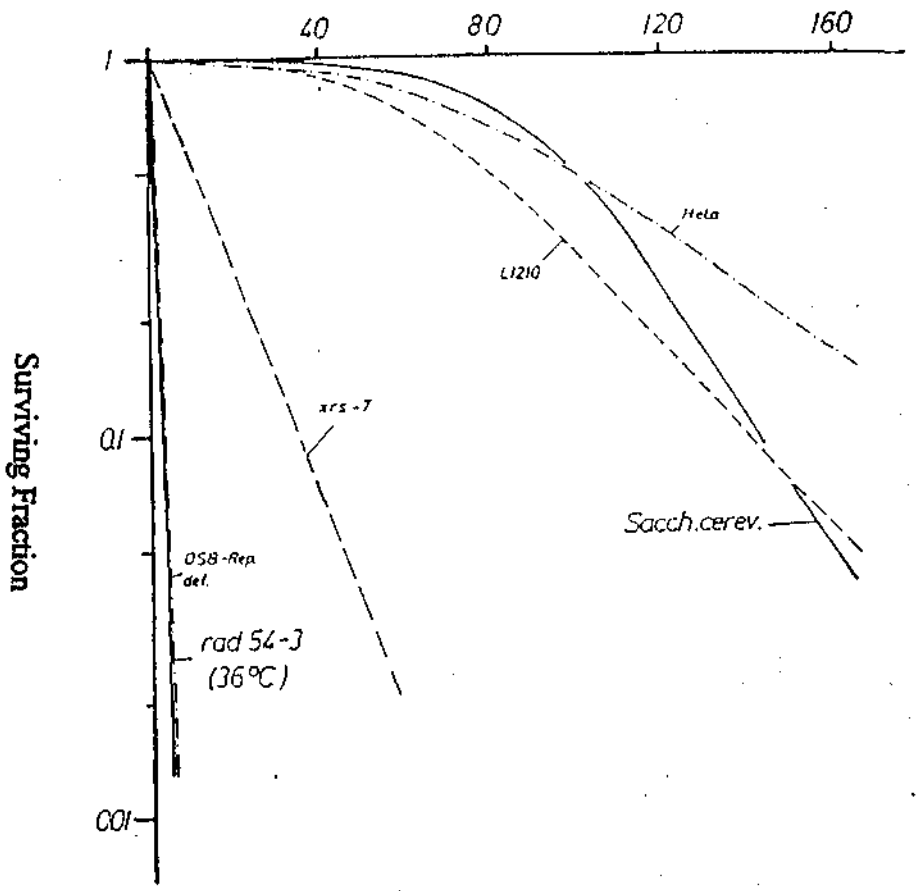


Figure 1.2: Comparison of survival curves of mammalian and yeast cells.

(After Frankenberg and Frankenberg-Schwager, 1990).

hypothetical survival curve of a completely DSB repair-deficient mammalian cell mutant which may be killed by one DSB per cell, is seen to be nearly coincident with the survival curve of the mutant yeast rad54-3 (Frankenberg-Schwager and Frankenberg 1990).

As can be seen from figure 1.2, there is striking similarity between the radiation response of yeast and mammalian cells. Thus, yeast seems to be a useful model system in which basic radiobiological research can be carried out (Frankenberg-Schwager and Frankenberg 1990).

1.2 An Overview of Previous Studies

The heaviest ions up to uranium were first employed by Schöpfer *et al.* (1978, 1980) to study the survival of dried yeast, by Schäfer *et al.* (1978) with bacterial spores and by Kraft *et al.* (1981) with mammalian cells. These studies as well as those of Barendsen (1968), Todd and Tobias (1974) and Blakely *et al.* (1984) revealed that the relative biological effectiveness (RBE) for cell killing increases with LET up to about 100-200 keV/μm and that for higher values of LET, a more complicated dependence on particle track structure emerges with a strong influence of particle velocity rather than LET (see Kiefer 1985, Kraft 1987 for reviews); a number of studies have confirmed these results for other biological endpoints. With regard to DSB induction several studies have been carried out mainly with sparsely ionizing radiations employing a variety of assays including sedimentation and neutral filter elution (see appendix A for a summary of results). The study of the DSB induction by densely ionizing radiation is a fairly recent event (see appendix B for a brief summary of results). It brought in its wake heightened interest regarding the question as to how the RBE-LET relationship found for cell killing would relate to the induction and repair of DSB (Lett 1992). There are, so far,

conflicting results with respect to the systems studied and the method of DSB detection applied. However, because of the anomalous movement of large DNA in sedimentation gradients, this assay cannot be used for DSB measurements in mammalian cells; even for yeast rather high radiation doses or fluences have to used in connection with the assay (Frankenberg *et al.* 1981). Previous efforts of various investigators to measure DSB-induction in mammalian and yeast cells are summarized in appendices 1.1 and 1.2.

Several methods have been established employing the recently developed pulsed field gel electrophoresis (PFGE) to detect DSB in mammalian cell DNA. Since intact mammalian chromosomes are too large to enter pulsed field gels, the methods reported so far resemble sedimentation or elution assays; the average DNA fragment size resulting from irradiation is determined (Ahn *et al.* 1991) or the fraction of DNA able to enter the gel after irradiation (Ager and Dewey 1990, Ager *et al.* 1990, Blöcher *et al.* 1989, Blöcher and Kuhni 1990, Iliakis *et al.*, 1991, Stamato and Denko 1990). On the other hand, yeast chromosomal molecules can be separated according to size by PFGE, and they form distinct bands in ethidium bromide-stained gels. With this technique, certain clear advantages should be mentioned; apart from the greater precision of the method, the small sizes of yeast DNA molecules and the relatively low cellular sensitivity coupled with the high sensitivity of PFGE permit the measurement of DSB in the dose-range of biological importance. Another advantage is that with the method, DSB and cell survival measurements can be made in the same dose-range. It is apparent that a study of DSB induction, especially for survival range doses, could lead to a deeper understanding of the physical and basic mechanisms underlying their formation which, in turn, is of fundamental importance in determining the chain of events leading to radiation-induced

cell death or cell transformation and many of the radiation-induced biological endpoints as well as an understanding of the various enzymatic reactions involved in their repair.

Compared to ionizing radiation, work with other DNA-damaging agents is easier because of the large number of agent-induced damages needed to kill the cell. For UV radiation, for instance, 400,000 thymine dimers are induced at a mean lethal dose. For ionizing radiation on the other hand, only 40 DSB and 1000 single-strand breaks. At the same radiation dose, the yield of total base damages is expected to be about five times the yield of single strand breaks. (Ward 1988).

1.3 The Present Work

In recent years, the electrophoretic technique has been applied to a greater extent than ever before for the resolution of large linear DNA molecules. The introduction of pulsed fields has greatly improved the effectiveness of the technique but the probem has always been in the measurement of the electrophoretic signal. Several methods have been outlined for quantification using photography (Sutherland *et al.* 1984, Ribeiro *et al.* 1989, Prunell *et al.*, 1977). In most cases, the reliability is low because the response of the film depends on factors like time and temperature of development. Thus, the manufacturers data of the film as well as the assumption that a linear response exists under the experimental conditions used should be accepted with care. Another disadvantage is that film development, washing, and drying are very labour-intensive.

Recently, video cameras were introduced as an alternative to conventional photography (Boniszewski *et al.* 1990, Freeman *et al.* 1990, Sutherland *et al.* 1987). These cameras have a linear response over a much larger intensity range and produce a high degree of reliability. The information of the gel is digitized by a frame grabber,

directly transferred to a computer and can be evaluated within reasonable time. Nevertheless, there are still problems with these systems. The camera lens can contribute to non-uniform photometric response due to geometrical factors like vignetting. Another problem is the background fluorescence due to ethidium bromide not intercalated with DNA or the thermal noise signals which are important if long exposure times are used.

There was, therefore, need to produce a straight-forward computer-assisted method of measuring the fluorescent signals from electrophoretic gels. Having obtained a method whereby DSB could be quickly and rapidly measured, it became necessary to test the method, with DSB measurement for X-rays and alpha particles and then extend it to heavy ions. For high-LET radiations and very heavy ions, in particular, a considerable amount of data has been accumulated on yeast cell killing (Manney *et al.*, 1963; Bertsche 1978 and Schöpfer *et al.*, 1982) but apart from the velocity sedimentation measurements of Frankenberg *et al.* (1981) and Akpa *et al.*, (1991), very little information is available on DSB-induction in yeast by very densely ionizing radiation. Other than strand-break measurements, there have been few studies of DNA damages. The problems in measuring other types of damage lie in the sensitivity required at biologically relevant doses. The sensitivity of the strand break assays relies on biophysical measurement of changes in macromolecular properties of the DNA; no such measurable change is induced by other types of damage except DNA-protein cross-links (Oleinick *et al.* 1990)

In the present work, DSB-induction in diploid yeast *Saccharomyces cerevisiae*, was measured by the PFGE-technique after the cells had been exposed to a variety of energetic heavy ions (provided by the UNILAC-facility at the *Gesellschaft für Schwerionenforschung*, (GSI), ^{241}Am α-particles and 80-kV X-rays. The derived DSB production cross-sections are compared with inactivation studies performed in parallel

for the same cells under identical conditions. After irradiation, the cells are lysed and the DNA purified. DNA samples are then embedded in 1 % agarose gels and electrophoresed in a CHEF-DR II system. After the electrophoresis, the gels are stained with ethidium bromide, placed on a U-V transilluminator and photographed with a digitizing camera. A specially developed computer software is then used to analyse the gels with a view to quantifying the ethidium bromide-induced fluorescence. The computer software has built-in mechanisms for subtracting background fluorescence and the camera's "shading" effect.

CHAPTER TWO

2.0 THEORETICAL BACKGROUND

2.1 Introduction

Heavy charged particles are usually more densely ionizing than X- or gamma rays or electrons. Their higher LET can have any of three possible consequences. The inactivation constant may change, the shape of the survival curve may be altered, and the physico-chemical mode of action may be different. Historically, high LET radiations became of interest because neutrons and α-particles were found to be 2-35 times as effective as X-rays, thus causing corresponding increases in the inactivation constant. This caused not only increased concern for health protection but it also created a crisis situation for target theory: the so-called sensitive volume-presumably the volume of an actual gene seemed unduly bigger when high-LET radiations were used. Later however, it was recognized that the effectiveness of high-LET radiations as measured by the inactivating constant always shows a decline at very high-LET values, probably because of the dissipation of energy that does not participate in inactivation. Figure 2.1 shows the relative distribution events for high and low LET radiation.

2.2 Interaction of Radiation with Matter

Observed chemical or biological changes induced by radiation result from chains of events. One may distinguish more or less distinct, consecutive, temporal stages in the response of a medium to irradiation. The first and physical stage is that of dissipation of radiant energy, followed by the physiochemical stage in which the primary products undergo secondary reactions. The third stage is the chemical stage. With condensed matter this stage may be subdivided into a track period, in which spatial inhomogeneities play an important role, and a subsequent uniform period. Finally, in the organism, there

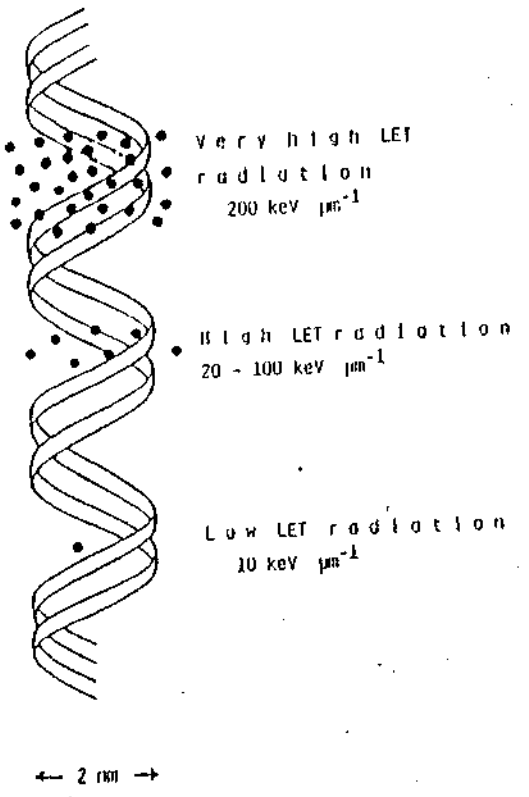


Figure 2.1: Relative distribution of ionization events for high and low LET radiation (After Coggle, 1983).

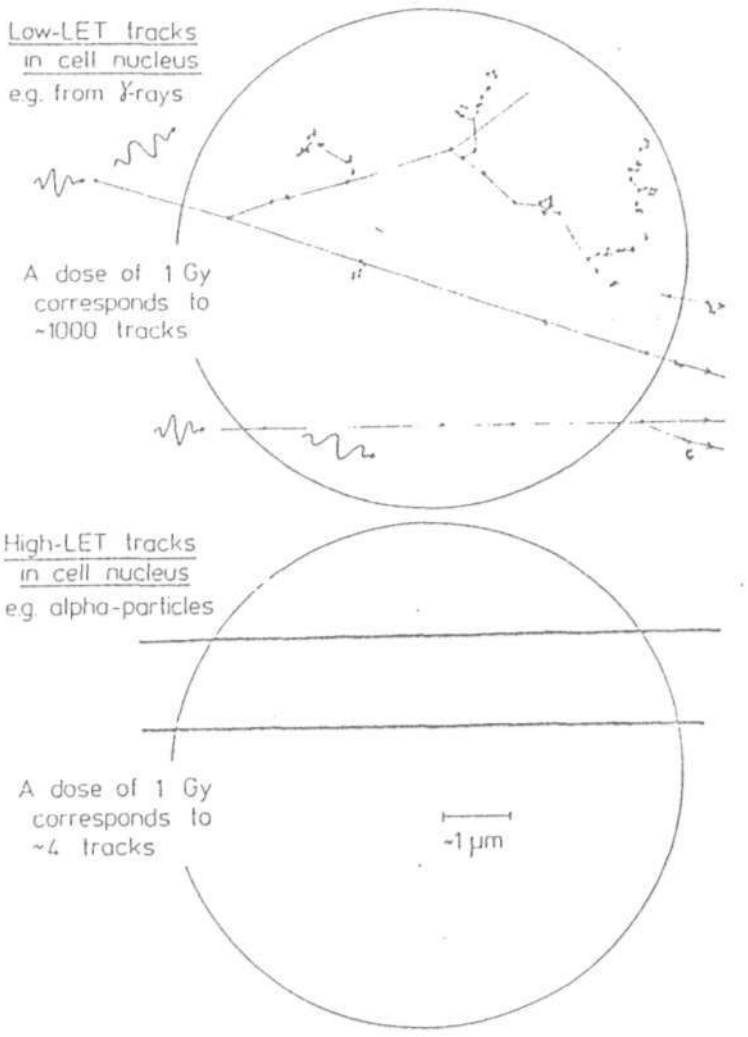


Figure 2.2: Tracks of low LET γ-rays and high LET particles through a cell nucleus. (After Goodhead, 1988).

follows a biological stage. The tracks of low LET γ-rays and high LET particulate radiation, through a cell nucleus, is schematically illustrated in figure 2.2.

2.2.1 Electromagnetic radiation

Electromagnetic radiations having sufficient energy to cause ionizations in the irradiated material interact by way of three processes: photoelectric absorption, Compton scattering and the production of positron-electron pairs in the medium. Other means of energy dissipation are of minor importance as far as the initiation of chemical changes is concerned. Photonuclear reactions occur at energies above 10 MeV, but these reactions deposit little energy in the medium and contribute only short-lived radioactivity. Low-energy radiations produce some coherent scattering, but the energy imparted to the molecules of the medium is not sufficient to produce chemical changes.

Photoelectric Absorption: In this process a low energy photon interacts with a bound electron and is absorbed, causing the ejection of the electron from 1st shell with energy given by

$$E_e = h\nu - E_b \quad \text{.....2.1}$$

where hν is the photon energy, E_b is the electron's binding energy and E_e is the electron's kinetic energy.

The likelihood of the photoelectric interaction per electron varies with E^{-3} and Z^{-3} where E is the photon energy and Z is the atomic number of the material. Thus the process predominates at low energies for materials of low Z (atomic number). In Biological materials, the photoelectric effect is most important for photon energies up to about 50 keV (Pizzarello, 1982).

In addition to the primary ionization that is a result of the photoelectric ejection of an electron, two other subsidiary processes may occur. The first is a filling of the vacancy created in the electron shell from which the photoelectron came. The jump of an outer electron to the inner vacancy is accompanied by the emission of characteristic X-radiation which may then produce its own ionization elsewhere in the medium. Sometimes the characteristic X-ray's energy is absorbed in the outer shells of the same atom, releasing electrons from these higher orbits. These so called *Auger electrons* do contribute substantially to the general distribution of the secondary effects.

Compton Scattering: Compton scattering frequently represents the predominant mode of energy loss by X- or γ-rays (e.g., ^{60}Co effects in water), in this process, the photons lose a portion of their energy by ejecting electrons from atoms. The ejected electrons, in turn produce ionization and excitation, whereas the scattered photons lose energy by interacting by way of either Compton scattering or photoelectric absorption.

Pair Production:In this process, the photon disappears and is replaced by a pair of particles- a positron and an electron. The energy of the photon goes partly to the rest masses of the two particles and partly to the kinetic energies E_p and E_e. The sum of the two kinetic energies must be equal to the energy in excess of the total rest energy:

$$E_p + E_e = h\upsilon - 2m_e c^2 \quad \text{.....2.2}$$

Where, h is Planck´s constant, υ is the frequency of the photon, m_e is the electronic mass and c is the velocity of light. Obviously the process cannot occur for photon energies less than $2\ m_e\ c^2 = 1.02$ MeV. The available kinetic energy can be divided in any proportion between the two particles, and in fact all proportions are equally likely.

Pair production can only occur in the Coulomb field of a nucleus, since the recoil of the nucleus is necessary to conserve momentum. The kinetic energy of the recoiling nucleus is negligible. The electron and positron produced as a result of the interaction of electromagnetic radiations with matter, are sufficiently energetic to induce ionized, excited, or both states in atoms and molecules in their surroundings. The positron eventually combines with an electron to generate, as a rule, two photons each having energy of 0.51 MeV. This radiation is generally referred to as "annihilation radiation". It is also possible for the positron to annihilate before losing all its kinetic energy, but this is much less likely. Annihilation with the emission of three photons can also occur with a small probability. The total cross section for pair production is zero below 1.02 MeV and increases generally above this energy. The cross section is very nearly proportional to Z^2, so that the effect is much more important in heavy materials. This energy loss process is only important with very high-energy gamma rays.

If a material substance is exposed to photons, all three interaction processes occur together, although with different contributions depending on the photon energy. The total interaction cross section is the sum of those of the single components. So that on a per atom basis:

$$\sigma_{total} = \sigma_{photo} + Z.\sigma_{compton} + \sigma_{pair} \quad \text{.....2.3}$$

The Compton cross section is multiplied by the electron number (equal to the nuclear charge Z of the atoms in the medium) since it is related to single electrons.

2.2.2 Interaction of particulate radiation with matter

The nature of particulate radiation: Two general types of particles can be distinguished on the basis of their *modi operandi* in interaction with matter: directly and indirectly ionizing particles. Directly ionizing particles carry a charge (e.g., electrons, protons and alpha particles) and have sufficient kinetic energy to produce ionizations by means of direct interactions with atoms and molecules. Indirectly ionizing particles are uncharged particles such as neutrons; these are also capable of interacting with the medium either through the agency of protons (fast neutrons), nuclear reactions (slow neutrons), or free electrons (X- and γ -rays) and, thus, of producing ionizations or excitations in atoms and molecules. The particulate radiations used in radiobiological studies are shown in table 2.1.

Table 2.1: Particulate radiations used in radiobiological studies.
(After Coggle, 1983)

Radiation	Rest mass (kg)	Charge (C)	Approximate energy used (eV)	(J)
α-particle	6.7×10^{24}	$+ 3.2 \times 10^{-12}$	$(1.0 - 200) \times 10^{6}$	1.6×10^{-13}
β-particle	9.1×10^{-31}	$- 1.6 \times 10^{-19}$	$(10 - 15) \times 10^{6}$	3.2×10^{-12}
Neutrons	1.7×10^{-27}	0	slow	
			0.025 - 100	4.0×10^{-21}
Neutrons	1.7×10^{-27}	0	intermediate	
			100 - 2000	1.6×10^{-17}
Neutrons	1.7×10^{-27}	0	fast	
			> 2000	$> 3.2 \times 10^{-15}$
Protons	1.7×10^{-27}	$+ 1.6 \times 10^{-19}$	1.0×10^{6}	1.6×10^{-13}
			30×10^{9}	4.8×10^{-9}
Deuterons	3.3×10^{-27}	$+ 1.6 \times 10^{-19}$	1.0×10^{6}	1.6×10^{-13}
			200×10^{6}	3.2×10^{-11}
^{7}Li	1.2×10^{-26}	$+ 4.8 \times 10^{-19}$	$(1.0\text{-}200)10^{6}$	$(1.6\text{-}320)10^{-13}$
^{11}B	1.8×10^{-26}	$+ 8.0 \times 10^{-19}$	$(1.0\text{-}200)10^{6}$	$(1.6\text{-}320)10^{-13}$
^{12}C	2.0×10^{-26}	$+ 9.6 \times 10^{-19}$	$(1.0\text{-}200)10^{6}$	$(1.6\text{-}320)10^{-13}$
^{14}N	2.3×10^{-26}	$+ 1.1 \times 10^{-18}$	$(1.0\text{-}200)10^{6}$	$(1.6\text{-}320)10^{-13}$
^{16}O	2.7×10^{-26}	$+ 1.3 \times 10^{-18}$	$(1.0\text{-}200)10^{6}$	$(1.6\text{-}320)10^{-13}$
^{20}Ne	3.3×10^{-26}	$+ 1.6 \times 10^{-18}$	$(1.0\text{-}200)10^{6}$	$(1.6\text{-}320)10^{-13}$
^{40}Ar	6.7×10^{-26}	$+ 2.7 \times 18^{-18}$	$(1.0\text{-}200)10^{6}$	$(1.6\text{-}320)10^{-13}$
π+(pions)	2.5×10^{-29}	$+ 1.6 \times 10^{-19}$	$(1.0\text{-}100)10^{6}$	$(1.0\text{-}160)10^{13}$
π-(pions)	2.6×10^{-29}	-1.6×10^{-19}	$(1.0\text{-}100)10^{6}$	$(1.0\text{-}160)10^{13}$

Charged particles, in general, lose energy in matter mainly through Coulomb interactions with atomic electrons. If the energy transferred to an electron is only enough to raise it to a higher energy level in the atom, the process is called *excitation*; if the electron is given enough energy to separate it completely from the atom, the process is called *ionization*. The two processes are closely associated, and together they constitute *energy loss by collision*. At energies below several times the rest energy of the moving particle, excitation and ionization account for the major percentage of the energy loss in all materials. Some of the electrons ejected in ionization processes may have large enough energies to produce further ionizations themselves; such electrons are called *delta rays*.

A number of other phenomena also occur when charged particles traverse matter. Interactions with the Coulomb fields of atoms, and particularly of atomic nuclei, result in changes in the direction of motion of the particle. If no kinetic energy is transferred to another form, the process is called *elastic scattering* such scattering is of minor importance for heavy particles but of great importance for electrons. Scattering through a large angle entails a large deceleration of the charged particle. This in turn may result in the emission a quantum of electromagnetic radiation, known as *bremsstrahlung*. If the speed of the particle through a medium exceeds the speed of light in the medium, radiation in the visible region known as *Cerenkov radiation* is emitted.

In general, when charged particles travel into matter, their paths are marked by excited and ionized molecules and atoms. The Coulomb field of the moving particle interacts with that of the electrons in the material and the collisions result in a transfer of the particles' energy into the absorber. They also interact with the Coulomb field of the nucleus and by so doing produce secondary X-ray emission. Ultimately, the particles

reach the end of their range of travel by giving up their kinetic energy in these interactions and then stop and are incorporated into the structure of the material.

Charged Particles - Alphas, protons and other heavy ions: Heavy charged particles have masses which are thousands of times greater than the mass of the electron. Thus there is a great difference in the velocity of these particles compared with the velocities of electrons having the same energy. A proton and an electron with the same velocity may ionize and excite molecules along their track in about the same proportion, but the energy of the proton would be more than 1000 times greater.

A proton having the same energy as an electron would be travelling with a much lower velocity and would therefore ionize a greater number of molecules along every part of its track to create a denser track. A doubly charged particle such as an alpha particle, makes a pattern of ionization which is four times that of a singly charged particle of the same velocity.

The track of a heavy charged particle is characterized by two important features. The first is its linearity which holds until the very end of the track when a small amount of deviation, called *straggling* occurs. The second is an increase in the number of ions formed per millimetre near the end of the track. When a heavy particle first enters a material medium, it produces ions at nearly a constant rate. As the particle slows down, the ionizations per mm increase until they reach a maximum a few mm from the end of its range. It then falls rapidly to zero as the particle stops. The maximum value occurs at what is called the *Bragg peak.*

Positively charged particles, of which the proton, deuteron and alpha particle are the most common examples, lose energy by elastic collisions. Secondary phenomena, such as

the production of delta rays, are a consequence of these collisions. Toward the end of their range, when the velocity of the particles approaches that of orbital electrons, the particles become neutralized. The neutral atom then loses energy by "knock on" collisions with atoms of similar size. Some of these target atoms are ejected from their chemical bonds, resulting in fragmentation.

2.3 Nature and Interaction of Radiation with Biological Systems

The physical processes of the interaction of photons and ionizing radiation with matter have been considered. These processes occur both in living and non-living matter and they are over in the extremely short time of 10^{-24} - 10^{-14} seconds (see table 2.2). The effect of all radiation on biological matter can be summarized as mutation and cell death but the pathways and basic mechanisms may be quite different, depending on the nature of both the radiation and the target molecule as well as the conditions surrounding the irradiation process. It is clear that radiation cannot produce any effect whatsoever unless it is absorbed; hence it would seem appropriate to start by considering the absorption process.

2.3.1 Alpha particles

The alpha particle is relatively massive, being about 7500 times as heavy as an electron. On passing through matter, such a positively charged particle exerts a strong attractive force on the negatively charged orbital electrons of the atoms near its path. This attraction may pull off one or more electrons, and the energy required for such an interaction causes the dissipation of some of the energy of the alpha particle. The resulting ionization leaves behind an ion pair. The interaction between an alpha particle and the atoms of the media through which it passes may not always be strong enough to

cause ionization, but may cause excitation. Excitations and ionizations are the most important ways in which alpha particles transfer their energy to matter (Coggle, 1983).

Table 2.2: Chain of events leading to radiation injury

(After Coggle 1983)

Event	Timescale
1. Initial interactions	
Indirectly ionizing radiation[a]	10^{-24} - 10^{-14}s
Directly ionizing radiation[b]	10^{-16} - 10^{-14}s
2. Physico-chemical stage	
Energy deposition as primary track structure ionizations	10-^{12} - 10^{-8}
3. Chemical damage	
Free radicals, excited molecules to thermal equilibrium	10^{7}s - hours
4. Biomolecular damage	
Proteins, nucleic acids, etc.	ms - hours
5. Early bilogical effects	
Cell death, animal death	hours - weeks
6. Late biological effects	
Cancer induction, genetic effects	years - centuries

[a] X-rays, γ-rays, neutrons
[b] Electrons, protons, α-particles

A fast moving particle is less likely to ionize a substance through which it is passing than a slower one. As a result of their mass, alpha particles move relatively slowly and so have ample time to ionize atoms of the media through which they pass. Also, because of their charge (2+) and their slowness, they give up all their energy in short dense, straight tracks which have a specific ionization (number of particles per unit track length). As the alpha particle penetrates deeper into the media more and more interactions occur, there is reduction in its speed, and this in turn increases the chances for further interactions.

Eventually, a peak, often referred to as the Bragg ionization peak, is reached followed by a decline to zero, when all the alpha particles's energy has been dissipated. Since alpha particles deposit their energy in such short tracks, they can be very damaging biologically if they get inside the cell (Wang and Willis, 1965).

2.3.2 Absorption of Photons

As has already been mentioned, photons interact with matter via the processes of photoelectric effect, Compton scattering and pair production; the energy of the incident photon determines which of these processes will play the dominant role in the absorption. Through these processes, ionizing electrons are produced and without these processes, the photons will travel straight through matter. This means that X and gamma rays have no absolute penetration depth in matter. The depth of penetration of a photon in a material depends on the energy of the photon and the atomic number of the material. What happens is that as a result of the complex, random interactions with matter, the beam of photons gets progressively weaker in intensity as it passes deeper and deeper into the medium - the beam is attenuated.

The absorption of X-ray and photons may be described by Beer's law as follows

$$I = I_0 e^{-\mu x} \quad \text{.....2.4}$$

where I_0 is the initial beam intensity

I is the beam intensity at thickness x

e is the base of natural logarithms

μ is the linear absorption coefficient

Actually, this equation applies to all monochromatic radiation traversing homogeneous material; in the case of composite matter and radiation it has to be replaced by appropriate integral expressions. It is also customary to use the mass attenuation coefficient μ/ρ instead of μ, with ρ being the density of the absorber. Attenuation is brought about by scattering (without energy loss) and energy transfer to the exposed medium. With regard to radiation action a distinction must be made between "energy transferred" and "energy absorbed", which is taken into account by introducing the energy transfer coefficient μ_k and the energy absorption coefficient μ_{en}, respectively. The first signifies the complete energy transferred to secondary particles in the form of kinetic energy by the initial ionization event, while the second includes only the fraction that is locally absorbed. All photon interactions (photoabsorption, Compton scattering and pair formation) lead to the production of electrons (and positrons, which play, however, a less important role since they combine readily after short distances). They are responsible for the actual energy deposition in the medium; the initial processes contribute only to a very small extent to the number of ionizations (Kiefer, 1991). Figure 2.3 shows the reduction of X- or γ-ray intensity as a function of absorber thickness.

To simplify comparisons between photons, the concept of *half value layer* (HVL) is used. The HVL is the thickness of the absorber which will reduce the intensity of a narrow beam of photons to one half. When the absorption of a homogeneous beam is exponential, the half value layer is

$$HVL = \ln\frac{2}{\mu} \qquad \text{.....2.5}$$

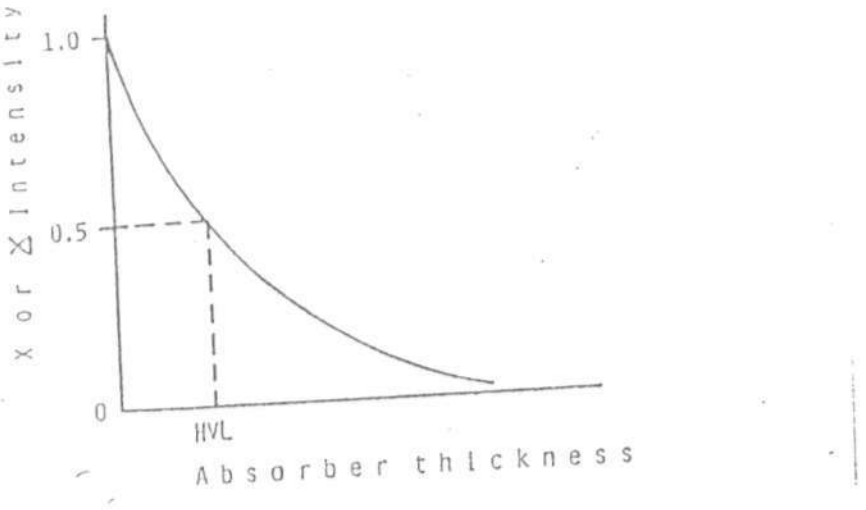


Figure 2.3: Reduction of X- or γ-ray intensity with absorber thickness. (After Pizzarello, 1982).

A second quantity, the homogeneity coefficient, uses the second HVL (that thickness in which the beam intensity is reduced from 1/2 to 1/4 its original value). The homogeneity coefficient is defined as (first HVL)/(second HVL). For a homogeneous beam the value is unity. Coincidence of both HVLs and a match of homogeneity coefficients ensures a reasonable match in beam characteristics.

2.4 Deposition of Energy by energetic ions

Accelerated heavy ions, in passing through solid matter, dissipate their energy by interacting with the target atoms (nuclear energy loss) and with the target electrons (electronic stopping). The nuclear stopping cross-section dominates the stopping process at specific energies below 10 keV/u and is only of minor importance in radiobiology. However, nuclear stopping is a biologically efficient process in which the energy is deposited in the vicinity of only a few atoms. Therefore, in measurements at very low energies a steep increase of the inactivation cross-section has been observed (Jung and Kürzinger 1968). For energies greater than 10 keV/u the electronic stopping cross-section dominates the stopping process. Energy loss is commonly given as "mass stopping power", which is related but not equal to LET (Kiefer, 1991). The rate of energy loss is proportional to the square of the charge of the particle and approximately inversely proportional to the square of the particle velocity. Thus the rate of energy loss of the particle increases in inverse proportion to the particle velocity, giving rise to a sharp maximum known as the Bragg peak near the end of the particle range. The particles capture electrons at very low velocities, and hence their effective charge is reduced, resulting in a decrease of the rate of energy loss. Accelerated heavy charged particles deposit energy in matter in a way which is fundamentally different from that of conventional ionizing radiations like X- or gamma-rays; they deposit large amounts of energy by single transversals through microscopic volumes. Ionizations are formed along

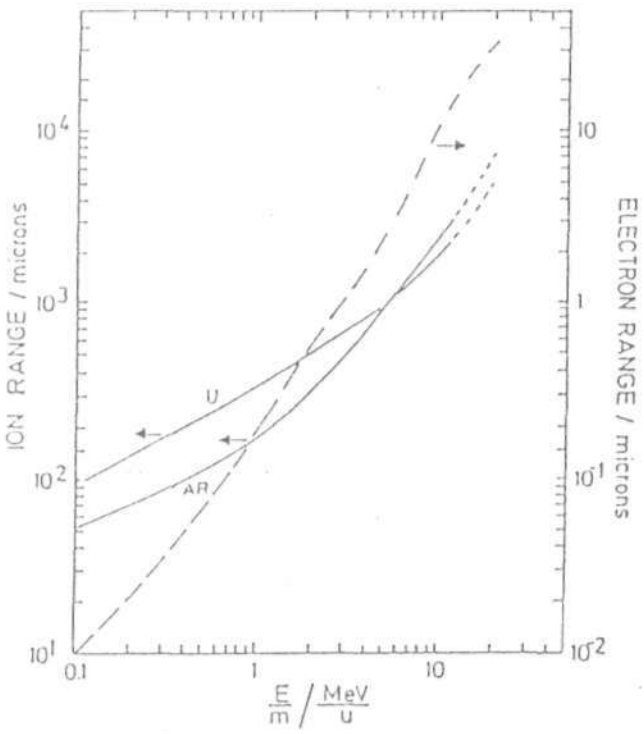


Figure 2.4: Range of heavy ions in water according to Northcliffe and Schilling. The range of the most energetic delta-electrons is also given. (After ICRU, 1970).

a well defined track whose radial extension depends on the particle energy while the ionization density is a function of its charge and velocity. The range of heavy ions in water is shown in figure 2.4.

For many purposes, the details of individual energy transfer events are not important. Instead, an approximation to the average energy lost by the ionizing particle is satisfactory. The most convenient approach is to calculate the collision stopping power, the mean rate of energy loss by the primary electrons, using the quantum mechanical formula derived by Bethe (ICRU, 1978a):

$$-\frac{dE}{dx} = \frac{4\pi e^4 Z^2 N}{m_e c^2 \beta} NZ \left[\ln \frac{2m_e c^2 \beta^2}{I(1-\beta^2)b} - \beta^2 - \sum \frac{C_i}{Z} \right] \quad \text{.....2.6}$$

where, -dE/dx is the rate of energy loss by the charged particle of atomic number Z and velocity ßc (c is the velocity of light). NZ is the number of electrons per unit volume in the medium, I is the mean excitation potential of the molecules of the medium, e is the electronic charge, and mc^2 is the rest energy of an electron. In this formulation, the cross sections are included in the mean excitation energy, I, and the shell corrections, $\Sigma(C_i/Z)$. The mean excitation energy can, in principle, be determined from the oscillator strengths, f_i, and corresponding excitation energies, E_i through $Z\ln I = \sum_i f_i \ln E_i$, but it is usually determined experimentally for one type of projectile and applied to others. The shell correction accounts for the effect of the electron orbital velocity on the energy loss. Approximations to the Bethe-Bloch have been described by Northcliffe and Schilling (1970), among others. When the velocity of the heavy particle is below the critical velocity for *Cerencov* radiation, the stopping power (that is,-dE/dx) is

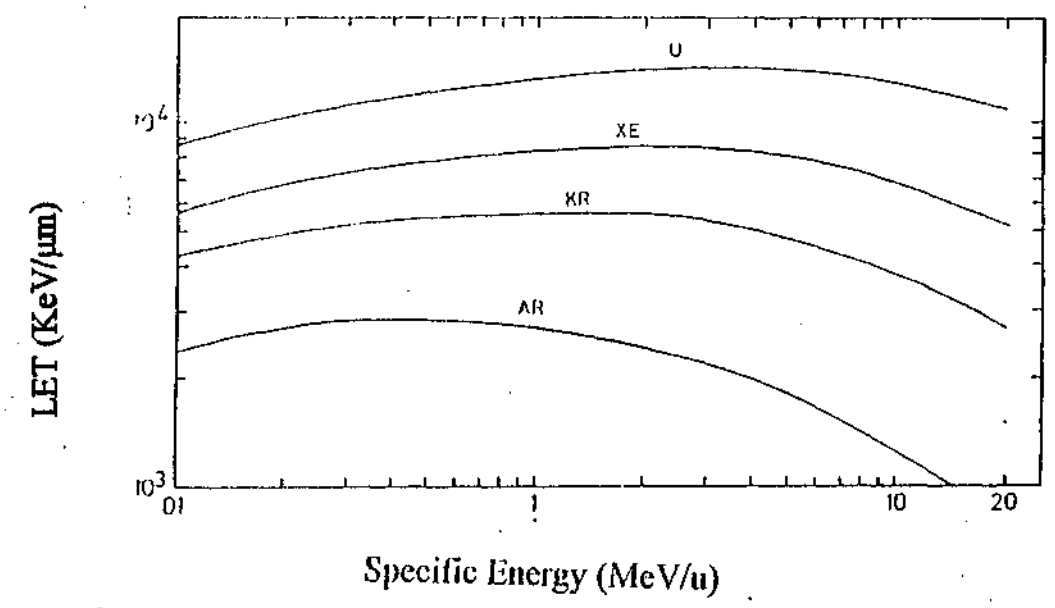
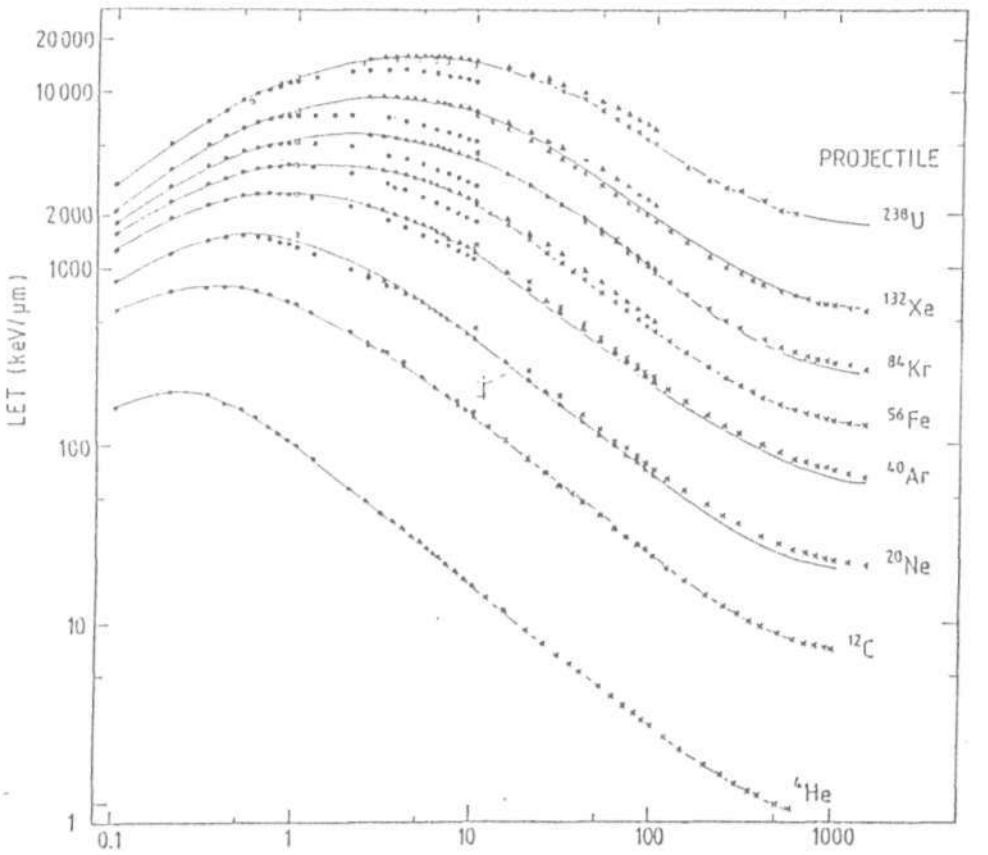


Figure 2.5: Stopping power as a function of ion specific energy.

(After Kraft, 1992).



Specific Energy (MeV/u)

Figure 2.6: Linear energy transfer of different ions in carbon.

(After Kraft, 1992).

equal to LET_{∞} (the subscript ∞ refers to the inclusion of all energies allowed by energy conservation).

If the numerical value of the ion energy in MeV is below $1/2Z_{eff}^{2}$, ions can alternately capture and lose orbital electrons. The ion then cannot be considered to have a constant charge, and a "root mean square [rms]" is assumed. To a first approximation, a plot of $(1/Z_{eff}^{2})S$ will be the same for all ions whose velocity is large enough that they are completely stripped of orbital electrons. Thus such a curve can be considered as a "universal curve" and departures from it at small velocities can be attributed to an effective rms number of electronic charges qZ_{eff}, where q is defined by the relation (Northcliffe and Schilling, 1970):

$$q^{2} = \frac{S_{ion}}{Z_{eff}^{2} S_{proton}} \qquad \text{.....2.7}$$

Where S= dE/dX and Z_{eff} is the effective charge of an atomic nucleus (ion) of atomic number Z. Figure 2.5 shows the stopping power as a function of ion specific energy for various ions while figure 2.6 shows the linear energy transfer of different ions in carbon.

2.4.1 Effective charge

If the velocity of the projectile exceeds the orbital velocity of its own electrons, these electrons are stripped off in the first few collisions and only the stronger bound electrons of the inner shells stay with the projectile. When the projectiles are slowed down, more and more electrons are captured and the charge state of the projectile is reduced until it comes to rest and is neutralized. The dependence of the projectile charge on the velocity

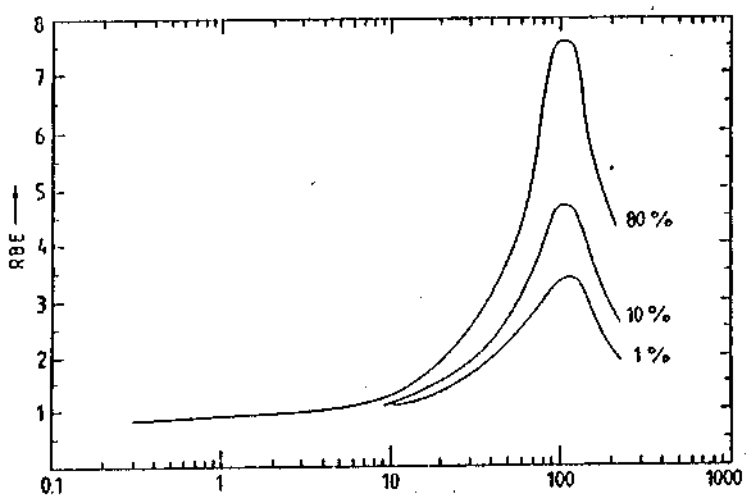


Figure 2.7: Relative biological effectiveness (RBE) as a function of LET.

(After Barendsen *et al.*, 1963).

has been approximated by Barkas and Berger (1963) with the expression in equation (2.8).

$$Z_{eff} = Z\left\{1 - \exp\left(-125\beta Z^{-2/3}\right)\right\} \quad \text{.....2.8}$$

Where Z is the atomic number of the projectile and β the velocity relative to that of light. It should be observed that the Z_{eff} values of Barkas represent the mean value of a broad charge state distribution. This mean value as well as the width of this distribution differs between gas and solid absorbers when compared at the same velocity. Due to the high collision frequency in a solid, more electrons from the inner shells are "pumped" by multiple collision into highly excited states from which ionization is produced more easily.

2.4.2 Energy loss, LET and RBE

The energy loss of heavy charged particles is mainly governed by the particle velocity. The velocity determines firstly the charge state and secondly the interaction mechanism between projectile and target. A variety of observations have shown that heavily ionizing particulate radiation (such as charged particles of atomic number greater than one) are several times more effective per unit dose, in producing biological effectiveness, than are X-rays. The concept of high biological effectiveness originated from the work of Zirkle (1980) who studied the lethal effects of α particles on cells. The studies of Zirkle and Tobias (1953) with helium and deuteron beams demonstrated that in addition to depositing dose at depth, these particles have increased effectiveness in the Bragg peak region, which led to the development of the term relative biological effectiveness (RBE) and LET (Blakely *et al.*, 1984). In order to differentiate, then, between the types of radiation, the International Commission on Radiological Units and

Measurements introduced as quality factor, the term 'RBE' which was attributed to the energy loss of the primary particle. The concept of quality factor is widely accepted in radiation research and is based on two assumptions:

1. The radiation effects caused by densely ionizing radiation are the same in their nature as those caused by sparsely ionizing radiation. But the energy deposition , that is the dose necessary to produce these effects, is different.
2. The quality of radiation can be characterized by the energy loss of the projectile or by the LET to the biological object.

The first assumption, the independence of the nature of the biological lesion from radiation quality was never a subject of critical review because many of the test systems used in radiobiology as for instance the most frequently used survival test are not sensitive to these differences. In contrast, the second assumption of the dependence of RBE from one single parameter like LET has always been a subject of intense research and controversy. From cloud chamber photographs as well as from tracks in nuclear emulsion, it is clear that particle tracks have lateral extensions and an inhomogeneous dose distribution inside the track. Besides, many biological experiments have shown that LET is not a good parameter for the description of the biological effects (Kraft *et al.*, 1992). Katz (1970) proposed an alternative method of specifying the quality of beams of ions, based on the conclusion that their effect on macromolecules, as well as on physical detectors, are attributable mainly to the delta rays ejected from their tracks as they pass through matter. According to this view, events in the track core are of much less importance than the distribution of the energy deposited by the delta rays. Their total energy varies as $Z_{eff}^{2}\beta^{-2}$, where β is the velocity of the ion relative to that of light. The energy density varies inversely with the square of the distance from the path of the

moving particle, up to approximately the range r_m of the δ-rays of maximum energy. According to Katz, therefore, the response of the macromolecules through which the ions pass should vary with $Z_{eff}^2\beta^{-2}$ provided their average radii are considerably less than r_m. Because the ions pick up electrons as they slow down, Z_{eff} may actually be less than Z. Calculations of Z_{eff}^2 as a function of β for atomic nuclei up to Z = 18, can be found in Butts and Katz (1967). However, in spite of the apparent success of the Katz view in his predictions about the inactivation of small macromolecules (enzymes and viruses) by ion beams, no single parameter can uniquely describe all features of the energy density variations, presumably because of the variety of energies of the electrons or other charged particles that are together responsible for energy transfers to the medium. Particle charge, velocity and fluence need to be defined before one can completely describe expected results. Alternatively, the effects can be described in terms of dose, mean dose-average LET∞ and charge. Blakely *et al* (1979) have illustrated this point in track-segment cell inactivation studies with high energy heavy particles. The relative biological effectiveness for cell killing as a function of LET is shown in figure 2.7.

There are, basically, two approaches which have been used for a more detailed description of the changes in biological response to heavy charged particles, the microdosimetric approach and the track structure modelling approach. In microdosimetry, small volumes of tissue having a diameter of 1 μm are simulated with gas-filled counters and the distribution of the energy deposition in these volumes is regarded to be the important parameter for the biological response (Zaider and Rossi, 1986). Clearly, the microdosimetric approach tries to take into account the inhomogeneous dose distribution inside the track as produced by the primary ionization of the projectile and the emerging electrons. In general, the microdosimetry of heavy ions

as primary beam particles, while in principle straightforward, is complicated by the highly energetic delta-ray distribution and the presence of nuclear spallation products. Most of the physical and chemical concepts underlying microdosimetry of particles have been recently reviewed (Booz *et al.*, 1990; Chadwick *et al.*, 1991). In a second approach, the track structure calculation of Katz *et al.* (1971), the grainy pattern of the energy deposition is not included. The dose is assumed to decrease continuously with the square of the radial distance from the centre of the track.

2.4.3 Distribution of energy deposition events

The processes by which a charged particle loses energy has been considered above; it would now be proper to consider the spatial distribution of energy deposition in biological material.

Since energy deposition is always due to the interaction of a whole spectrum of primary and secondary particles (even in the case of monoenergetic ions) and the secondary charged particle beam is usually composed of particles of different velocities and often of different charges, there is always a "distribution" of LETs. Such a distribution may be characterized by certain average values, the simplest one being the "track" or "number average" LET (L_T), defined by the expectation value of the distribution as follows (Kiefer, 1990):

$$L_T = \int fLf(L)dL \quad \text{.....2.9}$$

where all the events are treated as equally likely and fLf(L)dL is the probability to find a LET value in the interval L...L+dL.

The "absorbed dose" or "energy average" LET, L_D is used to calculate the relative contribution to the total energy deposited by the ionizing particle in the traversed medium. This is defined in equation (2.10)

$$L_D = \frac{\int fL^2 f(L)dL}{L_T} \quad \text{.....2.10}$$

where each event is weighted by its energy deposition and L_T is a normalizing factor (Kiefer, 1990).

Simply put, the average LET is calculated by estimating the proportion of the energy that is deposited within each LET interval, so that equal statistical weight is assigned to each unit of energy deposited while the absorbed dose-average LET as a whole is calculated by summing and averaging the contributions from all ionizing particles. As is obvious from the above expressions, the two "average LETs" can yield two different results if the variance of the distribution is non-zero. This depends on the kind of radiation and also on the cut-off energy chosen for specifying LET (Alper, 1979). The cut-off energy is related to the fact, which has already been touched upon, that some energy transfers (when ionizing radiation impinge on matter) may be large enough to result in the emission of electrons that can themselves act as ionizing particles; so in quoting a value for LET, it becomes necessary to stipulate the maximum energy loss per event that will be taken into account in the particular context. For example, if it is considered that energy losses of greater than 100 eV will not be relevant to the purposes for which the description of quality is required, the relevant LET is designated L_{100}. For some purposes it may be desirable to specify the LET in terms of total energy loss, which includes all energy transfers up to the highest energy delta rays or knock-on electrons that are kinematically possible; in this case the symbol L_{∞} is used. Generally speaking,

the linear energy transfer or restricted collision stopping power (L_Δ) of a charged particle in a medium is defined by equation (2.11).

$$L_\Delta = \left[\frac{dE}{dL}\right]_\Delta \qquad \text{.....2.11}$$

where, dL is the distance travelled by the particle and dE is its mean energy loss due to collisions with energy transfers less than some specified value Δ. The subscript Δ is usually specified in electron volts (eV) (Goodhead, 1987). Table 2.3 shows the track average LET for various radiations.

Table 2.3: Track average LET values for various radiations.

(After Pizzarello 1982)

Radiation type	$L_{\Delta,T}$ (keV/μm)
^{60}Co	0.237
22 MV X-rays	0.20
200 kVp X-rays	1.7
^{3}H betas	4.7
50 kV X-rays	6.3
5 MeV protons	10.0
Thermal neutrons	20.0
5.3 MeV alpha	43.0

A major limitation of the LET concept is that it ignores the finite width of radiation tracks. Unrestricted LET∞ totally ignores the width; energy restricted LET considers the main component of local energy deposition along the path of the primary particle but

does not include the energy deposited by the secondary electrons of energy > Δ, irrespective of whether this energy is deposited locally or at a distance from the primary particle. An alternative microscopic description is provided by calculated, or measured, radial distributions of mean energy deposition around particle tracks.

This approach is related to the concept of radius-restricted LET, L_r, (ICRU, 1970; Chatterjee *et al.*, 1973). It does not address the other main limitations of LET, namely fluctuations in electron energy loss and finite ranges of primary particles. A more detailed description of electron tracks has been proposed in terms of track entities such as "spurs", "blobs", and "short tracks" (Goodhead, 1987).

For particle radiation the fluence (that is, the number of particles impinging per unit area) is often more relevant than the dose (D). The two parameters are related by the stopping power or the linear energy transfer (LET) L as in equation (2.12).

$$D = \frac{L \cdot \phi}{\rho} \qquad \text{.....2.12}$$

where ρ is the density of the absorbing medium and ϕ is the particle fluence.

With heavy ions the number of cells hit by the particle varies considerably and can be described by a Poisson distribution (equation 2.13) (Kiefer and Schneider 1987).

$$p\nu(\phi) = \frac{(\sigma_o \phi)^{\nu}}{\nu!} e^{-\sigma_o \phi} \qquad \text{.....2.13}$$

Where, pν(ϕ) is the probability that the cell's sensitive site with cross-section σ_o receives just ν hits if exposed to a particle fluence ϕ and $\sigma_o\phi$ is the average number of hits.

2.5. Ion Sources and physical properties

Heavy ions also constitute an important fraction of cosmic galactic radiation (Curtis 1974, Adams *et al.* 1981). Their fluxes are, however, low (Kiefer, 1985). The energies cover a very wide range up to several thousands of GeV/u (Heinrich and Beer 1984). Energetic heavy ion can be produced by linear or circular accelerators (for review see Böhne 1984). Very high energies are obtainable by a combination of both, where a powerful linear accelerator is used as an injector for a synchrotron. This configuration is used in the BEVALAC facility at the Lawrence Berkeley Laboratory (Alonso *et al.* 1980). The UNILAC accelerator at the *Gesellschaft für Schwerionenforschung,* Darmstadt, Germany where most of the work in this report was performed, is a two-stage linear accelerator (Angert and Schmelzer 1977, Böhne 1984).

Accelerated heavy ions cover a wide range of values of LET. There is no general agreement in the literature about their actual values which mainly rely on theoretical calculations (Northcliffe and Schilling 1970, Ziegler 1980, Hubert *et al.* 1980). In general, it is found that the best agreement is obtained if it is assumed that the ion's effective Z_{eff} is not only a function of its energy but also of the absorbing medium (Bimbot *et al.* 1983).

2.5.1 Track Structure

The track of a heavy ion in matter is not infinitesimally small but widened due to the generation of δ-electrons. Its extension depends only on the ion velocity while the number of electrons produced per unit pathlength is proportional to Z_{eff}^2/β^2, where β is the ion speed relative to that of light in vacuum. The energy deposited per unit mass (energy density) falls off with radial distance (t) from the track centre. Chatterjee and Schäfer (1976) divided the track into a "core" and a "penumbra" region. They assume a

constant energy density in the first and a $1/t^2$ dependence in the other. Other track structure models have been presented by Butts and Katz (1967), Fain *et al.* (1974) Hansen and Olsen (1984) and Kiefer (1985) based on different assumptions and simplifications. While they all agree on the $1/t^2$ relation in the outer region, there is considerable disagreement about the actual value of the energy density and maximal extension, the 'penumbra radius'. While Chatterjee and Schäfer (1976) assume a sudden cut-off, others postulate an energy dependence in the outer region of (Butts and Katz 1967, Hansen and Olsen 1984):

$$\frac{1}{t^2}\left[1-\frac{t}{t_m}\right]^{1/\alpha} \qquad \text{.....2.14}$$

where t_m is the penumbra radius.

Penumbra effects play only a minor role with light ions because the electron density is low and so little energy is deposited outside the track core. However, with ions of higher atomic number the energy deposited even at the rim of the penumbra may be considerable and hence it may be expected that the radiobiological effects may also change. Therefore, at least for the very heavy ions, an adequate theory that can take into account the effect of the penumbra region as well as that of the core becomes imperative; this has been the goal of the various track theories. Figure 2.8 shows the penumbra radii according to different beam models as a function of ion specific energy.

Generally speaking, track theory describes the interaction of a charged particle with a detector through the joint application of the radial distribution of dose and the dose-response after irradiation. There exists a number of track structure modelling approaches. In the model as developed by Katz *et al.* (1985) good approximation to the

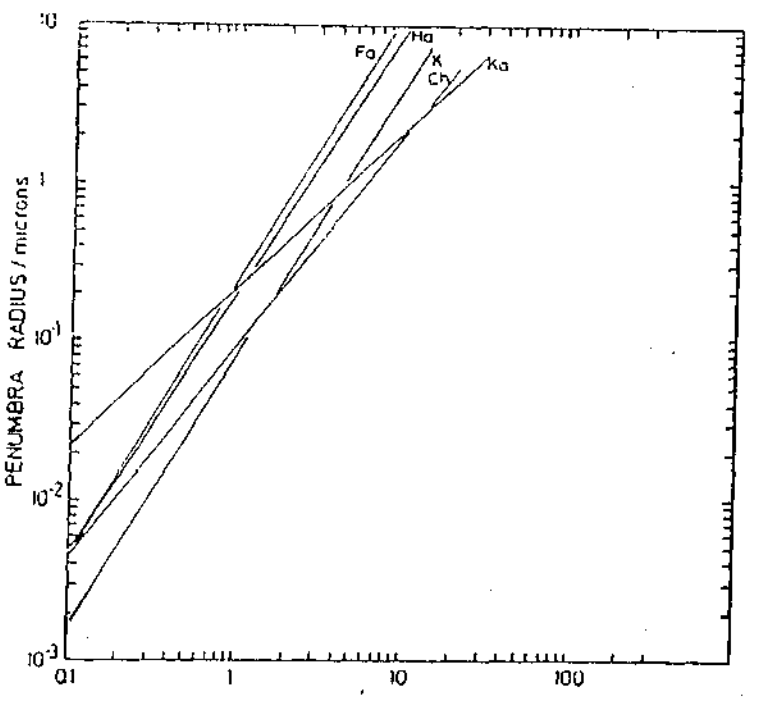


Figure 2.8: Penumbra radii according to different beam models as a function of energy. (After Kraft, 1992).

inactivation measurements of different biological objects as well as the LET-dependence of other biological endpoints has been achieved. An outgrowth of one track structure model was the prediction of particle track structure effects due to "thin-down" regions within the energy dense regions of the tracks that would yield "hooks" of inactivation for individual particles as a function of LET (Katz *et al.*, 1971). This was further confirmed by the experimental work of Kraft and his co-workers (Kraft *et al.*, 1984; Wulf *et al*, 1985; Kraft, 1987 and Kraft 1988) with very heavy ions (uranium ions of LET > 10000 keV/μm, etc.). Recent studies comparing low energy protons and helium ions at LET values between 7 - 40 keV/μm have revealed that protons are more effective than helium ions in inducing both cell inactivation and mutation at the same LET (Perris *et al.*, 1986; Belli *et al*, 1986). Microdosimetric differences in track structure are supposed to be responsible for this unexpected difference in biological effectiveness at low values of LET, but more data need to be obtained before this can be confirmed.

One way of calculating the energy deposition as a function of distance from the track centre is to follow the path of each electron bearing in mind experimentally determined interaction cross-sections in a given medium. This `Monte-Carlo simulation' has been successfully used to compute the energy deposition by protons, alpha particles and electrons.

The other method is to start with the known cross-section for liberation of electrons and then use mathematical formulations to describe the initial pattern of energy paths.

In detailed Monte Carlo calculations in which the primary ionizations and cascade of electrons are followed up individually, the $1/t^2$ law of the radial dose distribution is confirmed but there is no evidence of a high energy deposition in the centre of the track (Krämer and Kraft, 1987). The same is true for microdosimetric measurements of the

radial ionization distribution (Metting *et al.*, 1988). In addition, measurements of the angular and energy distribution of the emitted electrons have confirmed the previous assumption of Bethe that the overwhelming part of the energy loss of the projectiles is transformed into kinetic energy of the emitted electrons (Schmidt *et al.*, 1988).

The original beam model of Butts and Katz is able to predict single strand break (SSB) induction but fails with DSB-formation and cell survival; Kiefer and Straaten (1986) proposed an improvement by adding the so-called `integral proximity functions' which embodies the idea that two energy deposition events have to occur within a certain distance for DSB production. A complete consideration of the subject is, however, beyond the scope this work.

2.5.2 Track Entities of energetic electrons: spurs, blobs, short tracks and branch tracks

The low-energy (<100 eV) losses create track entities called "spurs". If the particle is fast and lightly ionizing, the spurs are widely spaced and developed independently, that is, without interference from neighbouring spurs. If the particle is slow enough to be heavily ionizing, the spurs overlap and form a continuous column. Half of the energy deposit of a heavy particle is in the spurs. If the particle is lightly ionizing, such as a proton with energy of about 100 MeV, the spurs are well separated and isolated spurs form a good approximation of the track; an average spur may contain two or three radical pairs.

Track entities formed with energies a little above 100 eV are like spurs; however, for some higher value of the energy loss, a recoil electron energetic enough to give rise to spurs is formed and a short track results (Mozumder and Magee 1975).

2.5.3 Target size and Cross sections

Concepts closely related to LET are inherent in early target theory calculations such as those of Lea, who used the concept of radiation tracks to estimate the sizes of critical biological structures ("targets") from the observed effectiveness of radiations in inactivating, or otherwise damaging, the organisms under study. These methods were most applicable to simple biological systems which showed (1) a relative sensitivity per unit absorbed dose which decreased with increasing ionization density of the radiation and (2) a purely exponential dose-response curve. These properties were considered to justify the assumption that the biological effect was due to a single random "hit" anywhere in the target. Estimation of target size could therefore be made by comparison with physical calculations of absolute probability of a radiation track passing through the target and interacting with it. It soon became obvious that for most biological systems these assumptions were not justified: (1) for most higher organisms, including mammalian cells, the relative sensitivity increases with increasing ionizing radiation density up to a point, and (2) for low-LET irradiation of many mammalian cell types, the log-linear survival curve is "shouldered" rather than a simple exponential.

Assuming that the response of a biological system to a given radiation type is governed solely by the energy deposited in its sensitive sites, it can be shown that, in the case of exponential inactivation as in equation (2.16) (Kiefer and Straaten 1989).

$$\sigma = \sigma_o \left[1 - \int f_1(z) e^{-kz} dz\right] \quad \text{.....2.16}$$

where, σ is the inactivation cross section

σ_O, "the geometrical" cross section

z, "local dose" in the sensitive site

f1(z)dz, distribution density function of z for single particle transversals and

k is the sensitivity coefficient of the particular system under study

σ is an experimental quantity determined from the response curves.

σ_o is a composite parameter depending both on the extensions of the sensitive site and the track penumbra and is given by:

$$\sigma_o = \pi \left(r_\tau + r_p \right)^2 \quad \text{.....2.17}$$

where r_τ is the target radius and r_p is the penumbra radius. The sensitivity coefficient k is assumed to be constant for a given system and may be taken from γ- or X-ray survival curves.

2.5.4 Radiation Quality

It is evident that the processes of energy loss by all types of ionizing radiation are complex, so `quality' is impossible to specify in any simple way. Further and as mentioned above, energetic charged particles give rise to a distribution of LETs in matter. It is not quite clear what factor should be used in weighting the various portions of the LET distribution in order to obtain a realistic evaluation of the LET distribution from the biological point of view. One function which has often been used in this regard is the quality factor (QF). In direct relation to this is the concept of relative biological effectiveness (RBE). Before much was known about the biological effects of heavy charged particles, Stokes proposed the use of neutrons in radiotherapy. However, early attempts at a radiotherapeutical use of neutrons failed because the RBE of neutrons given by the effectiveness of their recoil nuclei, mostly protons, helium and carbon ions,

was underestimated. In a classical experiment, Barendsen and co-workers measured the RBE of light ions like deuterons and α particles compared to the effectiveness of x-rays.

Although the term RBE can be applied to a variety of biological endpoints, its definition and method of determination remain the same. RBE is usually given as a ratio of doses from different radiation sources to produce the same effect. Since X-rays were first discovered and were most easily available, they were used as the basis for comparison. This selection turned out to be fortuitous since the RBE is relatively constant in the X- and γ-ray region. RBE is determined from the following equation:

$$\text{RBE} = \frac{\text{absorbed dose from 250 kV X-rays to produce a certain effect}}{\text{absorbed dose from another radiation to produce the same effect}} \quad \ldots\ldots\ldots\ldots 2.18$$

Since the "absorbed dose" is used, the differential penetration properties of various energies do not influence the RBE calculation. An examination of the individual survival curves shows, in general, a loss of the shoulder with higher-LET irradiation. Thus the value of RBE must change with the survival level, from a high value at high survival to a low value at low survival.

The RBE can be measured for several endpoints: cell survival, chromosomal aberrations, mutations etc. Although the actual curves for the responses as a function of the dose may vary in shape, the pattern for RBE variations with LET is quite similar for various endpoints. For many biological endpoints, RBE increases with LET to a certain point (100 keV/ μm) and then decreases abruptly. Based on target theory, this pattern can be explained by the necessity of inactivating one or more targets several times. The more densely ionizing radiations (high LETs) are more effective up to a certain point, beyond which the energy is wasted and the RBE decreases. The relationship is even

more complex with charged particles, since the LET varies with the depth of penetration (Raju *et al.*, 1976).

The term RBE is related to the term *quality factor* used in health physics for protection standards in that both attempt to equalize the various forms of radiation. However, the RBE does so for a biological endpoints. On the other hand QF is assigned a number based on physical considerations (Grosch and Hopwood, 1979).

2.5.5 Microdosimetry

The unsatisfactory features of "average LET" and average "dose" as specifications of radiation quality have led to a search for their replacement by more appropriate concepts. Linear energy transfer, defined as the energy transfer by an ionizing particle per unit path length takes no account of the stochastic nature of energy-deposition events, which assumes high importance when small mass elements are considered, because the quantity "energy per unit mass" cannot be singled-valued, in this case, but follows a distribution. Ionizing radiation deposits energy in discrete packages which are the result of interactions with the atoms of the medium through which it passes. These packages are distributed non-uniformly throughout the irradiated volume. Not only the average energy deposited per unit mass (that is, the absorbed dose), but also the number of energy deposits as well as their spatial distribution may be expected to influence the effect of the radiation on biological and other structures. Radiations which differ in the number, size and distribution of energy deposits might, therefore, be expected to cause different effects for the same absorbed dose. This is what is quantified, as far as the biological effect is concerned, as RBE for a given radiation.

For a thorough appreciation of these differences between radiations, one should, of necessity, begin with an appropriate description of the manner in which the energy is

initially deposited. This, in turn, requires detailed information on the structure of the tracks generated in an irradiated medium. A full description of all the interactions which occur in an irradiated medium is extremely complex. A complete description of the biological structures in an irradiated organism is likewise complicated and impracticable. To get round these difficulties, concepts have been developed which relate some of the principal features of the absorption of ionizing radiation in matter to the size and nature of the structures being affected. The branch of radiation research concerned with these problems is called "microdosimetry" in contradistinction to dosimetry which is concerned with *dose* at the macroscopic level. Although a prime motivation for microdosimetric studies has been the application to biological systems, microdosimetry itself can be regarded as a purely physics activity. Its techniques and methods provide physical descriptions of radiation fields and their interactions with matter. However, the major impetus and applications have always been in relation to biological problems (Goodhead, 1987).

The term microdosimetry originated when Rossi and his co-workers developed a conceptual framework and the corresponding experimental methods for the systematic analysis of the energy distribution of energy deposition in irradiated matter. Stochastic quantities , such as *the specific energy, z* and the *lineal energy,* y were defined and measured.

The "specific energy" z is the microdosimetric analogue of dose. It is defined as the energy dE deposited locally in a small volume divided by its mass dm:

$$Z = \frac{dE}{dm} \qquad \text{.....2.19}$$

Here, Z is a stochastic quantity fluctuating according to statistical laws and may be described by a distribution function f(z)dz. For heavy charged particles the variations of specific energy in a given microscopic volume are due to changes in hit number, distance from the track centre and fluctuations of energy deposition (energy straggling) (Kiefer, 1988).

Another related concept often used in relation to microdosimetry is `lineal energy', defined as the quotient δE by d, where δE is the energy imparted to the matter in a volume during an energy deposition event and d is the mean chord length in the volume of interest (ICRU, 1971). The description of such quantities like *specific energy* and *lineal energy* and their probability distributions are the central concepts in microdosimetry. At the same time, other important microdosimetric parameters like radial track distribution, point kernel and proximity functions have been developed to enable a composite description of the spatial energy deposition. Mention should also be made here about the microdosimetric concept of "energy deposits". This is the energy which remains at the locus of interaction in the form of excitations and ionizations after all nuclear reactions and mass energy transformations have taken place and all energetic particles have been emitted. It represents the most elementary quantum of local energy deposition of radiation to matter, being directly related to the formation of primary radiochemical products as starting points for elementary biomolecular damage. The energy deposits can be used to describe track structures of charged particles in matter and to evaluate the energy imparted to a sensitive volume (Ebert, 1983).

2.5.6 Energy density

Heavy charged particles deposit large amounts of energy by single transversals through microscopic volumes. The spatial pattern depends on the number of hits

received and is highly inhomogeneous. The number of hits may be assumed to follow a Poisson-distribution. The important parameters (Kiefer, 1988) are the number of particles per unit area - the fluence - and the cross-section of the sensitive volume (SV), that is, the nucleus. The probability $p_d(i)$ to receive i hits is given by equation (2.20) (Kiefer, 1988).

$$p_d(v) = e^{-\sigma_{sv}} \frac{\phi(\sigma_{sv}\phi)^v}{v!} \quad \text{.....2.20}$$

where σ_{SV} is the cross sectional area of the sensitive volume and Φ the particle fluence. Energy density may then be defined as the expectation value of specific energy in infinitesimally small volumes for single particle transversals as a function of distance from the track centre. The energy deposited by a single transversal is not single-valued but follows a distribution which is a function of particle type and the shape and size of the SV. To determine this distribution the spatial pattern of energy deposition has to be known. Since accelerated heavy ions interact with the shell electrons in the atoms of the exposed medium, the energy deposition does not remain localized since the liberated electrons may be imbued with high energies. Part of the energy do get transported over some distances by these δ-electrons. This implies that the track has a finite width, called *penumbra* radius r_p (Kiefer, 1988). The extent of this penumbra radius is not yet clear. The model of Kiefer and Straaten (1986) yields:

$$r_p = 0.0616\left(T/m\right)^{1.7} \quad \text{.....2.21}$$

Where T is the ions kinetic energy in MeV and m, its mass in atomic mass units and r_p given in μm.

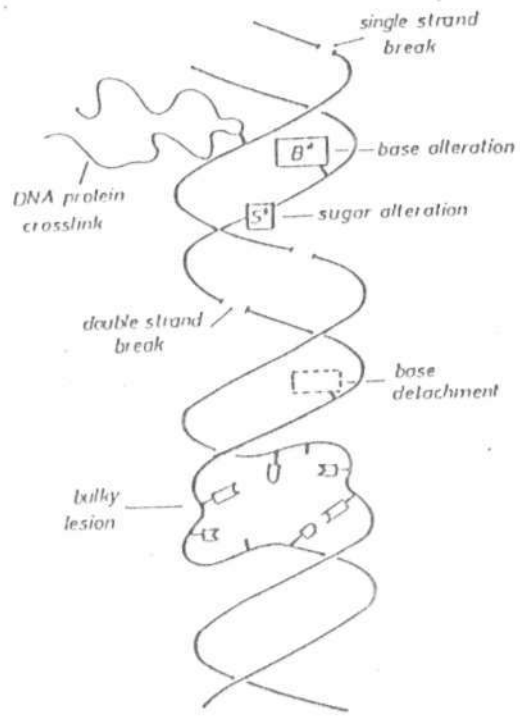


Figure 2.9: Lesions induced in cellular DNA by ionizing radiation.

(After Frankenberg-Schwager, 1989).

Thus it appears that ions of equal T/m possess similar track structures. With the above considerations, an "SV local dose" may be defined as the expectation value of the specific energy in the sensitive volume which varies with hit number and distance from track centre. The dose D is then obtained by averaging the "SV local dose" over all hit numbers and distances. Thus, it can be shown (Kiefer, 1988) that :

$$D = \sigma_0 \Phi \, z \qquad \text{.....2.22}$$

where, z is the average energy deposited per mass element by a single transversal, σ_0 is the cross section of the sensitive volume (assuming spherical (SVs) and Φ is the particle fluence.

Another relationship between particle fluence and the dose is given in equation (2.23).

$$D = \frac{L \, \Phi}{\rho_m} \qquad \text{.....2.23}$$

Where, L is the linear energy transfer or stopping power of the ions

and ρ_m is the density of the exposed medium.

2.6 Targets in Biological Cells

Deoxyribonucleic acid (DNA) is considered to be an important target for radiation damage in living cells, whether the result of the exposure is inactivation of proliferating capacity, mutation, or chromosomal aberrations. The effect of ionizing radiation on DNA has been studied quite extensively under various conditions, including irradiation of acqeous DNA solutions, dry DNA, viral DNA and DNA in living cells. Figure 2.9 is a schematic illustration of lesions induced in cellular DNA by ionizing radiation. The interruption of the nucleotide strand is one of the most serious kinds of damage to the

macromolecular structure of DNA. These strand breaks may concern either one strand of the double helix (single strand breaks, SSB) or both strands (DSB). It is widely agreed that the most important target molecule in living cells is the DNA, but since that recognition, two very different schools of thought have emerged. One school of thought, based on measurements of cell survival after track segment irradiation of mammalian cells (Barendsen *et al.*, 1963) held that:

(a) the biological target was small (5-10 nm diameter) and that the inactivation of one such site would cause the effect;

(b) the energy required to inactivate was a few hundred electron volts;

(c) this "threshold" energy could either be deposited instantaneously by a single passage of sufficiently high LET or "blobs"; or

(d) by two or more tracks passing through the target volumes before the damage due to the first "hit" or track passage had been repaired by enzymatic processes

The initial slope of low-LET mammalian cell survival curves is thought to be due to the small, but sufficient, proportion of high-LET "blobs" deposited by low-LET radiation. The shoulder (that is, increasing slope with dose) on low-LET survival curves was at first thought to be due to the necessity to accumulate "hits" in process (d). When it was clear that targets of 5-10 nm could rarely be hit by more than one track at the doses of a few grays where the shoulders occurred, condition (d) was replaced by "saturable repair" (Alper, 1979). It is basically a single-hit, small target-volume theory with repair assumed to be proficient for the first gray or so of low-LET irradiation, but becoming saturated or overwhelmed (or overtaken by misrepair) after a few grays, so that the survival curve becomes a steeper exponential.

The alternative hypothesis is the dual radiation action of radiosensitivity (Kellerer and Rossi, 1972). In this theory two sublesions must be produced, within a distance of about 0.4 μm so that they can interact and cause the biological effect. This theory leads to a linear (intratrack) plus the, rather controversial, quadratic (inter-track) dependence of effect upon dose. Among other consequences, the large interaction distances make low-LET radiation appear so inefficient at low doses that the RBE could rise above 100. The large interaction distances (based on the average ion-cluster spacing for the mean inactivation doses of 1-2 Gray for low-LET irradiation) differ strikingly from the 10 nm or so of the other theory. When the dual action theory was applied to risk estimates, very high values of quality factor were obtained. The dual action theory has been shown to be wrong in the dimensions of its interaction distances, although it converges to the other theory by assuming a distribution of interaction distances that is strongly skewed towards very small distances (Fowler, 1989).

The experiments that first indicated targets of nanometer, rather than micrometer, size were track segment experiments carried out on single layers of mammalian cells irradiated with heavy ions having a range of LETs from low (< 30 keV/μm) to past the peak of the RBE curve, where the effectiveness per particle track decreased because of overkill (Barendsen 1964; Barendsen *et al.* 1960, 1963).

2.6.1 Chemical changes induced by ionizing radiation

Having considered the physical processes of the absorption of photons and ionizing radiation, it is appropriate now to examine the next step in the chain of events which may lead to a biological effect. Here an extrapolation must be made from the physical system previously discussed, where matter was considered as a sea of atoms, to the biological state where matter consists of molecules of various sizes and various degrees of

complexity. The interaction of radiation with these molecules is thought to be similar in nature to that with individual atoms.

2.6.2 Formation of radicals

Ionization is not a selective process. Any atom or molecule in the path of a radiation may be ionized. The predominant constituents of a complex system will stand the best chance of being ionized and the chief constituent of living material in its functional state is water. In marine forms, water may comprise more than 96% of the organism. Many human tissues are made up of 70-80% water; in vegetative cells its fraction lies between 40% and 50% but even in bacterial spores it is still around 20%. Thus, water is identified as the most probable material in which the ionizations caused by radiation may occur. The resulting chemical products may react with biologically important organic molecules and thus be indirectly responsible for an observable effect. Since water does not absorb optical radiation between 200 and 800 nm, it is not directly relevant for photobiology. The situation is completely different for ionizing radiations because in this case most of the energy is, in fact, absorbed by water (Kiefer, 1991). Thus for an understanding of radiobiological effects the radiation chemistry of water is of extreme importance.

Free radicals:. Free radicals are electrically neutral atoms or molecules having an unpaired electron in their outer orbits. The concept of unpaired electrons can be explained using the Bohr model of the atom with its K, L, M, N, etc. shells, whose population is limited by the Pauli exclusion principle. The electron quantum state is determined by a number of parameters, one of these being spin, which may have two values only. In stable atoms and molecules, orbital electrons occur in pairs with opposite spin values. A free radical is formed by radiation when an atom is left with one of its outer orbital electrons unpaired with respect to spin. Free radicals are usually very

reactive since they have a great tendency to pair the odd electron with a similar one in another radical or to eliminate the odd electron by an electron transfer reaction. Free radicals can therefore be electron acceptors (oxidizing species) or electron donors (reducing species).

2.6.3 Radiation chemistry of water

When pure water is irradiated, in the absence of oxygen it is ionized or excited. Excitation is often followed by a homolytic splitting of the molecule (Coggle, 1983):

$$H_2O \xrightarrow{\text{radiation}} H_2O^+ + e^- \text{ (ionization)} \quad \text{2.23}$$

$$H_2O \xrightarrow{\text{radiation}} H_2O^* \longrightarrow H\cdot + OH\cdot \text{ (splitting)} \quad \text{2.24}$$

The primary products are H· (hydrogen atoms), OH·, H_2O^+ and electrons. All these species possess unpaired electrons and hence are free radicals.

The electron (e^-) will travel through the water, losing energy by various processes, until it is captured by another water molecule converting the latter into a negatively charged molecule:

$$e^- + H_2O \longrightarrow H_2O^- \quad \text{2.25}$$

This process is a relatively slow one and the electron may become hydrated, that is, surrounded by water molecules in such a way that the dipoles of several molecules are orientated towards the negative charge of the electron.

Apart from free radicals, stable molecules like water, hydrogen and hydrogen peroxide may also be formed in the process. The reactivities and rate constants for

reactions of these species with many molecules have now been measured, mainly by pulse radiolysis techniques. Their chemistry is that of free radicals and they can therefore abstract hydrogen from organic molecules, RH,

$$RH + H^{'} \longrightarrow OR^{'} + H_2 \quad \text{.....2.26}$$

These radicals result in new radical species. The primary as well as the secondary free radicals $R^{'}$ can react with biologically important molecules and cause radiobiological damage. These reactions are generally held to be important in the so-called `indirect' action of radiation. Indirect action, thus involves the acqeous free radicals as intermediaries in the transfer of radiation energy to biological molecules. In contrast, the direct action of radiation involves the simple interaction between the ionizing radiation and critical biological molecules. The water radiolysis products is shown in table 2.4, for low LET radiation.

Table 2.4: Initial and final yields of water radiolysis products for low LET radiation (After Buxton, 1987)

Product	Initial Yield $(100\ eV)^{-1}$	Final Yield $(100\ eV)^{-1}$
e_{aq}^{-}	4.78	2.7
$OH^{\cdot}$	5.6	2.7
$H^{\cdot}$	0.62	0.45
H_2	—	0.45
H_2O_2	—	0.7

The increased effectiveness of radiation in the presence of oxygen is known as the "oxygen effect". The increased yield of damaging free radicals has been proposed to account for the effect. The reaction of oxygen with acqeous free radicals such as H and

e^-aq lead to the production of the relatively stable hydroperoxy radicals (HO_2) and to hydrogen peroxide:

$$O_2 + H^{'} \longrightarrow HO^{'}_2 \quad \text{.....2.27}$$

$$2HO^{'}_2 \longrightarrow H_2O_2 + O_2 \quad \text{.....2.28}$$

Alternatively, if an organic biologic molecule (RH) becomes a free radical either directly or indirectly it may interact with oxygen as follows:

$$R^{'} + O_2 \longrightarrow RO_2^{'} \text{ (an organic peroxy radical)} \quad \text{.....2.29}$$

These reactions are tantamount to fixation of biological damage and occur at a rate of about thirty times other competing reaction like $R^{'}$ + cysteine or other hydrogen donor to give RH, that is reconstitution (Coggle, 1983).

DNA free radicals can be formed by direct ionization as well by the attack of water radicals, mainly as OH radicals. These radicals are most susceptible to chemical modifications resulting in more stable products. Either the DNA-free radicals may be chemically restored by reduction involving hydrogen donation from sulphydryl compounds such as glutathione (GSH) or they may be oxidized by molecular oxygen or other electro-affinic compounds leading to stable altered DNA structures.

On the average, about 17 eV is needed to create a hydroxyl radical in water. The initial yields of the respective species are expressed in terms of G-values, which can be defined as the number of a given radical produced per 100 eV of deposited energy: G_{OH} = 5.88, G_H = 0.88, G_{e^-} = 5.0 and $G_{H_2O^+}$ = 5.00. How these initial values depend on LET is not clear at the present time.

In acqeous solution, DSB of DNA are formed only by coincidence of two single strand breaks at a distance of about 10 base pairs, this distance *h* being dependent on the ionic strength of the medium. Thus DSB are formed *in vitro* with a quadratic term of the dose as well as with a linear response, due to pre-existing SSB during handling of the DNA solutions. This relationship can be expressed by the equation:

.....2.30

Where B_1 is SSB per nucleotide and per gray, B_2 is the DSB per nucleotide pair and per gray, A_1 is pre-existing SSB per nucleotide in the DNA strand, and h is the distance of SSB opposite on the DNA strands to form a DSB, expressed in nucleotide pairs. Both SSB and DSB may be formed by an attack of OH radicals, where details of the radical reactions have been studied on the radical C4 position of the deoxyribose (von Sonntag *et al.* 1981). By irradiating single nucleosides or nucleotides, it can be shown that there is an equal distribution of the radical attack on the five carbon atoms in the deoxyribose.

2.6.4 Routes to damage production

Radiation damage to an intracellular molecule can be traced through several distinct stages. The steps which lead to the production of chemically stable damages are:

1. Physical deposition of energy (10^{-18} s).
2. Production of primary radicals on the target molecule and in molecules surrounding the target - "direct" and "indirect" effect (10^{-12} s).
3. Reaction of radicals on surrounding molecules with target molecule (10^{-8} s).
4. Reactions of unstable target radicals leading to chemically stable damage (10^{-3} s)

These steps occur sequentially and the approximate time necessary for each step is as indicated.

2.7 Lesions Induced in DNA by Ionizing Radiation, their Measurement and Repair

A number of lesions can be detected in the DNA of eukaryotic cells treated with ionizing radiations. They include DNA-protein cross-links (DPCs), base alterations and base detachments, sugar alterations, bulky lesions, i.e. clusters of base damage, single and double strand breaks. The structural damage produced by ionizing radiation can be described as denaturation and degradation of the DNA molecule. DNA-protein cross-links are formed by covalent linkage between DNA and proteins of the nuclear matrix. The main areas of the DNA involved in this linkage are those containing actively transcribing, and presumably also replicating sequences (Frankenberg-Schwager 1990). A relatively high amount of about 6000 DPCs is observed per normal, unirradiated cell of Chinese hamster V 79 lung fibroblasts in exponential growth. In general, DPCs are induced at a rate four times higher than double strand breaks for the same dose level (Ramakrishnan *et al.* 1987). Radiation-induced DPCs are thought not to play a role in radiation-induced cell killing (Frankenberg-Schwager 1990).

Radiation-induced SSB in the DNA were first demonstrated using the alkaline sucrose gradient velocity sedimentation technique. Extreme alkaline conditions (pH 12) are used to split the DNA lengthwise into its constituent strands. The cells are layered onto a specifically prepared sucrose solution and centrifuged at high speeds. The DNA strands sediment at specific velocities which can be related to their molecular weight. If the DNA has been irradiated and a number of breaks induced, then the lengths of the strands (and hence their molecular weight) will be less than the unirradiated control DNA. SSB can also be determined using the alkaline elution technique.

It has been shown that the number of SSB is linearly related to the radiation dose over a very wide range, from less than 0.2 Gy to 60,000 Gy. The efficiency of induction of SSB varies with a number of biochemical factors, but recent measurements give values for the average energy required of between 10 and 20 eV per break for low LET radiation. Under normal conditions a significant proportion of SSB are induced via a mechanism involving the `OH· radicals of water. This has been proved using chemicals known as 'OH· radical scavengers'. The number of SSB induced by radiation in oxygenated mammalian cells is 3-4 times that found in cells irradiated under hypoxic conditions.

The repair of SSB in mammalian cells is very rapid and efficient. It is thought to occur by a mechanism called `excision repair'. This involves the excision of the length of nucleotide strand containing the defective piece of DNA and uses the complimentary (undamaged) strand as the template for the resynthesis of a new length of DNA. The process is enzymatically controlled and temperature dependent, with no repair occurring at $0^{o}C$. The first step in the process is the recognition of the site of the distortion or disruption when an incision is made by endonuclease enzymes (figure 2.10a). The incision is followed by the complete excision of the lesion and sometimes a wide area around it. The gap produced is then filled with new nucleotide bases by the action of DNA polymerases using the opposite and undamaged as template (figure 2.10c). When this `repair replication' is complete the new section of DNA is linked to the intact DNA by enzymes called ligases (figure 2.10d).

The most important of radiation-induced lesions, with respect to cell killing or mutation-induction is the DSB, which can be formed either by a single ionizing event or

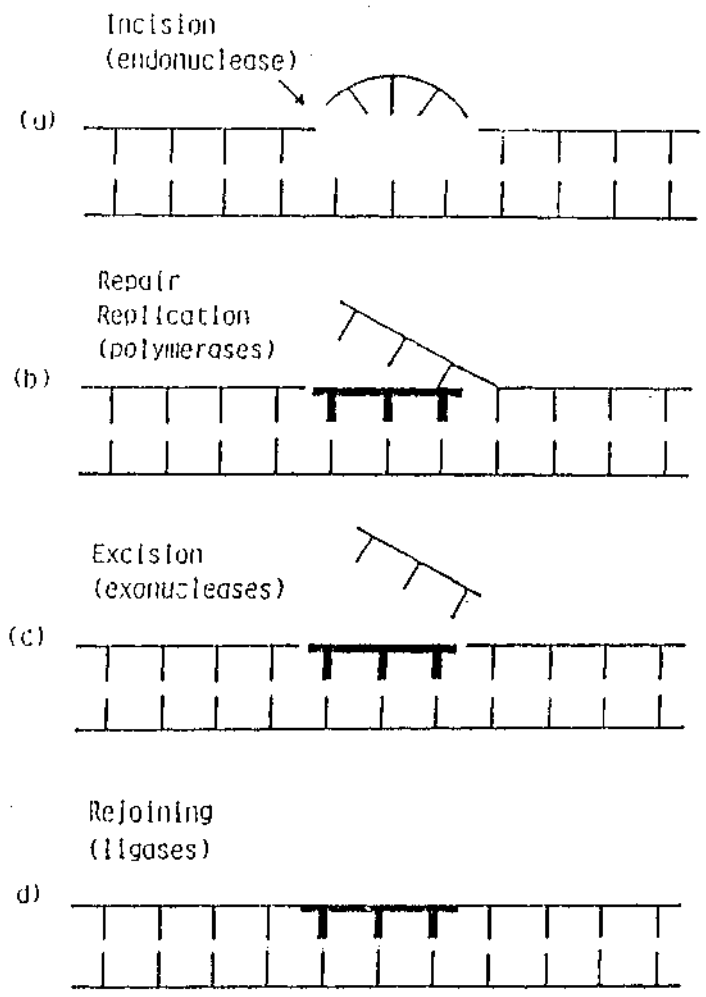


Figure 2.10: Excision repair mechanism for DNA single strand breaks.

(After Coggle, 1983).

by the coincidence of random single strand breaks on the complimentary strands. Measurement of DSB has been made by neutral gradient sedimentation methods. The neutral biochemical conditions do not split the DNA molecules into single strands and the number of DSB is measured by the decrease in the average molecular weight of the DNA pieces. However, the technique is only capable of distinguishing between relatively small pieces of DNA (1 - 3.0 x 10^9 Dalton molecular weight) and so relatively large radiation doses have to be used. The neutral elution, DNA unwinding technique as well as pulsed field gel electrophoresis have also been applied for DSB measurements.

The repair of DSB is conceptually difficult to imagine. The nucleotide base sequence may not be available The nucleotide base pairing may not be available on either strand and there may be no continuity between the two `free ends'. However, there is irrefutable evidence that in yeast, bacteria and mammalian cells that radiation-induced DSB can be repaired (Kiefer, 1990), but the methods used can only detect whether the free ends of a broken DNA molecule have joined together and cannot indicate whether the original base pairing of the genetic code has been re-established. The methods cannot detect the presence of the so-called `misrepair' or `error-prone repair' which might be a cause of significant genetic damage. A theoretical model has been proposed by Resnick (1976) to explain how radiation-induced DNA DSB might be repaired. According to the model (see figure 2.11), the repair starts by the enzymatic excision of parts of a single strand for each of the broken ends, leaving single-stranded pieces. These single strands are then imagined as associating with homologous and undamaged strands in such a way as to allow for recombinations. The undamaged strands have to be cut by an endonuclease in two places and a reciprocal exchange of the DNA helices occurs. The recombination will leave two small and larger single-strand gaps. The small one can be sealed by ligase

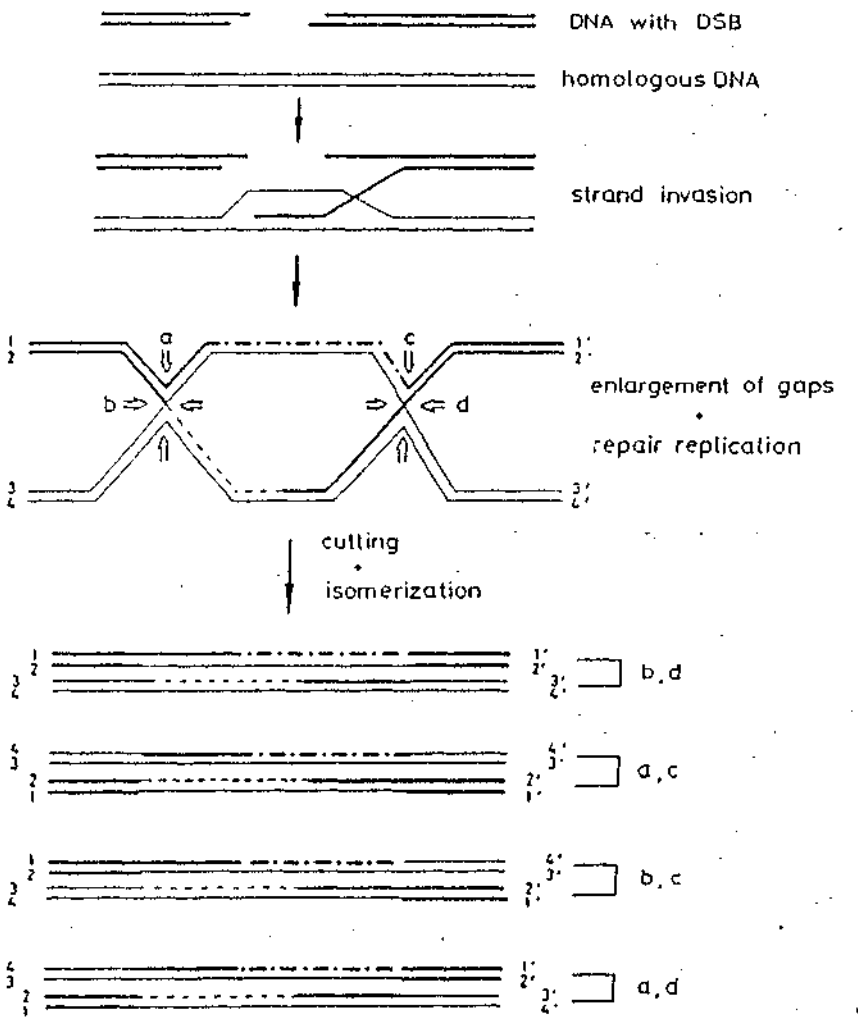


Figure 2.11 A scheme for DSB repair by recombination in yeast.

(After Kiefer, 1990).

enzymes and the larger gaps by the repair replication. It must pointed out that there is as yet no experimental evidence to prove or disprove the outlined theory (Coggle 1983). There is some controversy regarding the dose-response for DNA double strand breakage by ionizing radiation. While some investigators using the sedimentation assay report a linear response, others using the neutral filter elution method report a linear-quadratic dose response. However, more recent studies have shown that the response is a linear one (Akpa *et al.* 1992, Löbrich *et al.* 1993b).

Base damage to the pyrimidine and purine bases of DNA has, for some time now, been recognized and measured. Such damage which is found to be linearly related to dose, is thought to arise via interaction with aqueous free radicals such as OH·. Radiation-induced base damage is more frequent in biological cells than single and double strand breaks. The excision repair mechanism appears to be responsible for the rapid and efficient removal of the damaged bases. In prokaryotes, unrepaired base damage is an important determinant in survival.

2.7.1 Techniques for double strand break measurement

The main techniques, currently in use, for DSB measurement include sucrose velocity sedimentation and neutral filter elution. The velocity sedimentation method (discussed in section 2.7), provides an absolute measure of DNA DSB since the system can be readily calibrated using DNA standards of known molecular weight. It has come to accepted as the `golden standard' used to calibrate other systems. The chief criticisms of the sucrose sedimentation method are its low sensitivity, probably due to the high background of breaks from DNA shearing resulting from cell manipulation after lysis, and the anomalous effects in cells with large genome (Whitaker *et al.*, 1991). In filter elution method-first described by Bradley and Kohn (1979), cells are lysed directly on a

filter and a buffer solution is pumped through the filter to elute DNA. Fractions of eluted DNA are then collected over a period of time (usually, about 16 hours) and the amount of strand breakage is deduced from the rate of DNA elution. Although this technique is highly sensitive, too many extrinsic factors affect the DNA elution rate: pH of lysis (Evans *et al.*, 1987, buffer composition (Koval and Kazmar, 1988), cell cycle (Okayasu *et al.*, 1988; Sweigert *et al.*, 1988) and lysis condition (Bradley and Kohn, 1979). Further, it has been stressed that this method does not measure DSB but only the `swelling of the DNA gel' which is influenced not only by DSB but also by damage to the chromatin (Wlodek and Olive 1990). Also, results obtained by the filter elution method have caused some controversy as to the interpretation of the dose response and repair kinetics, which are in conflict with those obtained by sedimentation methods (Blöcher, 1990). Both sedimentation and elution methods, in the main, detect a decrease in the average molecular weight of DNA from an organism due to lesions induced by various agents. These methods are either very laborious or ambiguous (Blöcher *et al.*, 1989). Besides, they often involve radioactive labelling of the DNA, limiting their applicability to established cell lines and excluding non-growing cell populations.

In recent years, electrophoretic techniques have gained much attention. The application of the pulsed field technique in DNA DSB determination in yeast was pioneered by Mortimer and co-workers (Contoupoulou *et al.* 1987, Cook and Mortimer, 1991).

2.7.2 The electrophoretic technique

Molecules of RNA, DNA and protein can be separated according to size by electrophoresis. This technique depends upon the fact that dissolved molecules in an electric field move at a speed determined by their charge-to-mass ratios. For example, if

two molecules have the same mass and shape, the one having the greater charge will move faster toward an electrode. Many successful techniques of electrophoresis are in general use. For example, paper electrophoresis is widely used for small molecules such as amino acids and nucleotides. A sample is deposited in a small spot on a filter paper (or other porous membrane); the paper is then soaked with a conducting solution and move in the plane of the paper at a rate related to their charge.

Nucleic acids in solution generally have a negative charge at neutral or alkaline pH because of the ionization of their phosphate groups. In principle, therefore, if DNA fragments of different lengths are placed in a gel matrix in an electric field, they will migrate towards the anode, and their mobility will depend on their size. However, nucleic acid molecules consisting of long chains have almost identical charge-to-mass ratio, no matter their lengths, because each residue contributes about the same charge and about the same mass. Also, many proteins that differ in shape and mass have almost equal charge-to mass ratios. Therefore, if electrophoresis of nucleic acids and proteins were simply carried out in solution or on paper as is done for small molecules, little or no separation of molecules of different lengths would be achieved. To get round these difficulties, molecules are now most commonly subjected to electrophoresis not in a liquid solution but in the form a gel, a semisolid material made of agarose (a plant polysaccharide) or of a synthetic polymer such as polyacrylamide. The size of the pores in such gels limits the rate at which molecules can move through them. Nucleic acids that have identical charge-to-mass ratios migrate slowly through the pores of the gel. Even very long nucleic acids chains (containing from 10,000 to 20,000 residues) that differ in length by a few percentage points can be separated from one another, and each individual

can be isolated in mixtures containing chains of 500 nucleotides or less (Rickwood and Hames, 1982).

Protein chains can also be separated according to length. Both before and during electrophoresis, the proteins are continuously exposed to the detergent SDS (sodium dodecyl sulphate, a common commercial cleaning agent found in toothpaste). Approximately one molecule of detergent binds to each amino acid. At neutral pH, the detergent is negatively charged so that the adjacent negatively charged SDS molecules repel each other, and forces the proteins with bound detergent into rodlike shapes endowed with similar charge-to mass ratios. Proteins in this state are said to be denatured. As with nucleic acids, chain length (which is equivalent to mass) is the determinant factor for the separation of proteins during electrophoresis through polyacrylamide gels containing SDS. Again, even the chains that differ in molecular weight by less than 1 percent can be separated (Maizal, 1971; O'Farrell, 1975).

Over the past few years, pulsed field gel electrophoresis (PFGE) has been developed for the resolution of large DNA molecules. Since it was first described by Schwartz and Cantor (1984), a number of variations of PFGE have emerged; these include orthogonal field alternation gel electrophoresis - OFAGE (Carle and Olson, 1984), field inversion gel electrophoresis - FIGE (Carle *et al.*, 1986; Dawkins *et al.*, 1987) and transverse alternating field gel electrophoresis - TAFE (Gardiner and Patterson, 1988; Stewart *et al.*, 1987). Intact chromosomal DNA molecules have been resolved from a number of lower eukaryotes including *Saccharomyces cerevisiae* and several parasitic protozoa (Kemp *et al.*, 1985). Electrophoretic methods have also been used in the separation of large human chromosomal DNA fragments generated with restriction enzymes that cleave the DNA infrequently. However, the problem with these systems, whose main

underlying difference is the configuration of the electrodes, is that the electric field is not uniform. The result is that the DNA migrates in such a manner that comparison of multiple samples across the gel becomes difficult (Chu *et al.*, 1986). This limitation can be overcome by using a contour-clamped homogeneous electric field (CHEF) system. The CHEF configuration , first described by Chu *et al.* (1986), uses multiple electrodes arranged along a polygonal contour and clamped to predetermined electric potentials, to produce a homogeneous field at every point inside the contour. The method has been used to resolve the chromosomes of the yeast *Saccharomyces cerevisiae* (Carle and Olson, 1984) as well as the chromosomes of the malarial parasite *Plasmodium falciparum* (Kemp *et al.* 1985, van der Ploeg *et al.* 1985) and other organisms. The chromosome sizes resolved are in the size range of 0.2 to 5.0 Mb.

2.7.3 Detecting the DNA migration

After separation the DNA or RNA is detected by ethidium bromide staining, or, if the samples are radioactively labelled, by autoradiography. The smallest amount of non-radioactive DNA which can be detected by ethidium bromide is less than one nanogram. The complex which formed between ethidium bromide and DNA has a fluorescence excitation spectrum with a maximum at 250 nm. In many experiments the samples are subjected to further analysis. The gel can be blotted, for example, to transfer the DNA or RNA molecules onto a membrane where they will be available for subsequent hybridization with radioactive probes; or stained bands of interest can be cut and the nucleic acid recovered for further studies.

2.7.4 DNA migration pattern in pulsed field gel separations

DNA molecules appear to be resolved into four zones on PFGE gels, most easily observed in separations of lambda concatemers where the size change between adjacent

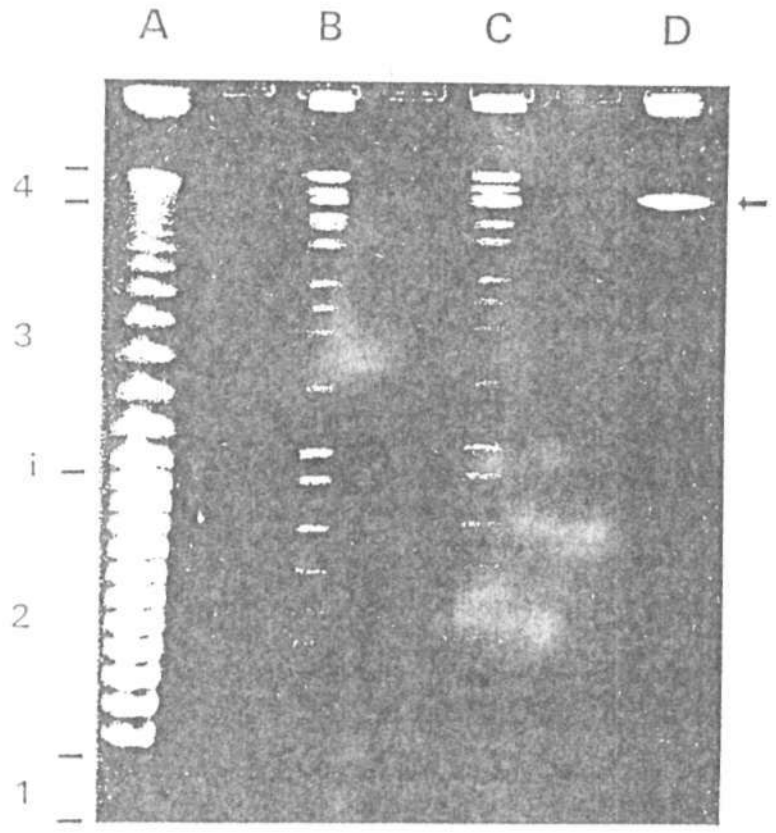


Figure 2.12: The four zones of DNA resolution.
(After Gemmil, 1990).

bands is always a fixed monomer size (figure 2.12, lane A). Zone 1 contains molecules below 30 to 50 kb that are resolved by sieving. Zone 2 contains multimers separated by size in a linear fashion, but with a slightly decreasing separation as band size increases. At a critical size (marked i in figure 2.12) the band compression reverses and separation between adjacent bands increases markedly; this position marks the inflection point (i) between zones 2 and 3. Zone 3 represents a region of enhanced resolution with the largest separation between adjacent lambda concatemers. Following this region of hightened separation, bands rapidly come closer until the compression zone (zone 4) is reached. The compression zone contains a collection of molecules small enough to enter the gel under the specific conditions of the electrophoresis but too large to be resolved. Unusual migration behaviours are associated with this zone (Gemmill 1990).

2.7.5 Shift of DNA between the four zones

As parameters of separation are changed , the size ranges of molecules within these zones are altered. At longer pulse times or higher field strengths, more molecules in the compression zone enter into the resolved zones (zones 1, 2 and 3). Changes in pulse time and field strength can cause larger molecules in the compression zone to become progressively trapped or to remain at the well or become smeared between the well and compression zone. A good understanding of the interrelationship between pulse time and field strength and the position a particular DNA molecule will occupy on a pulsed field gel is important for effective utilization of the technique.

2.7.6 The parameters governing PFGE separations

A large number of variables are known to affect the migration during PFGE. These variables include pulse time, electric field and shape, agarose type, agarose

concentration, temperature, buffer composition and ionic strength, DNA loading and the presence of DNA binding agents such as ethidium bromide. Thus, uncontrolled changes in one parameter can seriously hamper a correct appropriate interpretation of results.

2.7.7 Unusual migration characteristics of DNA in PFGE

The compression zone contains molecules that can enter the gel but are not separable with the given parameters. When yeast chromosomes are employed, this zone normally falls above the largest chromosomes present in the sample. The zone has a rather complex microstructure in which the smaller molecules appear 'stacked' in order from smallest to largest until a certain critical size is reached. Beyond this point, migration rate increases again with larger molecules migrating ahead of smaller ones in the zone. This mobility inversion continues until trapping dominates and retains larger molecules at the origin of the lane.

Non-monotonic separation on PFGE gels has been demonstrated by a series of two-dimensional separations by Löbrich *et al.* (1993a) for the two largest chromosomes (IV and XII) of the yeast *Saccharomyces cerevisiae.*

Trapping of large molecules in zero mobility states occurs for yeast DNA samples separated with conditions which can resolve all the 16 chromosomes. Another unusual migration behaviour is band spreading. This often occurs for large molecules (above 1.5 Mb) and can cause difficulties in the interpretation of results, especially when they are generated by Southern blot or hybridization.

2.7.8 Theoretical models

Direct observations in the light microscope indicate that DNA moves through agarose by oscillating among a complex repertoire of configurations. A number of

theories have been proposed (Levene 1992) which attempt to explain one or more electrophoretic feature. An early model assumes that DNA moves through the gel in fully extended conformations and that when the field is oriented by an angle more than 90° the DNA begins moving in the new direction led by what was formerly its back end. This simple model successfully predicts the separation of large DNA molecules in a pulsed electric field. However, it incorrectly predicts that the upper size limit of resolution is accompanied by zero DNA mobility.

A second model, the reptation model, pictures the motion of the DNA as a 'reptating' chain that crawls snakelike through a 'tube' in the gel in response to the electric field. As the DNA moves forward its leading end creates additional segments in the tube, each forward step being intrinsically in a random direction but with a bias in favour of the electric field direction. The reptation model is successful in predicting that continuous field will fail and pulsed fields will succeed in separating large DNA and that in a pulsed field the size limit of separation should increase proportionally to pulse time and is associated with a non-zero mobility. It also successfully predicts the phenomena of lateral band spreading and mobility inversion.

A third model, the chain model, views the DNA as a flexible chain moving through a lattice of obstacles. The chain is not constrained to move a tube but is free to adopt any configuration as it interacts with obstacles that represent the gel. Thus the DNA moves through a variety of extended and tangled conformations as it migrates in response to the field. Like the reptation model, the chain model successfully predicts that the separation of large molecules requires a pulsed field. However, chain model calculations require the power of supercomputers and have not yet addressed the phenomena of lateral band spreading and mobility inversion (Chu 1991).

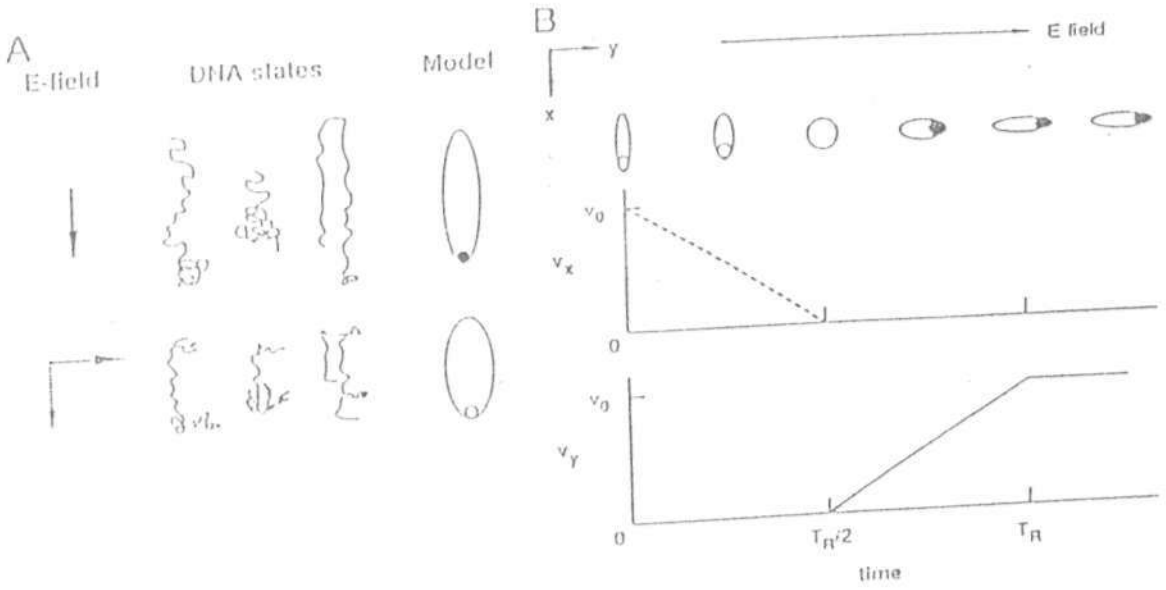


Figure 2.13: Bag model - the different DNA configurations as it passes through a gel. (After Chu, 1991).

The recently developed bag model (Chu 1991) combines aspects of both the reptation and chain models (see figure 2.13). Here the DNA is pictured as a deformable bag of a specific size and orientation, with three basic properties:

(i) Limiting velocity: In a continuous electric field, the DNA bag moves with a limiting velocity independent of its size.

(ii) Orientation: In a continuous field , the bag assumes an elongated shape with an orientation aligned with field direction and a defined leading end.

(iii) Memory: When the field is oriented, the bag responds by undergoing gradual deformation with a reorientation time that increases with size, while retaining a time-dependent memory for its previous orientation.

The bag model does not treat any interaction between the DNA and the agarose, but supplies a universal curve including anomalous migrations which can be compared with experimental data.

2.8 Measurement of Radiation Dose

The direct measurement of the energy absorbed by biological material is very difficult; consequently radiation doses are often based on ionization effects in air using ionization chambers of varying types. Radiation produces ionizations in air and other gases and the ionization current can be measured by applying a potential difference between the two electrodes in a gas-filled chamber. The resulting electric current between the two electrodes is a measure of the amount of ionization the radiation has produced in a definite volume of the ionization chamber. By conversion, and due allowance for ion recombination within the chamber, the current reading may then be used to indicate the absorbed dose in Gray.

Since neutrons are uncharged they do not directly ionize matter and indirect means have to be used. Fast neutrons can be detected by causing them to interact with hydrogen atoms and it is the recoil of the protons which ionizations. So, fast neutron monitors have a hydrogenous material, for example polythene, incorporated in their volume. To measure thermal neutrons, ionizations chambers filled with either boron trifluoride (BF_3) gas or lined with a layer of boron are used. The capture of neutrons by the boron involves the emission of α particles and it is the latter that cause the detectable ionization currents. The use of ionizations in air is the most important dosimetric method, but there are other systems some of which are briefly described below.

Thermoluminescent dosimeters: When lithium fluoride and many other crystals are heated after being exposed to radiation they emit light. The process is called "thermoluminescence". The absorption of radiation causes free electrons to be trapped in the lattice imperfections in the crystalline structure. These trapping levels lie between the valence and the conduction band. If the crystal temperature is raised the electrons are excited from the trapping levels to the conduction band and then return to the valence level (the stable state) with the emission of light the intensity of which is a measure of the dose received by the crystals. Thermoluminescent devices respond over a wide range of doses (10 μGy - 1 kGy) of X-rays, γ-rays, electrons and protons. Thermolunescent devices may be used as powders in capsules or sachets or used as small rods or discs which can be annealed after one exposure and used over and over again. Thermolunescent dosimeters (TLDs) are widespread in laboratories for personnel monitoring.

Photographic Films: Photographic emulsions consist of silver halide crystals or grains dispersed in gelatin. Radiation absorbed in an individual grain forms a latent image, and

the chemical action of development reduces the grain to silver. The blacker the film is, as measured by densitometry, the more dose it has received. Film badges are the main form of personnel monitoring in radiation protection.

Scintillators: Scintillation detectors convert the radiation energy of ionizing particles into pulses of light. The size of a pulse is proportional to the energy deposited in the crystalline or liquid scintillant. Most scintillators have to be calibrated against other dosimetric devices because there is hardly a linear relationship between the dose and the pulse of light which is detected by photomultipliers and recorded electronically.

Optical dosimeters: Certain types of glasses and plastics become increasingly opaque with increasing radiation dose.

Solid state counters: Some semi-conductors show an altered electric conductivity during exposure to radiation. This method is analogous to the ionization chamber measurement, except that the current is flowing in the solid semi-conductor crystals and not in the gas of the ionization chamber.

Chemical dosimetry: Ferrous sulphate dosimetry is an accurate method of absolute dosimetry. Ferrous sulphate is converted to ferric sulphate when irradiated. Chemical titrations with potassium dichromate or ceric sulphate may be used to determine the amount of ferric ion present. Alternatively, the ferric ion yield may be assayed using an ultraviolet spectrophotometer, measurements being made at 304 nm. The yield is proportional to the dose received.

CHAPTER THREE

3.0 MATERIALS AND METHODS

3.1 Yeast Strain

Cells of the diploid yeast *Saccharomyces cerevisiae* strain 211*B were used in the experiments. The strain, which was constructed by Brendel and Fäth (1974), is homozygous for the tempI-3 marker conferring auxotrophy for 2'-deoxythymidine (5'-dTMP) (Frankenberg-Schwager *et al.* 1979). It is a petite lacking mitochondrial DNA and was generously given to us by Dr. M. Frankenberg-Schwager GSF, Frankfurt. The cells were grown to stationary phase at 30°C in a growth medium consisting of the following: Bacto agar 20 g/l, Glucose 20 g/l, Yeast Nitrogen Base w/o amino acids 6.7 g/l, Cassamino acids w/o vitamins 2 g/l, plus 2 ml/l of the following: 0.01 M 5'-dTMP, 50 mg/ml Isoleucine and 50 mg/ml Leucine.

For the DSB repair experiments, the mutant strain rad 54-3 was used. The cells are designated X754.6D x X754.3B and are homozygous at the rad 54 locus. It originated from M. Budd and was given to our laboratory by M. Frankenberg-Schwager of Göttingen, Germany. Cells were grown on succinate agar (1% yeast extract, 2% bacto-peptone, 2% sodium succinate, 2% agar) (Frankenberg *et al.* 1984).

3.2 Irradiation Conditions

3.2.1 X-ray and Alpha irradiation

The X-ray source used is a spectral analysis tube type FA 100/3 with tungsten anode and beryllium window (Müller, Hamburg). The tube was operated at a constant condition of 80 kV, 30mA with no additional filters for the soft component. Dose calibration was done by chemical (Fricke) dosimetry.

Chemical (Fricke) dosimetry

Fricke dosimetry is based on the oxidation of an aerated ferrous sulphate solution by radiation. To make the Fricke solution, 0.392g of ferrous sulphate and 0.058g of sodium chloride are dissolved in 12 ml of 0.8N sulphuric acid and then made-up to one litre with triply distilled water (Fricke and Hart, 1968). Dose rates were determined by irradiating 3ml aliquots of the Fricke solution for known durations. The optical density of the irradiated solution was then measured at 304 nm (the wave length at which the optical absorption is less than 0.05% of that of the ferric ions) using as a control, the unirradiated solutions. At 25°C the G-value of the ferric ions is 15.5 and the molar extinction coefficient of ferric and ferrous ions are 219.0M^{-1} cm^{-1} and 1.0M^{-1} cm^{-1} (at 304nm) respectively. Under the above stated conditions, the dose (D) according to Fricke and Hart (1968) is given by

$$D(Gy) = 2.756 \times 10^2 \times Dp \quad \text{.....(3.1)}$$

where Dp is the difference in optical density between the irradiated solution and the control.

The dose-rate is therefore calculated as follows:

$$X-ray\ dose\ per\ unit\ time = \frac{2.756 * 10^2 * D_p}{Irradiation\ time} \quad \text{.....(3.2)}$$

A plot of the differences in optical density as a function of irradiation time was made and from the slope, the dose-rate was determined. The dose rate was 132 Gy/minute.

Alpha Irradiation was performed using an ^{241}Am source (Amersham). The α-source (sp. act. 70 Bq/m^2) covered a 0.047 m diameter and rotated during irradiation. The cells were exposed in monolayer on a filter 0.0085 m from the surface of the α source. The mean residual energy of the α particles at the exposure position was 3.5 MeV, corresponding to a mean L_{100} of 65 keV/μm and can therefore penetrate the yeast cells exposed in monolayer. The dosimetry was performed as described by Bertsche (1977). The dose rate was 23.4 Gy/min. Briefly, the α-source is placed in an irradiation box at a fixed distance from the sample and the fluence rate, ϕ, at the exposure position measured with a solid state counter. This is then converted into "dose", D, by using the expression:

$$D = (L.\ \phi)/\rho \quad \text{.....(3.31)}$$

Where L is the LET of the α-particles = 65 keV/μm

and ρ is the density of the biological material = 1000 kg/m^2

All irradiations were done in open air and under normal atmospheric pressure (1.013 Newton/m^2); X-irradiation in solution, α-irradiation on membrane filters.

3.2.2 Heavy ion irradiation

The UNILAC accelerator of the *Gesellschaft für Schwerionenforschung* (GSI) was used as a source of heavy ions (figure 3.1 shows the biological working station at accelerator site in Darmstadt, Germany). It is a two-stage linear accelerator. The first part accelerates the ions to a specific energy (total energy divided by the ion mass) of 1.4

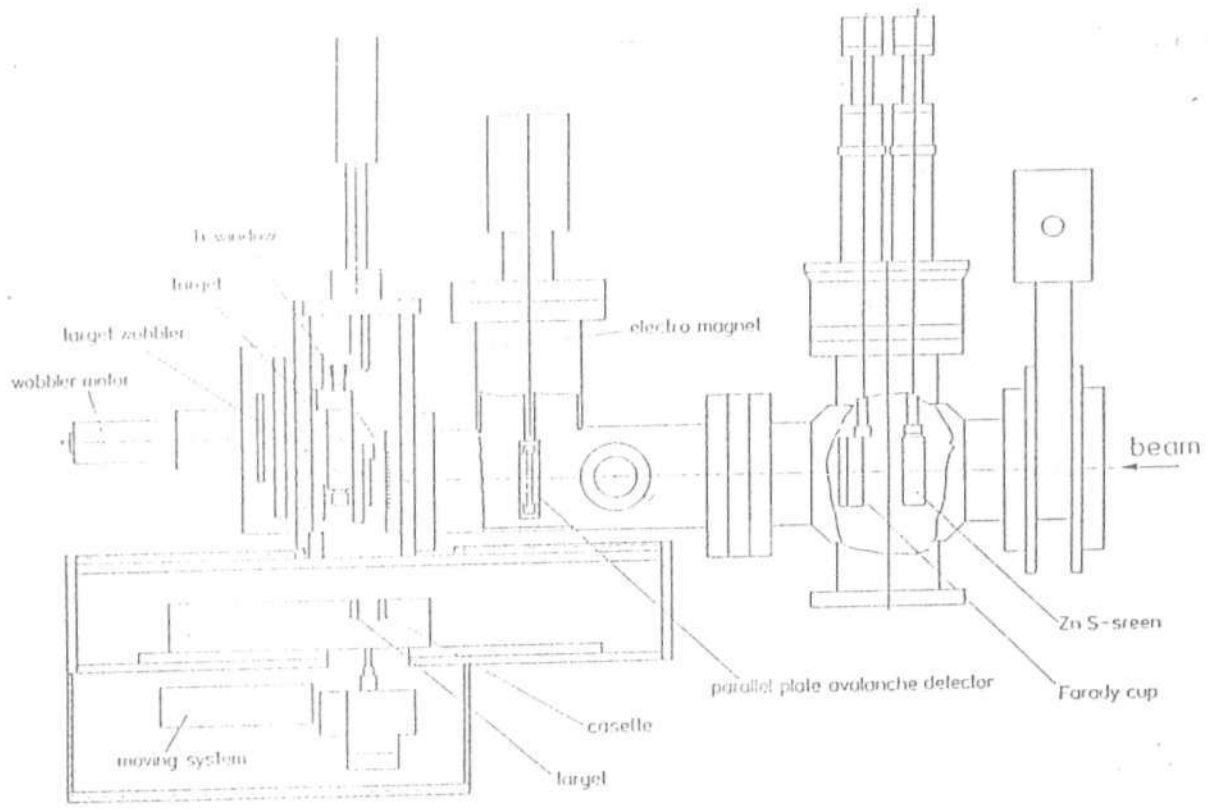


Figure 3.1: The biological working station at GSI, Darmstadt, Germany. (After Kraft, 1987).

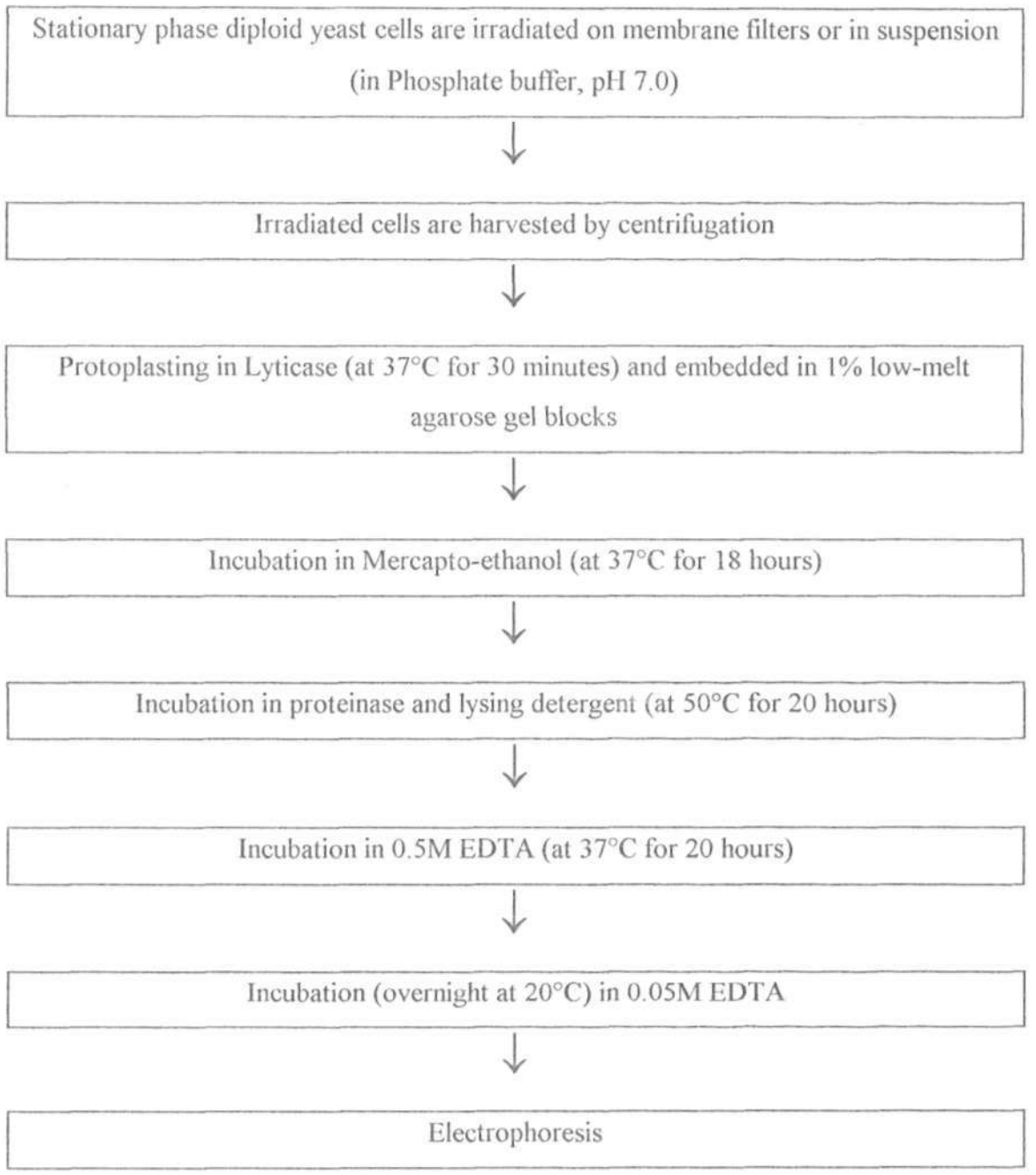


Figure 3.2: **Sample preparation for DSB meassurement**

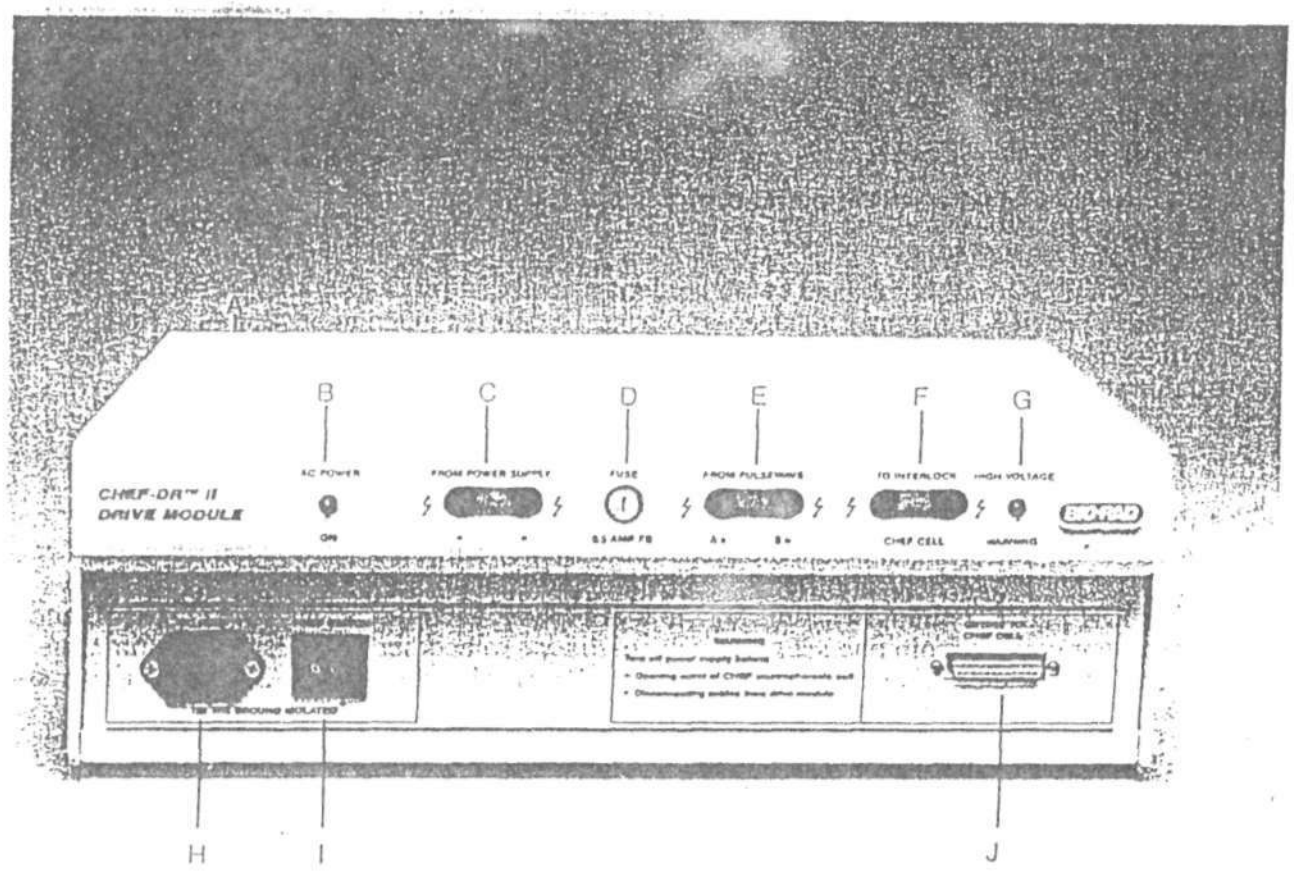


Figure 3.3: The CHEF-DR II drive module.
A. Drive module power switch; B. AC power indicator; C. Leads from power supply; D. 0.5 Amp fuse; E. Leads from pulsewave 760 switcher; F. Interlock to CHEF-DR II electrophoresis cell; G. High voltage indicator light.

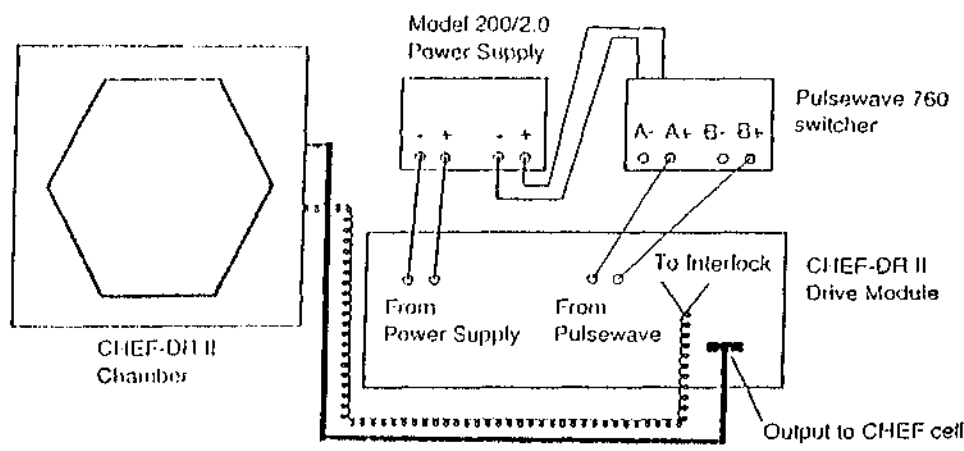


Figure 3.4: Wiring of the CHEF-DR II system

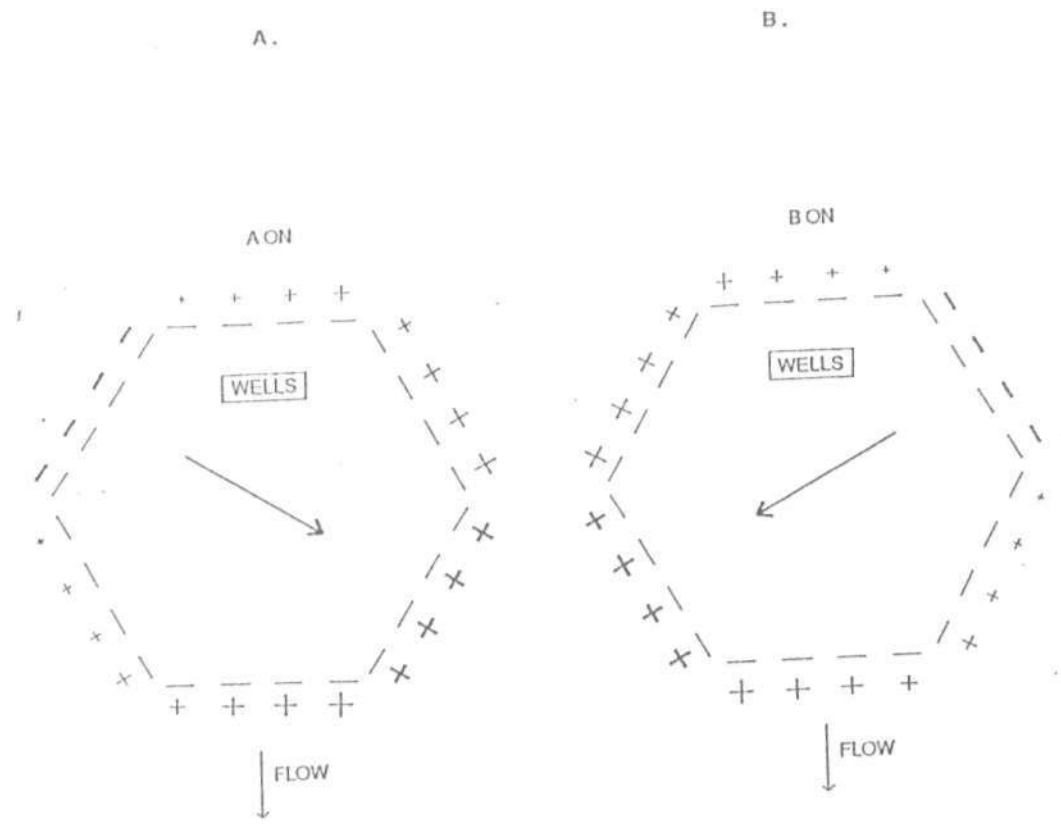


Figure 3.5: Voltage clamping by the CHEF-DR II system

MeV/u. By colliding with a stripper-foil they loose large fractions of their electrons, yielding a higher effective charge, so that they can be brought up to final energies of up to 20 MeV/u by the second stage (Angert and Smeltzer 1977). Cellular samples were exposed on membrane filters, in a special gas-tight enclosure with a remote-controlled sample-changer (Kraft *et al.* 1980). The ion current is monitored by the measurement of secondary electron emission from a carbon foil mounted upstream in the beam line close to the exit window. Fluence determinations were performed by exposing glass plates at the site of the window; after irradiation the glass plates etched for 1-2 minutes with each particle track developed as a small hole of 0.4 μm diameterand counting the tracks after etching. The number of tracks is then determined with a scanning electron microscope (for details, see Fleischer 1965). Figure 3.2 is a flow diagram showing the various steps in the sample preparation process. Figure 3.3 shows the CHEF- DR II drive module; figure 3.4 shows the wiring of the system and figure 3.5 illustrates the voltage clamping.

3.2.3 DNA preparation and gel electrophoresis

A modified form of the method of Schwartz and Cantor (1984) was used to prepare the DNA for electrophoresis. Briefly, after irradiation (5 x 10^7 cells per sample) about 10^8 cells were pelleted (3000 rpm at 4°C) and washed twice in 0.05 M EDTA, pH 8. The cells were then protoplasted in Lyticase (Sigma) for 20 minutes at 37°C and encapsulated in low melt agarose blocks after which they were incubated in LET buffer (0.5 M EDTA pH 8, 0.01 M Tris pH 7.5, 7.5% 2-mercaptoethanol) for 20 hours at 37°C in NDS buffer (0.01 M Tris pH 7.5,).5 M EDTA pH 8, 1 % Laurylsarcosine, 1 mg/ml Proteinase K) for 19 hours at 50°C. Preliminary experiments have demonstrated that the lysing conditions used are optimal for the DSB measurements. Finally, the plugs were cut to pieces containing about 2 x 10^7 cells each.

A CHEF II PFGE system (Bio-rad) was used to separate the yeast samples. Electrophoresis in 1% pure grade agarose (Bio-rad) was carried out in 0.5 x TBE buffer (0.045 M Tris, 0.045 M Boric acid and 1 mM EDTA) with each run consisting of two modes In first mode an initial and final switch time of 60 seconds was used with a run time of 15 hours, while in the second mode the initial and final switch times were 90 seconds with a run time of 8 hours. The run-temperature was 14^{o}C in both modes.

3.2.4 System and Processing

The ethidium bromide-stained gel is placed on top of a UV-transilluminator (Bachofer Transilluminator 312 nm, Fa. Bachofer, Reutlingen) whose filter has the maximum of transmission at 312 nm. A glass plate is placed on top of the transilluminator filter to define the position of the gel.

The fluorescence light passes through some optical glass filters (Fa. Schott, Mainz) before input into the camera to separate it from the UV and other undesirable light. There are first two glass filters for the absorption of heat (KG1 and KG3) and then an orange glass (OG590) and a blue-green glass (KG1BG38). The maximum of transmission of these 4 filters is at 570 nm with a transmission grade of 45 % while the transmission grade at 530 and 640 nm, respectively is only 10 %. Thus, the filter system is appropriate for the transmission of ethidium bromide fluorescence light, with a maximum at 590 nm.

The fluorescence is recorded using a tube camera Hamamatsu C2400-08 (Hamamatsu Photonics Deutschland GmbH, Herrsching) along with the control unit. A lens in front of the camera forms an image of the gel. The video output of the camera is in the form of standard CCIR. In front of the sense head is a photon amplifier based on

the principles of a MCP which can be steered by the control unit. An electronic amplifier positioned behind intensifies the signals for further use and can also be steered by the control unit. The analogue image data from the camera is transformed by a 512 x 512 x 8 bit frame grabber (Leutron LFS-AT image processing card; Leutron Vision AG) into 256 different values. The images in the digital form can be displayed at a resolution of 518 x 480 pixels on a high resolution NEC Multisync 2D colour monitor (with a Trident 8800 VGA 512 kB graphic card) or stored on magnetic disc or tape for later analysis. Each gel picture requires memory space of 262144 B. A second monitor is used for the display of the text menu. Figure 3.6 is a schematic representation of the video imaging system.

Since the UV-transilluminator does not supply a homogeneous picture (it consists of 6 tubes) a luminescence plate was used as a homogeneous source for the corrections described below. This was achieved with a phosphorescent foil (W. Maier GmbH + Co, Villingen-Schwenningen) fixed on top of a glass plate.

3.2.5 Recording the gel picture

The software (written in Pascal and Assembler) of the electronic imaging system provides different modes for the recording of a picture. The LIVE-mode is used for the representation of the momentarily transferred image while the FREEZE-mode shows a statue of the finally transferred image. One problem concerning the use of tube cameras is the relatively high amount of rustle because the integration time for one picture is fixed and cannot be increased as with CCD-cameras. A possibility to circumvent this problem is the oversampling of many pictures. With the command SELECT OVERSAMPLING FREQUENCY, up to 255 pictures can be added to average out the rustle. However, the choice of a high number is only meaningful if the intensity remains constant during the

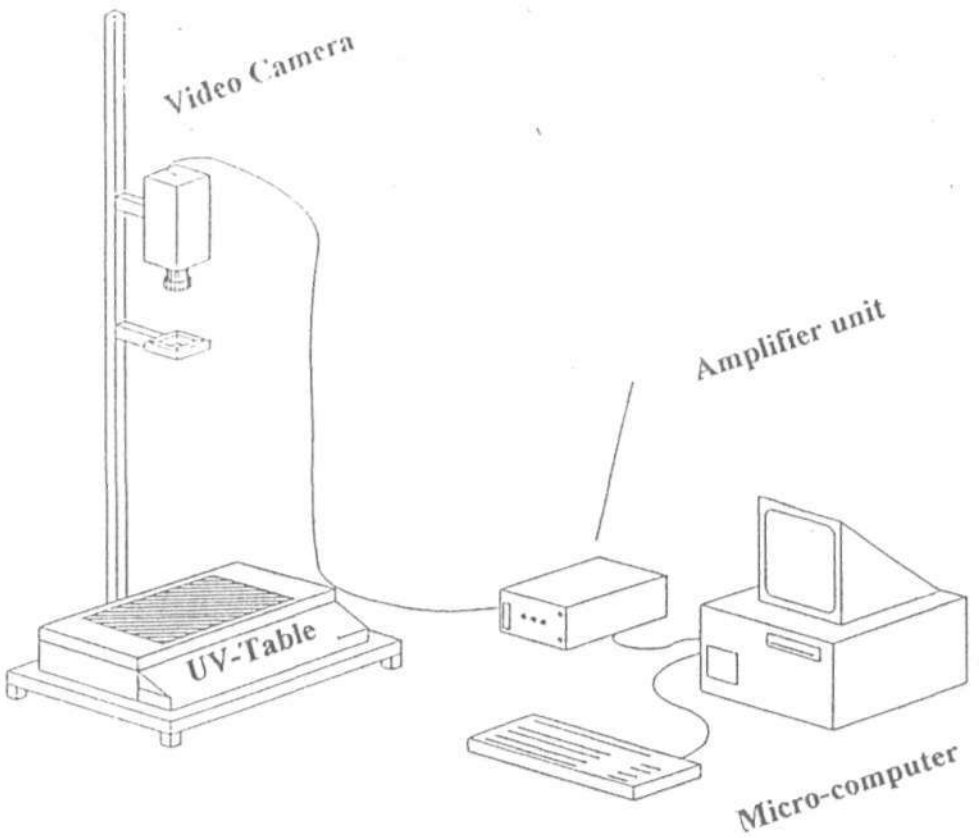


Figure 3.6: The video imaging system.

time which is needed for the recording of all the pictures (about 3 pictures per second can be taken). To study the decrease of fluorescence with time the MAKE MOVIE-mode can be applied. It permits the recording of pictures in defined time intervals (the shortest time which can be used is 1s). Another useful command for the recording of images is GRID ON/OFF. With that command it is possible to display a grid at the monitor to achieve a positioning of the gel in agreement with the x- and y-direction of the computer pixels.

3.2.6 Corrections and Evaluation

The software for the correction and evaluation of the pictures again written in Pascal and Assembler consists of three parts. First of all the image data have to be corrected with regards to background and shading effects. A shading is present in each optical system due to effects like vignetting and means that a homogeneous signal is not detected with constant intensity values. This effect is strong if a tube camera is used. Beside the optical shading, a camera specific shading is present due to the electron beam inside the tube - the sensitivity is not uniform for all pixel detector elements in the image plane. Pixel detector elements positioned relatively far away from the centre of the image plane get loaded by the electron beam for a shorter time than pixels close to the centre. Besides that the electron beam is focussed at the centre of the image plane, the pixels at the borders are reached with a defocused beam. These effects lead to a decrease of sensitivity with increasing distance from the centre.

The first part of the correction and evaluation software is the programme "KOR". It displays the image in two different colours, blue for intensities of pixel elements less than a defined intensity border and red for the others. The intensity border can be changed in steps of one or ten pixels. If the border intensity is 0 all pixels have the colour red and if

it is 255 all are blue. This kind of display becomes very useful for the performance of the corrections.

For an exact quantitative evaluation the background fluorescence, due to unbound ethidium bromide, has to be subtracted from the gel picture. The best way to achieve this is the subtraction of a gel without DNA which was stained and destained along with the gel that contains the DNA. Such a subtraction procedure performed with commands of the program KOR lasts only few seconds. A necessity is that both gels are recorded with the same conditions of the camera (with the same sensitivity of the photon amplifier and the electronic amplifier). Another possibility concerning the background subtraction is the construction of a homogeneous image with KOR and the subtraction afterwards. But this can easily produce errors because a homogeneous background due to unbound ethidium bromide will not result in a homogeneous image (because of the shading effect), which is in that case used for background subtraction. Thus, this second background subtraction method is only useful if the DNA is extended over a limited area that the shading is negligible. Figure 3.7 is a schematic illustration of the different steps in gel processing after electrophoresis.

After the described background subtraction the image should represent only fluorescence of DNA-bounded ethidium bromide. For the correction of the shading effect - the sensitivity is not uniform for all pixel detector elements in the image plane - the image of the phosphorescence plate has to be used. This image shows decreasing values with increasing distance from the centre of the image. We devised again two methods for correction, one is called elliptical correction and the other point-area correction. The image of the phosphorescence plate is displayed in the red-blue modus with a border intensity that the pixel elements close to the centre show the colour red

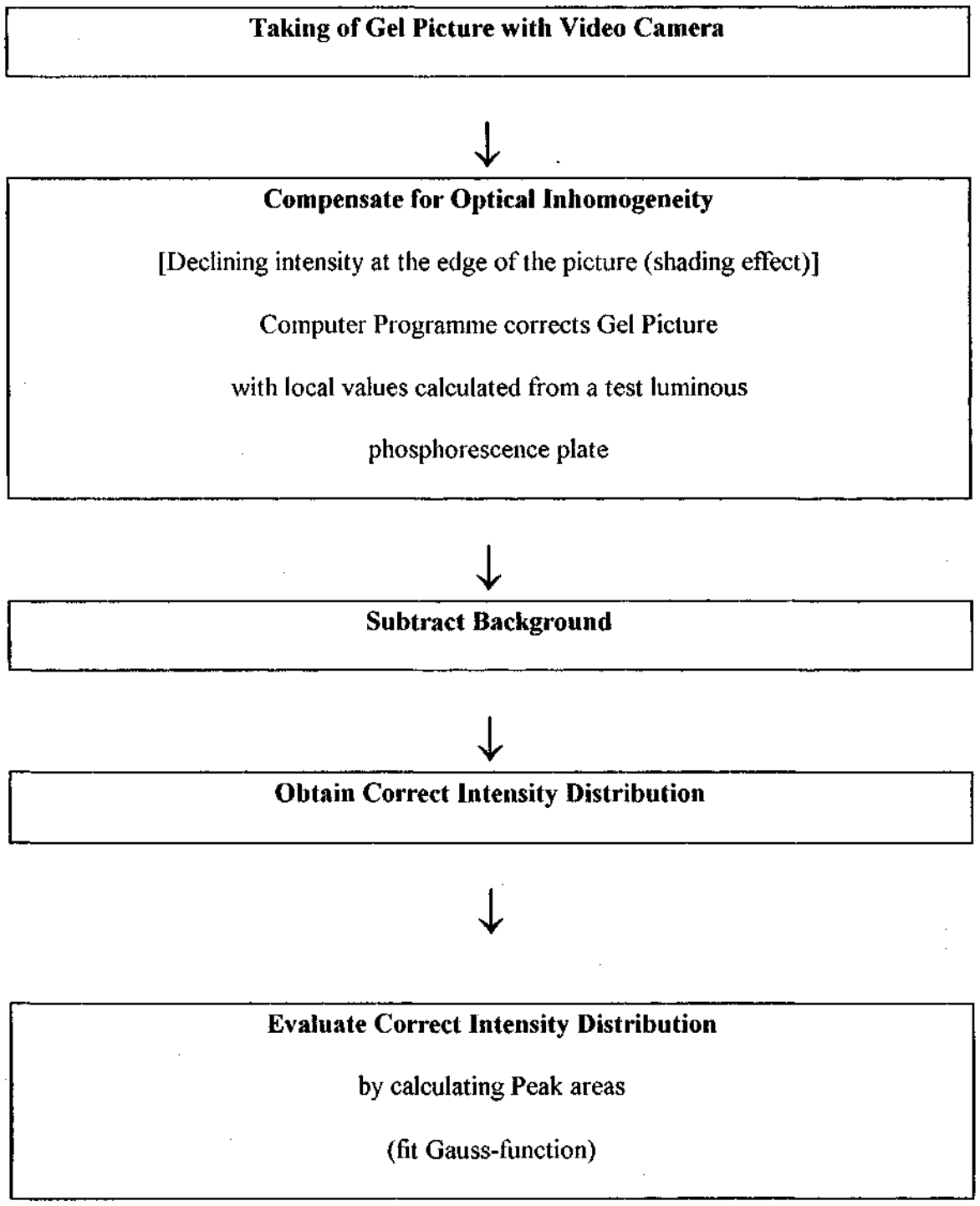


Figure 4.5: Schematic diagram showing the different steps in gel processing after electrophoresis

and the others the colour blue. An ellipse is then fitted to that image and the parameters of the ellipse (centre, radius and eccentricity) were saved. This should be done for a lot of border intensities. The centres of all ellipses get then averaged and the eccentricity as a function of the radius is fitted to a straight line. It was found that the eccentricity is increasing with increasing distance from the centre. The shading correction is then performed in such a way that each pixel element of the gel for evaluation is multiplied with a factor determined by the phosphorescence plate. In case of an elliptical correction this factor is calculated by the average intensity of all pixels positioned on the same ellipse as the pixel for correction divided through the average intensity of the pixels around an area (7 x 7 pixels) of the centre. In case of the point-area correction the factor is determined by the average intensity of the pixels around an area (7 x 7 pixels) of the pixel for correction again divided through the average intensity of the pixels around an area (7 x 7 pixels) of the centre. The shading correction procedure for a picture of 262144 Byte lasts about 2 minutes for both methods.

A necessity for the performance of both shading correction methods is the independence of the shading from the intensity of light. In order to investigate this a lot of images of the phosphorescence plate were recorded with different amplification conditions of the photon and the electronic amplifier. The phosphorescence plate was excited with a bulb for at least 5 minutes to achieve saturation and pictures were taken in defined time intervals (with the command MAKE MOVIE). After about 1 minute the phosphorescence decreased to 1 %. For this reason an oversampling frequency of 1 had to be used for the recording of the plate resulting in a relatively high scattering. As a result of these series of pictures with different amplification conditions and phosphorescence intensities the shading effect was found to be independent of the

camera amplification and the intensity of light. The correction of each picture with each of the others results in a homogeneous image. Thus, for the correction of the gel pictures any phosphorescence plate can be used. It is not necessary for the shadowing correction to take an image of the phosphorescence plate along with the gel, as it is the case for background subtraction.

The second part of the correction and evaluation software is called EVA(luation). This program displays the intensities of the images in 256 different grey values, the higher the intensities the brighter the respective pixels. A cross can be moved by means of the computer mouse over the image and the intensity and co-ordinates of each pixel get displayed on the second screen by pushing a key. This command is useful if a rough overview of the image is desired.

Another command enables the drawing of a rectangle of any size on the image screen. This rectangle can again be moved over the image by the computer mouse and the average intensity of the enclosed pixels as well as their number is displayed on the command monitor by pushing a key. This mode is applied if the fluorescence inside a defined region - e.g. the fluorescence of a DNA band - has to be quantified.

In order to study a fluorescence distribution over the image an arbitrary region of the picture can be defined for calculation. The intensities of the pixels inside this region are averaged in the x-direction and the distribution is produced in y-direction and shown along with the image on the same screen. It can then be saved on hard disk for further application. This evaluation mode is for example used if some DNA bands, separated with an electrophoresis system, have to be quantified independently. Even if the bands

are not separated very well and the fluorescence of some pixels can not be attached to the bands unambiguously, the fluorescence distribution is useful for further calculations.

The third part of the correction and evaluation software starts with the distribution made by "EVA". "ADA" displays it on screen and parts of the distribution can be extended to make details visible. There are now two possibilities for integration; with the first mode borders (y_{min} and y_{max}) can be set for a numerical integration. This method is almost the same as the rectangle evaluation in the program EVA. It averages the pixel intensities inside a region in the x-direction and sums up these values for the y-direction while the rectangle evaluation produces an average intensity value of all pixels inside the marked region.

The second mode adapts any mathematical function to the distribution which is then integrated analytically. If for example some Gauss functions are adapted to a distribution of separated bands, the co-ordinates of the maximum of each band serve as starting parameters and the integral of each band is calculated analytically. But also other functions can be used for curve fitting. This method is very useful for the quantification of DNA bands which were not separated completely.

3.3 Reagents and Buffers

The following reagents and buffers were used:

Spheroplasting Solution

0.5 M EDTA, pH 8.0

7.5 % ß-mercaptoethanol (BME)

10 Mm Tris pH 7.5

Digestion Buffer

0.5 M EDTA pH 8.0

10 mM Tris pH 7.5

1 % Lauroyl sarcosine

2mg/ml Proteinase K

Complete Medium

Bacto agar 20 g/l

Yeast Extract 5 g/l

D(+)Glucose 20 g/l

Table 3.1 lists the ions used and some of their physical parameters. Stopping powers were calculated according to Kiefer (1987), penumbra radii after Kiefer and Straaten (1986). (Relative effectiveness for DSB induction and inactivation were calculated using the respective values for 80 kV X-rays).

Table 3.1: Physical parameters of the ions

Heavy ions	E MeV/u	r_D µm	Z^2_{eff}/β^2
α	0.88	0.05	1680
C	3.4	0.49	4349
C	18.0	8.39	958
O	2.9	0.38	8293
O	8.0	2.11	3473
O	10.7	3.46	2663
Ar	5.7	1.19	19415
Ne	14.4	5.74	3108
Ne	15.0	6.15	2996
Ni	12.1	4.27	2319
Kr	11.2	3.74	36929
Xe	14.0	5.47	59145
Au	9.3	2.73	123491
Au	11.7	4.03	111002



Approx. Size (Kb) Sample well	Chromosome #
2,200	XII
1,600	IV
1,125	XV, VII
1,020	XVI
945	XIII
850	II
800	XIV
770	X
700	XI
630	V
580	VIII
460	IX
370	III
290	VI
245	I

Figure 4.1: Separation pattern of the Bio-rad length standard performed in a 1% gel. (After Bio-rad, 1993).

CHAPTER FOUR

4.0 RESULTS

4.1 Size separation of Yeast DNA

The banding pattern for yeast chromosomal DNA is shown in figure 4.1 together with the size-distribution of the molecules for the electrophoretic conditions used in this work. Two-dimensional electrophoretic experiments demonstrated, however, that the two largest chromosomes (XII and IV) are inverted with respect to their positions (Löbrich *et al.* 1993a). This fact is made use of in the calculation of DSB yields or production cross-sections.

4.2 Gel fluorescence as a function of DNA content

In order to check the validity of the outlined approach, the fluorescence as a function of DNA content was studied by using DNA with a known concentration. Different DNA amounts were loaded in the wells and the gel was stained and destained in the same way as is used in all the experiments. The ethidium bromide fluorescence was then measured as described; figure 4.2 shows the resulting curve. One finds a linear response in the range up to 100 ng. Since our gels usually contain not more than 70 ng of DNA (in the first band), it is clear that one is always working within this linear range. The two curves in the figure were measured with two different amplification conditions of the camera which represent the lower and upper limit of the conditions used for all the experiments. They show that linearity is independent of the amplification conditions.

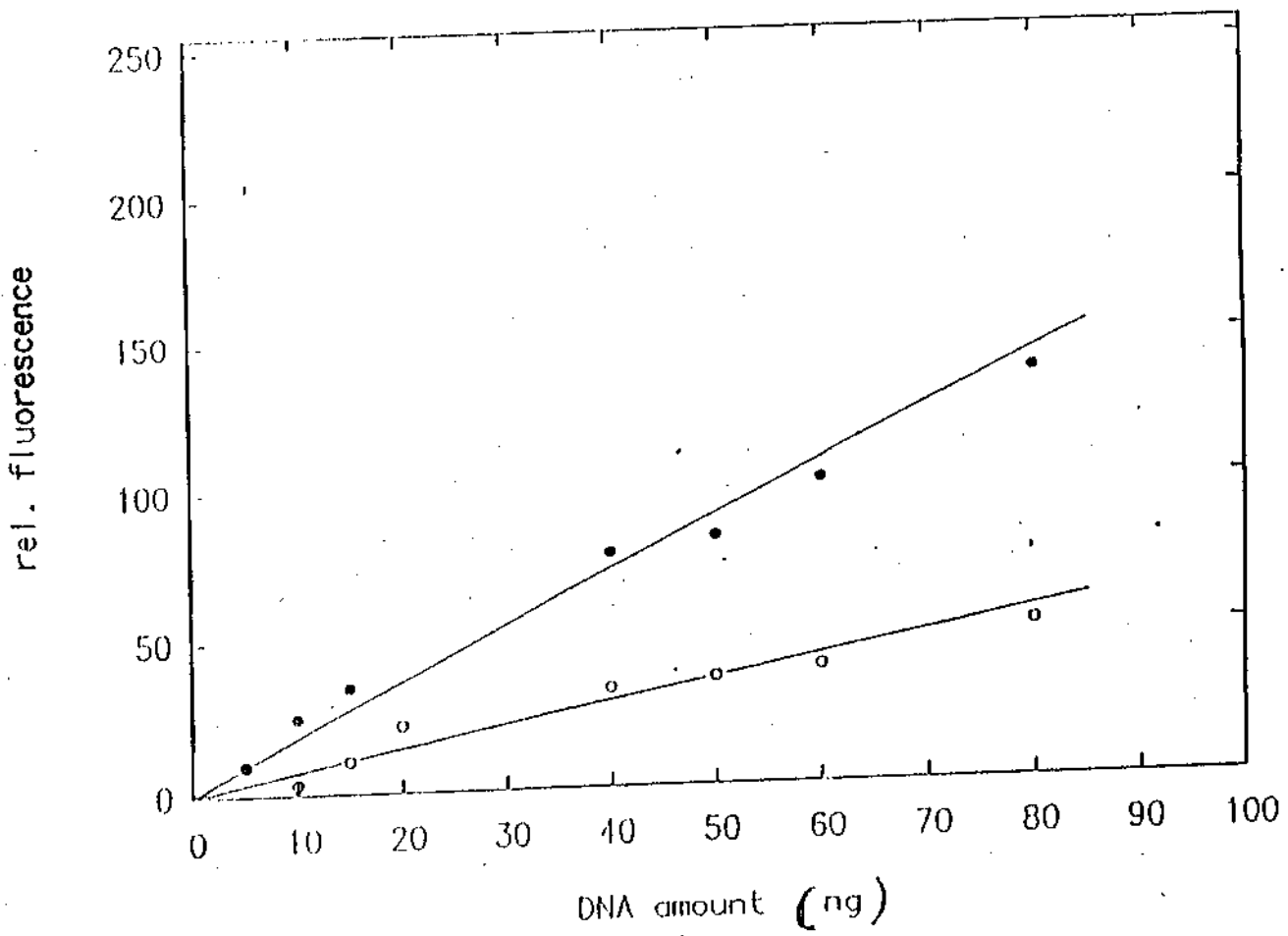


Figure 4.2: Ethidium bromide fluorescence as a function of DNA concentration.

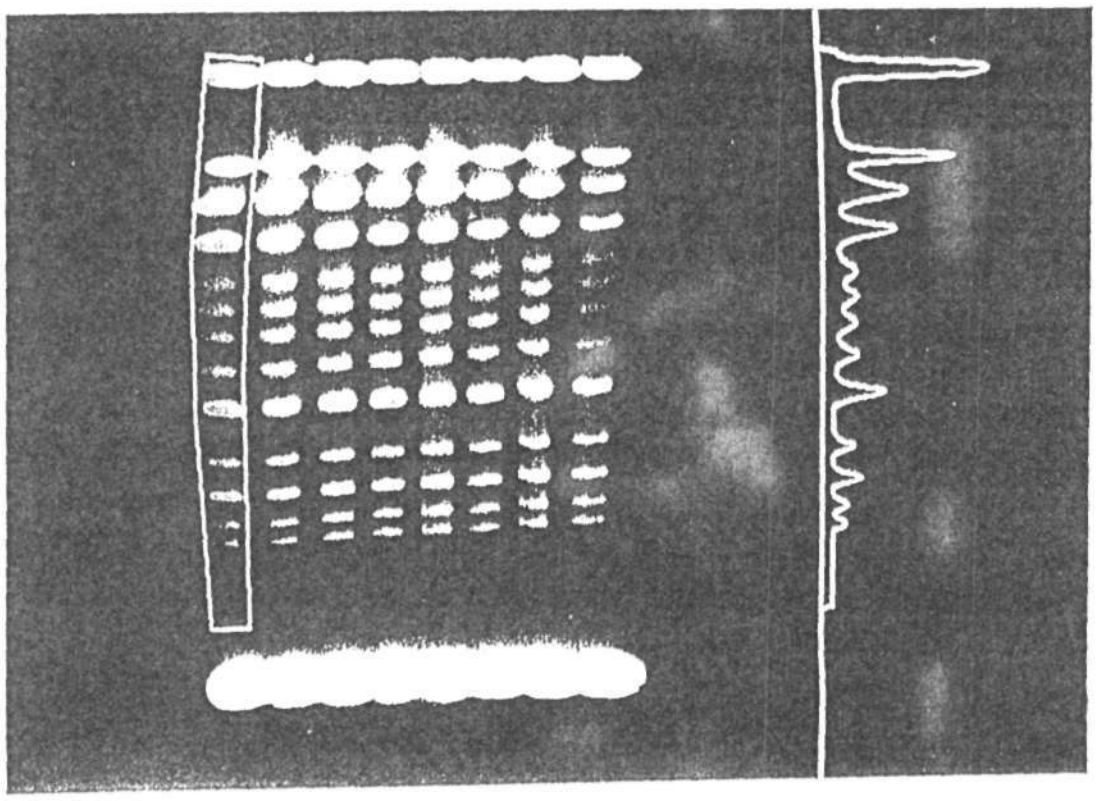


Figure 4.3: An uncorrected gel picture of unirradiated (first two lanes on the left) and Irradiated (lanes 3 - 8, with X-ray doses of 14.7, 29.3, 40.0, 58.7, 88.0 and 103 Gy) yeast DNA after electrophoresis. The intensity distribution on the right corresponds to the marked lane.

4.3 Correction of the Electrophoretic Gels

After electrophoresis, the next step in the evaluation procedure is the correction of the gel pictures with respect to background fluorescence, etc. Figure 4.3 is a picture of the uncorrected gel with two sets of wells; the lower set was inserted after the run and used as reference plugs, as described in section 3.2.5. The distribution on the right corresponds to the marked lane. The X-ray dose increases from left to right of the picture, the first two on the left being unirradiated controls. In both the gel picture and the distribution a high background is visible.

The gel is now corrected with regard to the background (by subtracting a gel without DNA) as well as the camera's shading effect. For the control sample only a very small background is left, while in the irradiated samples a smear (increasing with dose), presumably due to fragments, still remains (picture not shown). The cause of the little smear in the control is not immediately clear. It could be due to RNA or DNA fragments resulting from shear forces during the DNA preparation or the electrophoresis. Another suggestion is that it could be due to unbroken DNA pieces of the smaller chromosomes which, for some unknown reasons, are not completely separated by the electrophoresis. The gel is then scanned around the unirradiated sample lanes to determine the minimum intensity. This value of intensity is used to make a homogeneous background for subtraction (as described above); the picture obtained after this last step is shown in figure 4.4. This is the gel finally used for the evaluations. The densitograms corresponding to the marked lanes are shown on the right of each gel picture. The intensity distributions before and after the corrections is also shown in figure 4.5.

In the gels shown in figures 4.3 and 4.4 chromosome XII is not visible. However, the uppermost band is likely to be contaminated by fragments arising from this chromosome.

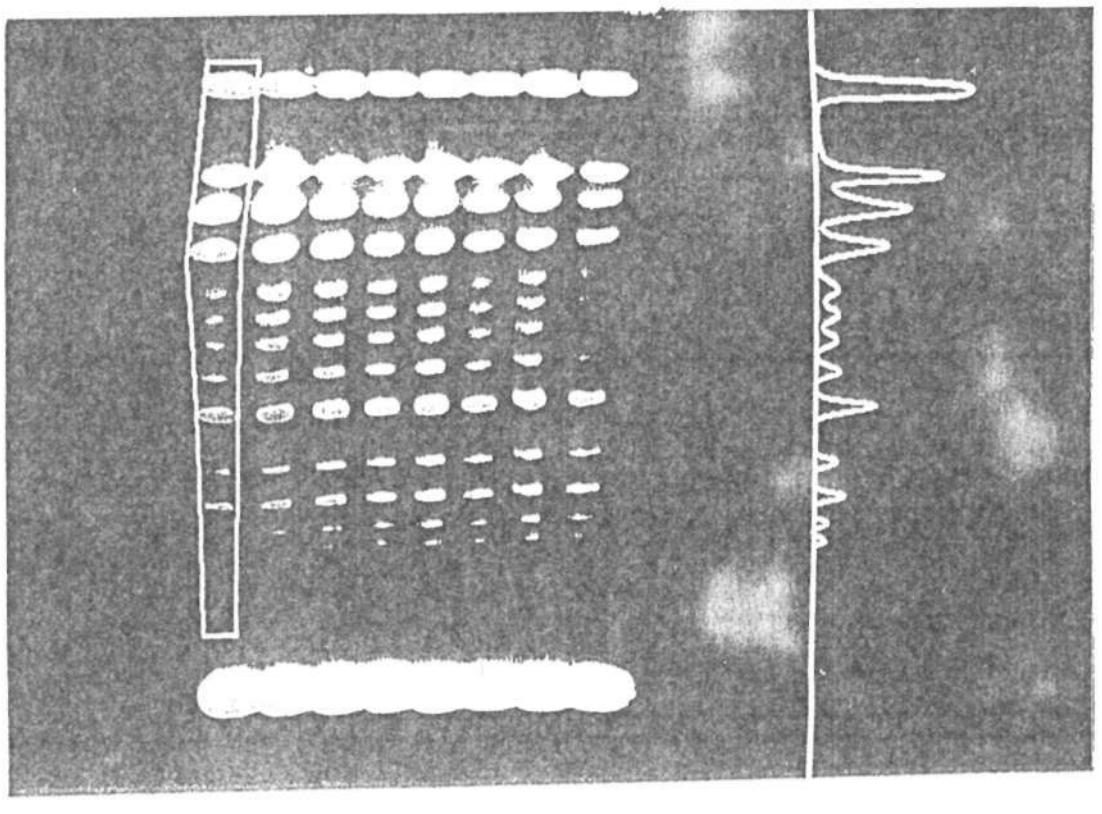


Figure 4.4: The gel picture (figure 4.3) after all the corrections.

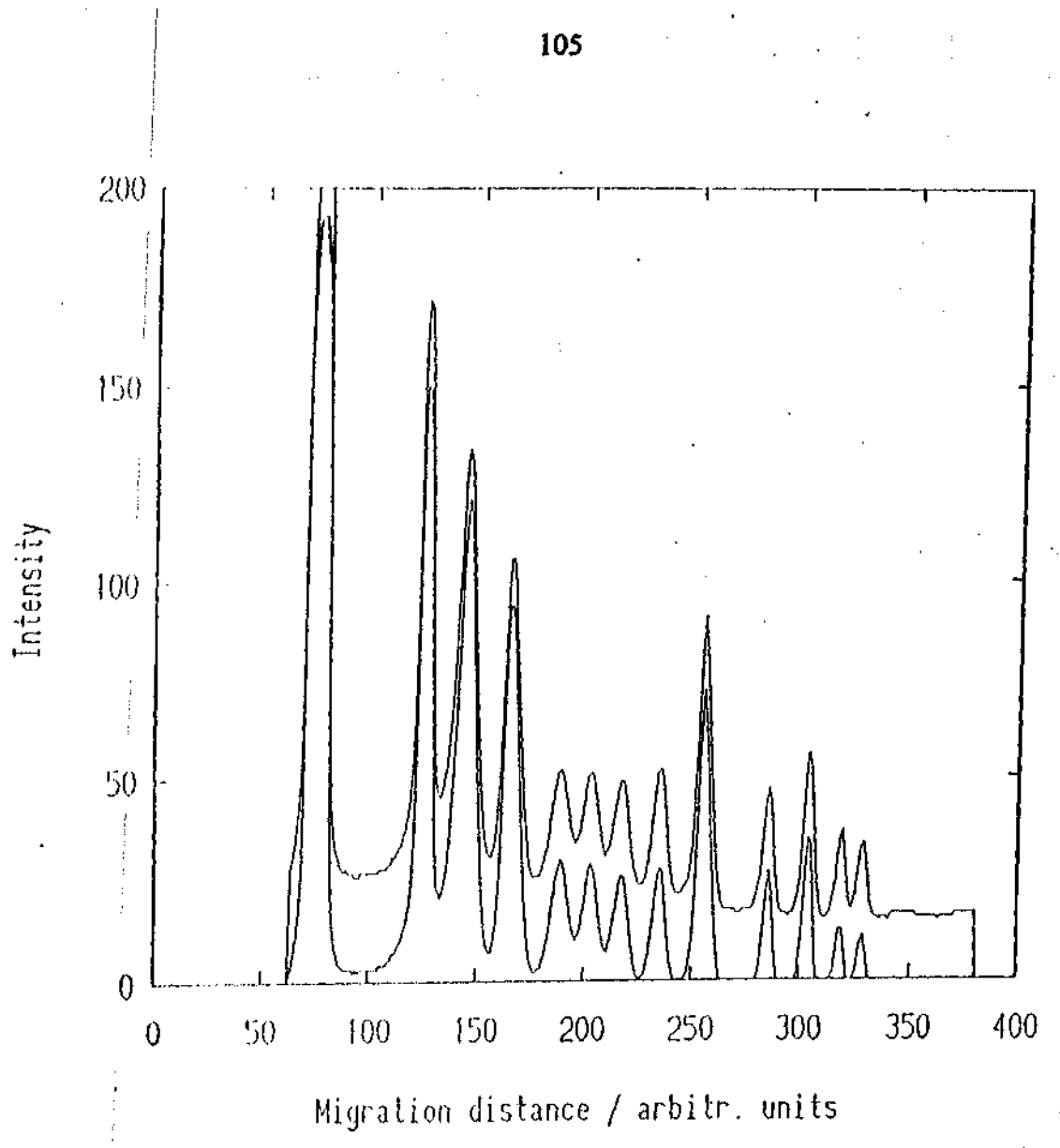


Figure 4.5: Intensity distribution curves before and after the electrophoretic gel corrections

However, the exponential nature of the relative fluorescence curves suggests that this is only a minor effect.

4.4 Quantification of the Band Fluorescence

Band fluorescence was measured by integrating the area under the peaks. Because it is impossible to use exactly the same amount of DNA in all the sample plugs, and this condition is necessary in order that the fluorescence of a given band in an irradiated sample could be compared to a corresponding one in the unirradiated sample, it was necessary to have reference plugs containing the same amount of DNA as the samples used in the electrophoresis. This was achieved by cutting the original plugs into two identical parts, one was used in the run and the second placed, as reference, in the agarose gel after electrophoresis. Both the reference plugs and the separated bands were then stained under the same conditions. Since the difference in DNA content of the reference plugs and the first bands is one to two orders of magnitude, they were photographed with two different amplifications of the camera. The fluorescence of the first band of the irradiated samples was then compared to that of the control; the variations in the DNA amount in the sample plugs were eliminated by the use of the corresponding reference plugs. The results show an exponential decrease of the first band fluorescence with dose.

4.5 DSB-induction by 80 kV X-rays and 3.5 MeV α-particles

The relative fluorescence curves for 80 kV X-rays and 3.5 MeV α-particles are shown in figures 4.6 and 4.7, respectively. The 'relative fluorescence' is obtained by comparing the fluorescence of the first band of an irradiated sample with that of the unirradiated but electrophoresed control.

After the corrections described and based on the assumption that the dose which results in a decrease in fluorescence of the first band to 37% gives rise to one DSB per molecule, the DSB yield was calculated from equation (4.1):

$$Y_{dsb} = \frac{F_r}{M_1} \quad \text{.....4.1}$$

Where F_r is the slope of the relative fluorescence-dose curve and M_1 is the mass of the chromosome in the first band. The different steps in the gel processing procedure is shown in figure 4.5.

The assumption of randomly distributed breaks is, of course, not necessarily valid (especially with regards to α-particles and heavy ions) and needs further elucidation by analysing the size distribution of the DNA fragments. Previous experiments, with the electrophoretic conditions used for the gels in the presented report, have demonstrated that chromosome XII (the biggest chromosome) is either very faint or not at all detectable . In the case where it is visible, a mobility inversion occurs for the two largest chromosomes (Löbrich *et al.* 1993a) and this means that the first band actually corresponds to chromosome IV of length 1.6 Mbp (Mortimer and Schild, 1985) and molecular weight of $1.6 \times 10^6 \times 667$ g/mol.

The DSB induction rates, based on the assumptions that the induced breaks are randomly distributed, the uppermost band corresponds to chromosome IV and neglecting any contamination effects, were determined to be $(8.2 \pm 0.4)10^{-12}$ $(g/mol)^{-1}Gy^{-1}$ and $(14.8 \pm 0.5)10^{-12}$ $(g/mol)^{-1}Gy^{-1}$ for the 80 kV X-rays and 3.5 MeV α-particles, respectively. This yields an RBE for the α-particles of 1.8 ± 0.1.

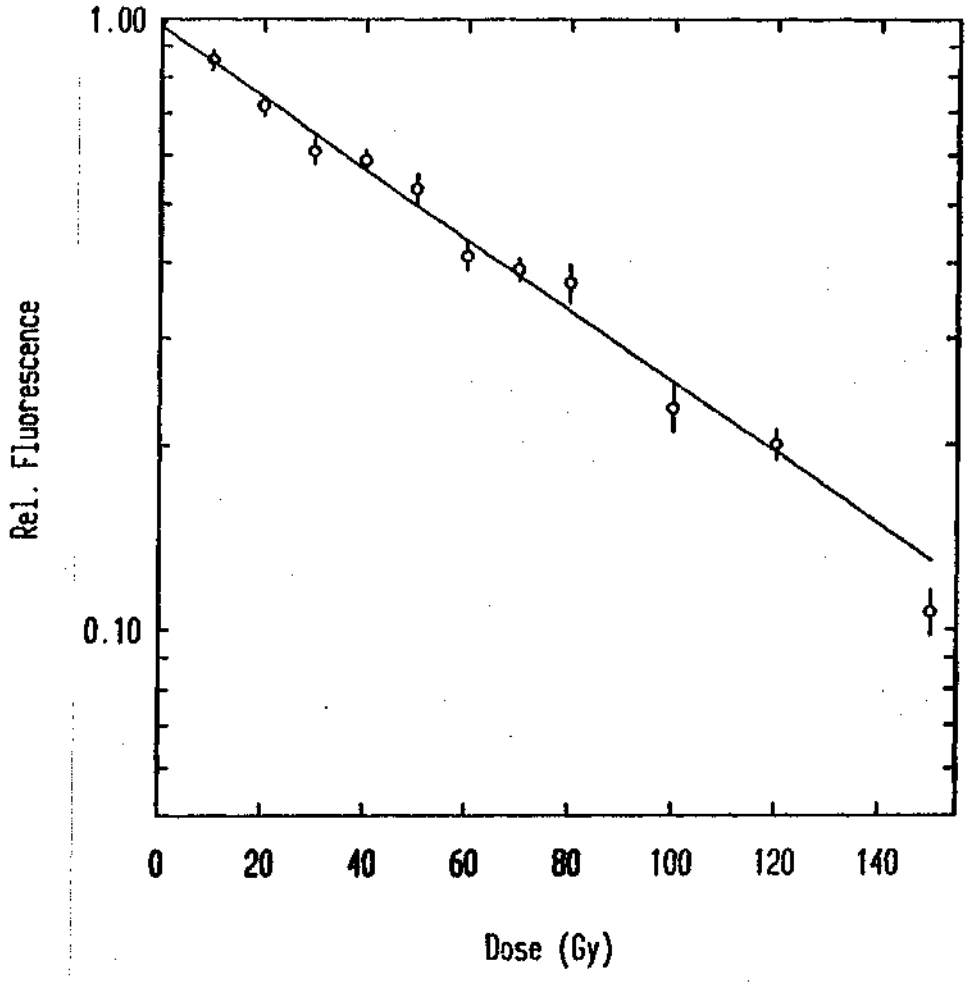


Figure 4.6: Relative fluorescence curve for yeast (211*B) after 80 keV X-ray irradiation

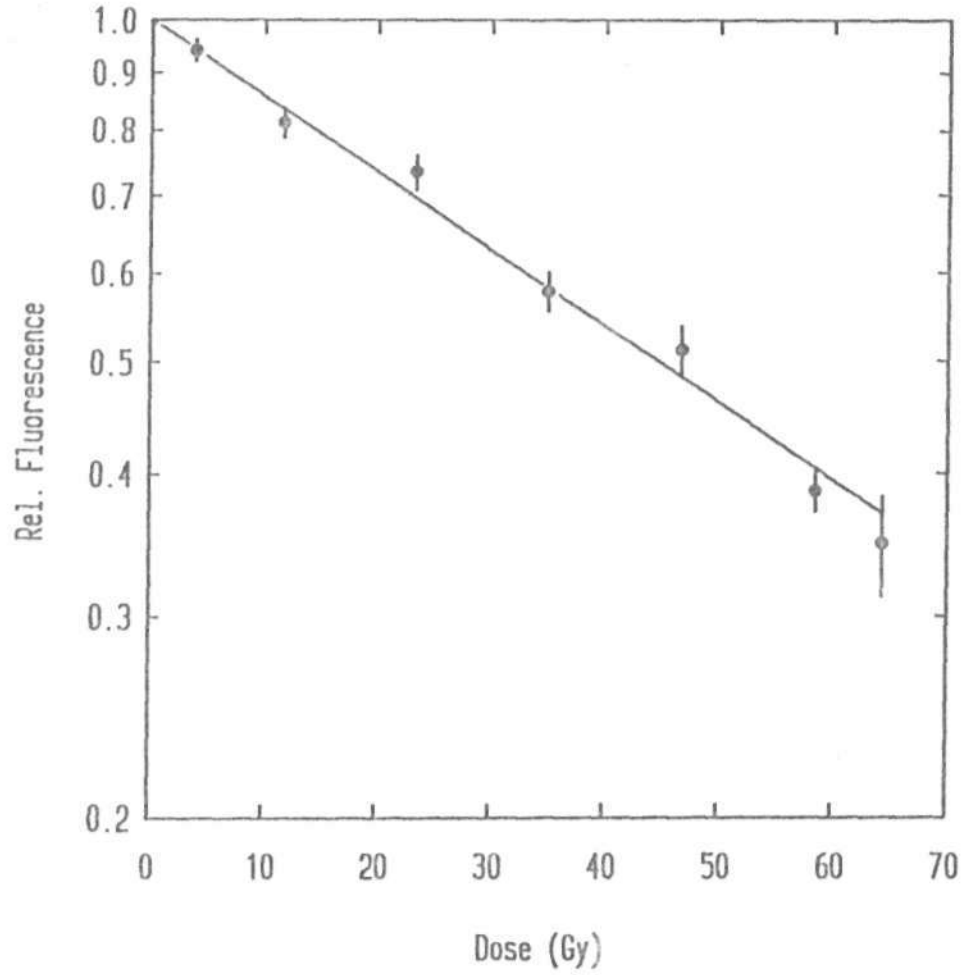


Figure 4.7: Relative fluorescence curve for yeast (211*B) after α-particles irradiation

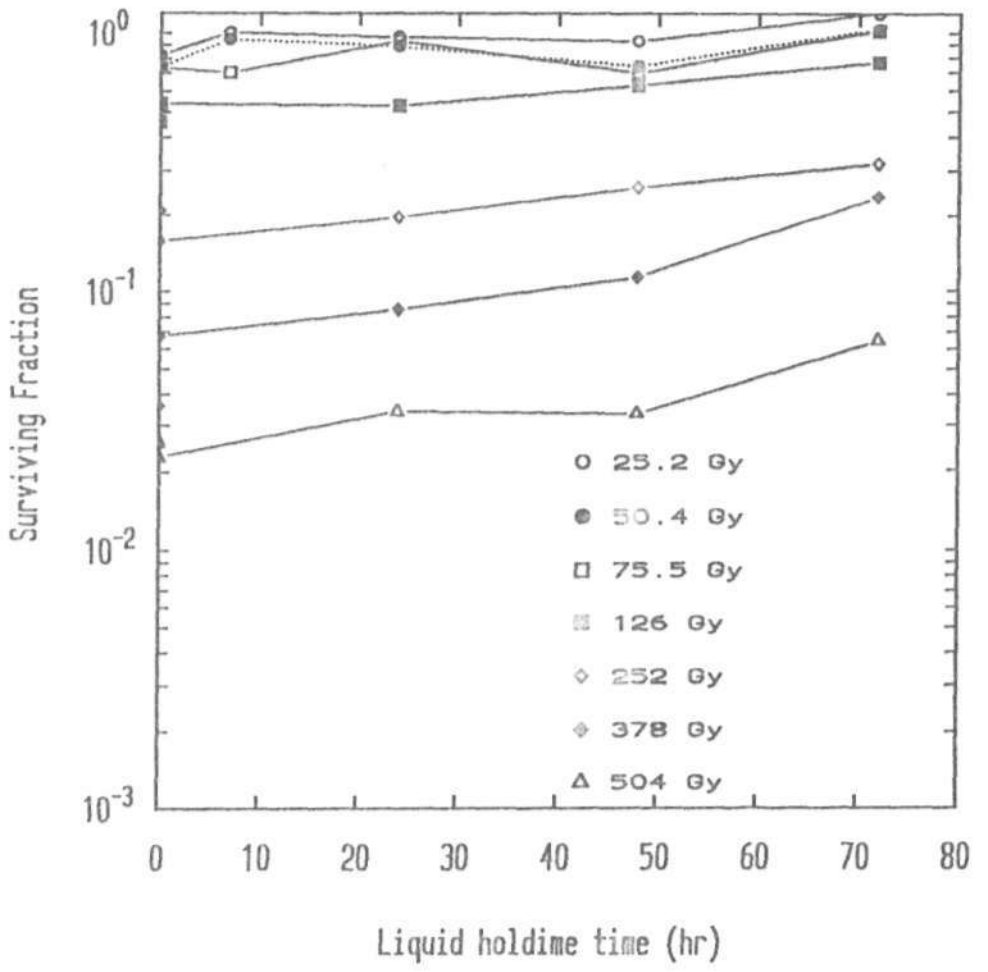


Figure 4.8: Yeast (rad 54-3) survival curves after incubation in phosphate buffer

4.6 DSB Repair

Repair studies were performed using the temperature conditional diploid yeast strain rad 54-3 which is known to be capable of DSB repair at 23°C but not at 36°C. Liquid holding recovery was carried out in phosphate buffer (pH 7). The irradiation was carried out with 80 kV X-rays, after which the yeast samples were held, at 23°C, in the buffer for 7, 24, 36, 48 and 72 hours before being assayed for DSB induction as well as survival. The "survival" curves in figure 4.8 demonstrate that during the period of incubation, the viability of the cells is unaffected.

4.6.1 Survival after X-irradiation

The multi-target survival curves in figure 4.9 show the result of the repair; it is clear here that the longer the cells are kept in the incubation buffer the bigger the shoulder of the corresponding survival curve. This may be interpreted as exhibiting an enhanced repair if it is assumed that the shoulder of the survival curve is related to repair.

4.6.2 DSB repair kinetics after X-irradiation

Relative fluorescence curves for the rad 54-3 cells are shown in figure 4.10. The curves demonstrate the well known biphasic repair kinetics with a half-time of 2.5 h for the fast component and 12.5 h for the slow component. The curves also tend to show that within the first two hours of incubation after X-irradiation, a secondary effect takes place leading to more DSB. This may be due to an interaction of some of the some non-DSB lesions to form DSB; this effect also tends to increase with dose.

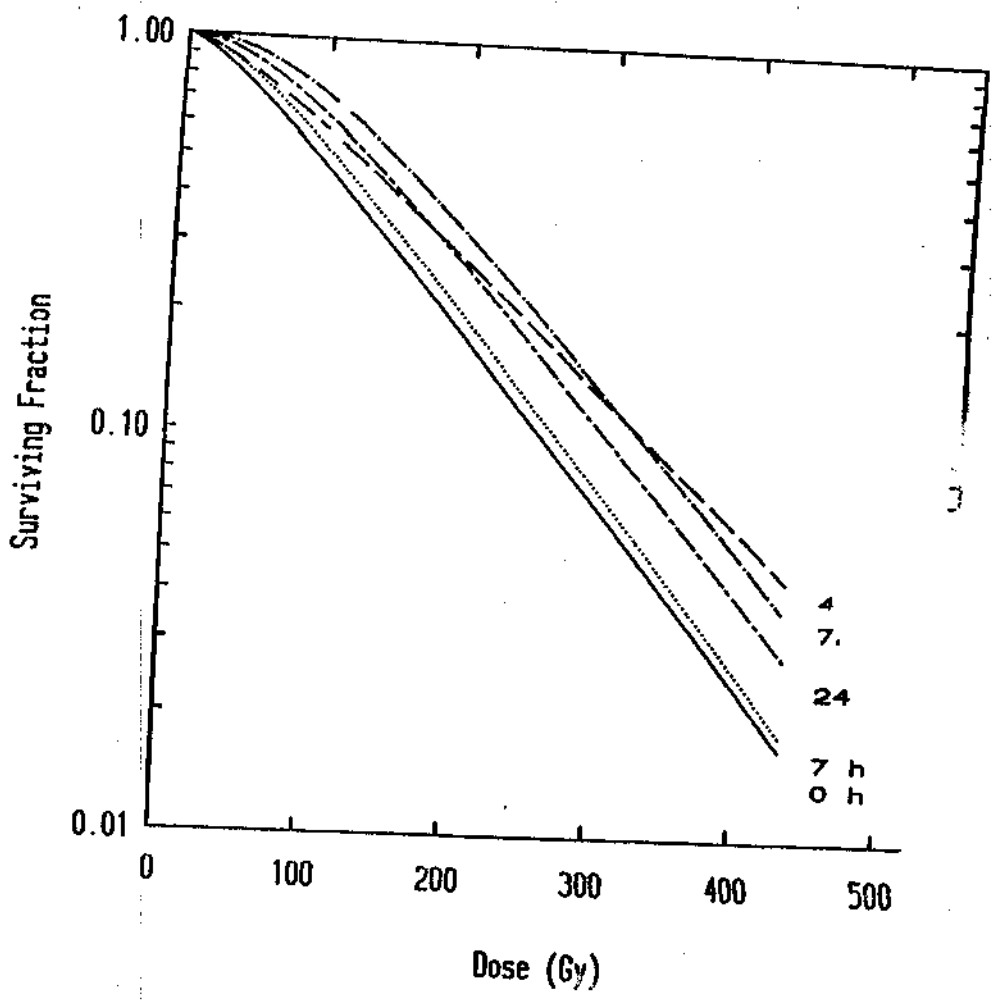


Figure 4.9: Survival curves for yeast (rad 54-3) after X-ray irradiation and incubation in phosphate buffer. For clarity, the experimental points have been removed (see appendix for the experimental data).

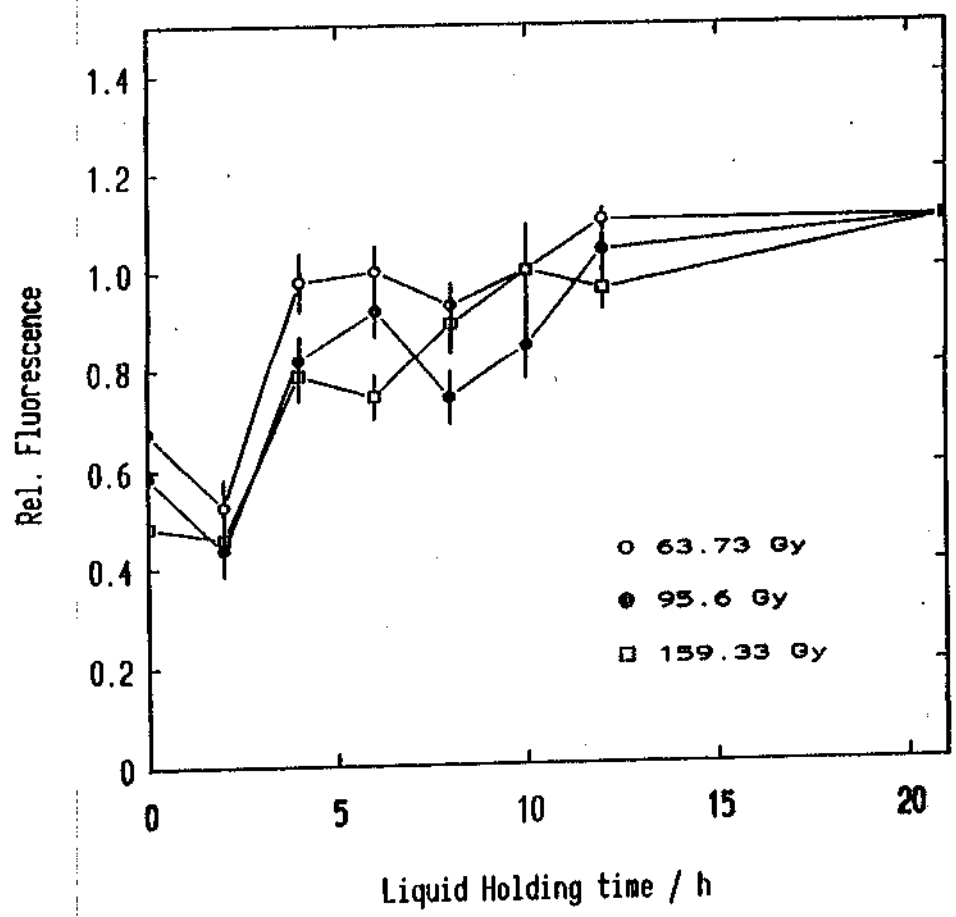


Figure 4.10: Relative fluorescence curves for rad 54-3 yeast cells after X-ray irradiation and incubation in phophate buffer

4.7 Heavy Ion Effects

4.7.1 Inactivation

The survival data were fitted to a multi-target function and the resulting curves are shown in figures 4.11, 4.12, 4.13 for low, medium and high LET, respectively The shoulders appear to be retained even after high LET irradiation; this appears however to diminish gradually for the higher LETs. The slopes of the final linear parts of the curves are presented as inactivation section in the table 4.1 together with the ion parameters. The RBE_{inact} was calculated using 80 kV X-rays as the reference radiation and in accordance with equation 2.18.

Table: 4.1:Inactivation Cross-section for the various ions

Heavy ions	E MeV/u	LET (keV/μm)	σ_i (10^{-8} cm^2)	RBE_{inact}
α	0.88	110	0.34 ± 0.05	0.7
C	3.4	329	0.41 ± 0.04	1.3
C	18.0	101	0.21 ± 0.01	2.2
O	2.9	604	0.67 ± 0.05	1.2
O	8.0	316	-----	-----
O	10.7	257	0.45 ± 0.01	1.8
Ar	5.7	1654	0.96 ± 0.05	1.2
Ne	14.4	316	0.37 ± 0.02	0.7
Ne	15.0	306	-----	-----
Ni	12.1	2283	0.88 ± 0.03	0.4
Kr	11.2	3586	1.10 ± 0.06	0.3
Xe	14.0	5975	3.80 ± 0.17	0.4
Au	9.3	11585	4.51 ± 0.43	0.4
Au	11.7	10863	4.20 ± 0.51	0.4

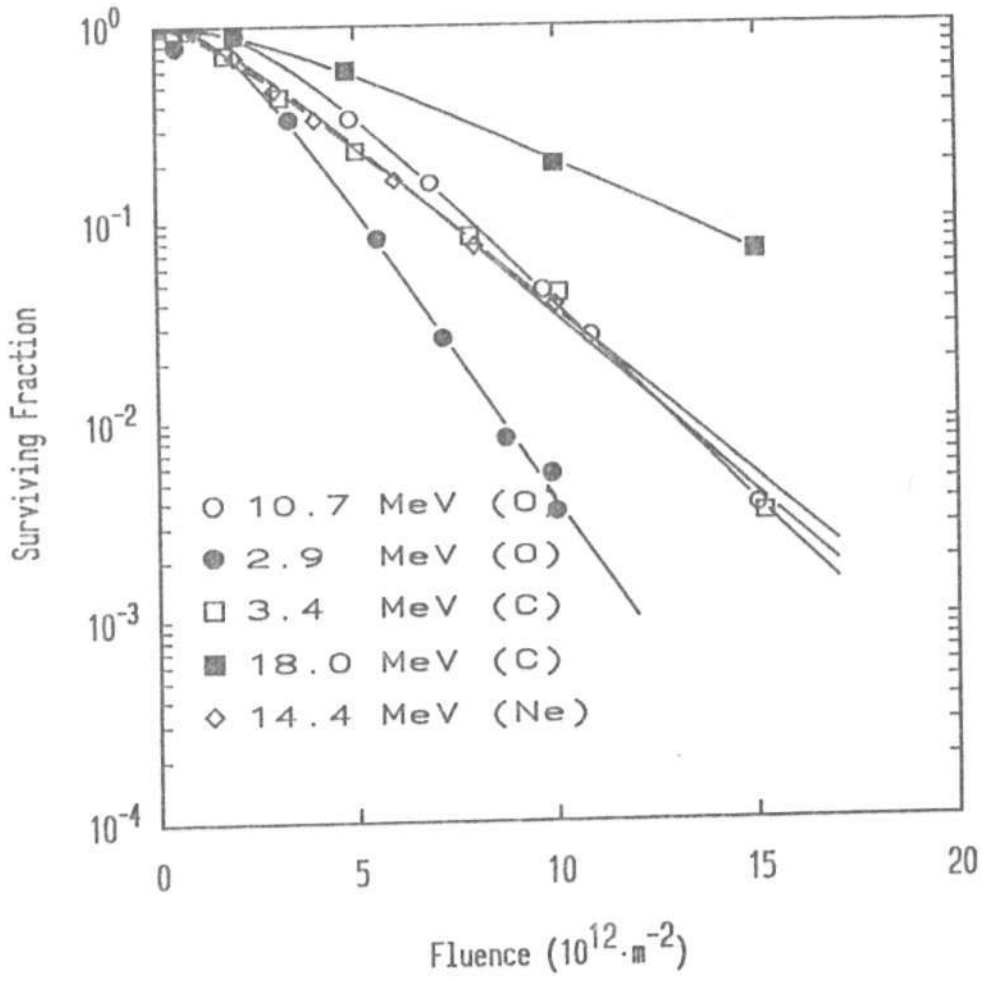


Figure 4.11: Survival curves for yeast (211*B) after low LET heavy ion irradiation

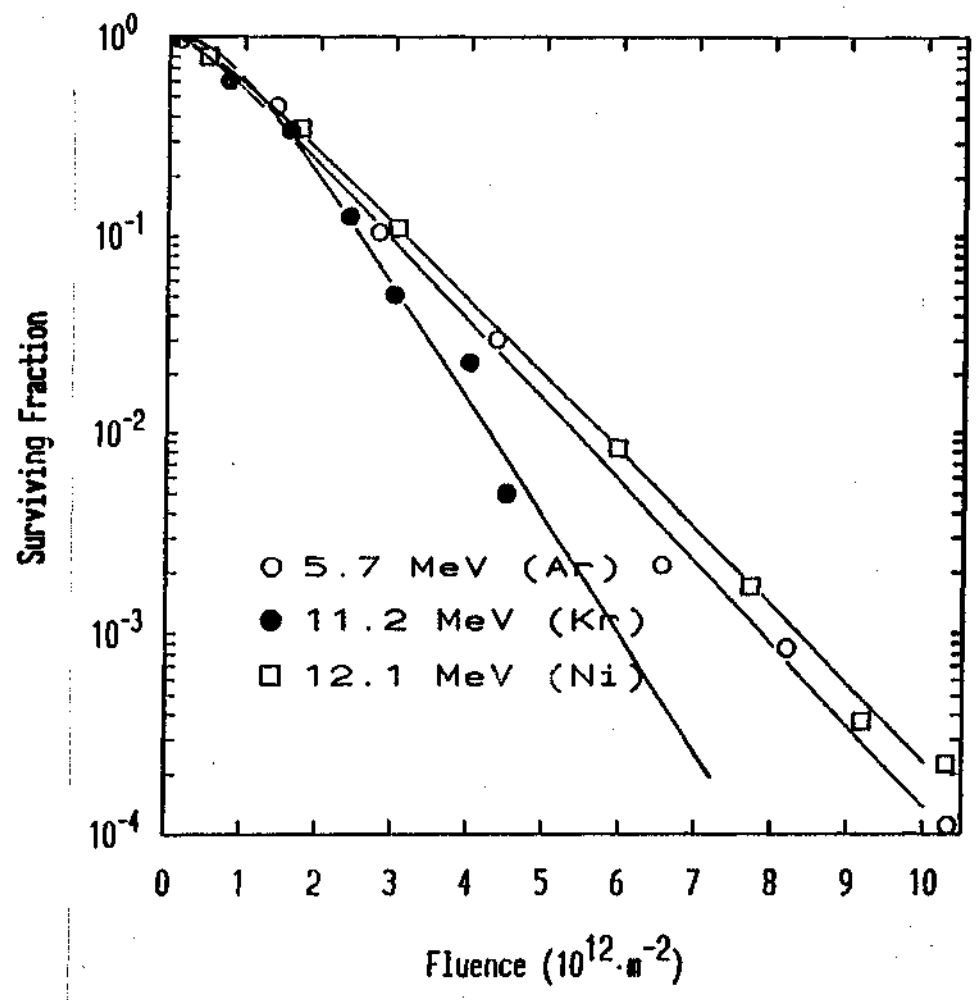


Figure 4.12: Survival curves for yeast (211*B) after medium LET heavy ion irradiation

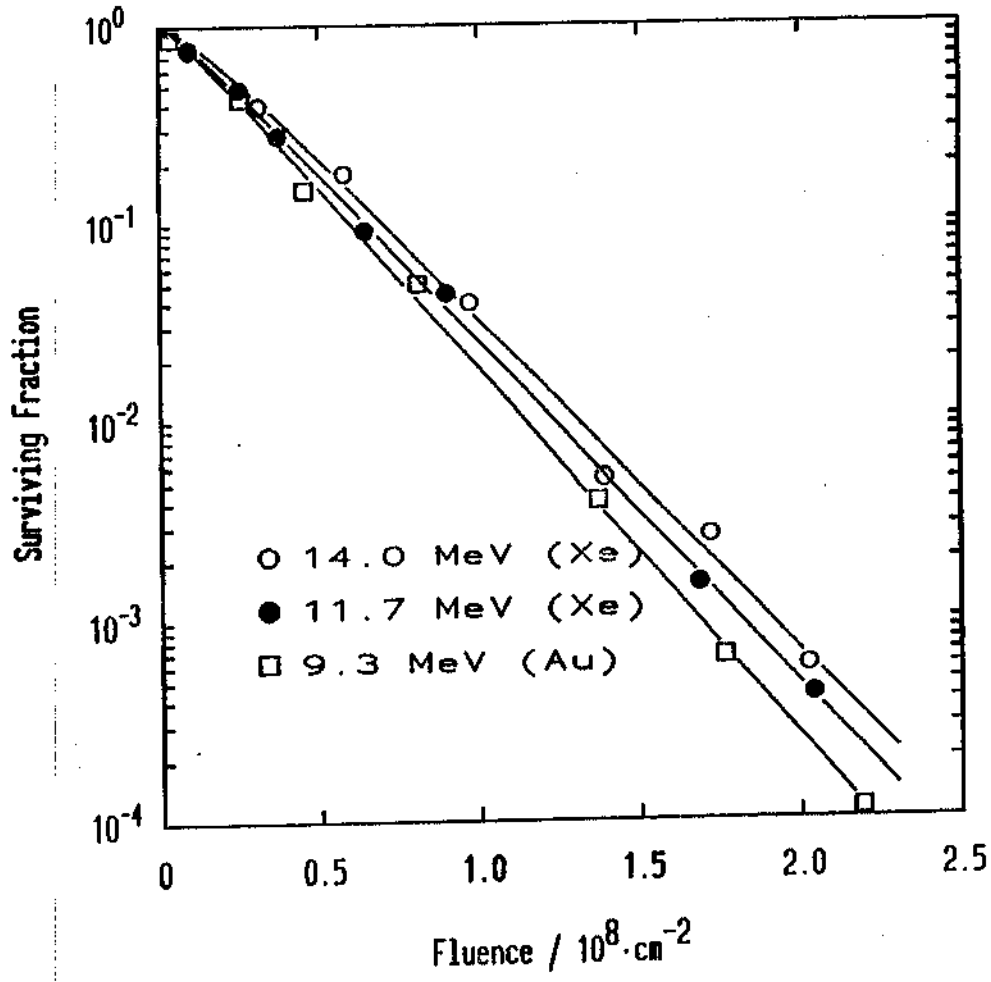


Figure 4.13: Survival curves for yeast (211*B) after high LET heavy ion irradiation

4.7.2 DSB induction

The relative fluorescence values obtained as stipulated in section (4.4) were fitted to an exponential function and slopes of the curves used to calculate the DSB production cross section as shown in the following equation:

$$\sigma_{dsb} = \frac{F_r}{M_1} \quad \text{.....4.2}$$

Where F_r is the slope of the relative fluorescence curve, and M_1 is the mass of the chromosome in the first band. This procedure assumes a random distribution of the induced breaks and this is not necessarily valid especially with heavy ion irradiation. This point obviously requires further elucidation because it is not improbable that what is measured in this technique may not be "breaks" but clusters of breaks. The derived DSB production cross sections (normalized to 10^9 g mol^{-1}) are presented in table 4.2.

Table 3.3: DSB production cross-sections for the heavy ions

Heavy ions	E (MeV/u)	LET (keV/μm)	σ_{dsb}(10^{-8} cm^2)	RBE_{dsb}
α	0.88	110	0.26 ± 0.051	1.78
C	3.4	329	0.39 ± 0.009	0.89
C	18.0	101	0.30 ± 0.031	2.27
O	2.9	604	0.71 ± 0.005	0.89
O	8.0	316	0.56 ± 0.037	1.34
O	10.7	257	0.42 ± 0.016	1.24
Ar	5.7	1654	1.10 ± 0.038	0.50
Ne	14.4	316	0.60 ± 0.017	1.43
Ne	15.0	306	0.64 ± 0.067	1.58
Ni	12.1	2283	0.95 ± 0.089	0.32
Kr	11.2	3586	1.05 ± 0.10	0.22
Xe	14.0	5975	4.90 ± 0.12	0.62
Au	9.3	11585	4.22 ± 0.17	0.28
Au	11.7	10863	4.85 ± 0.087	0.34

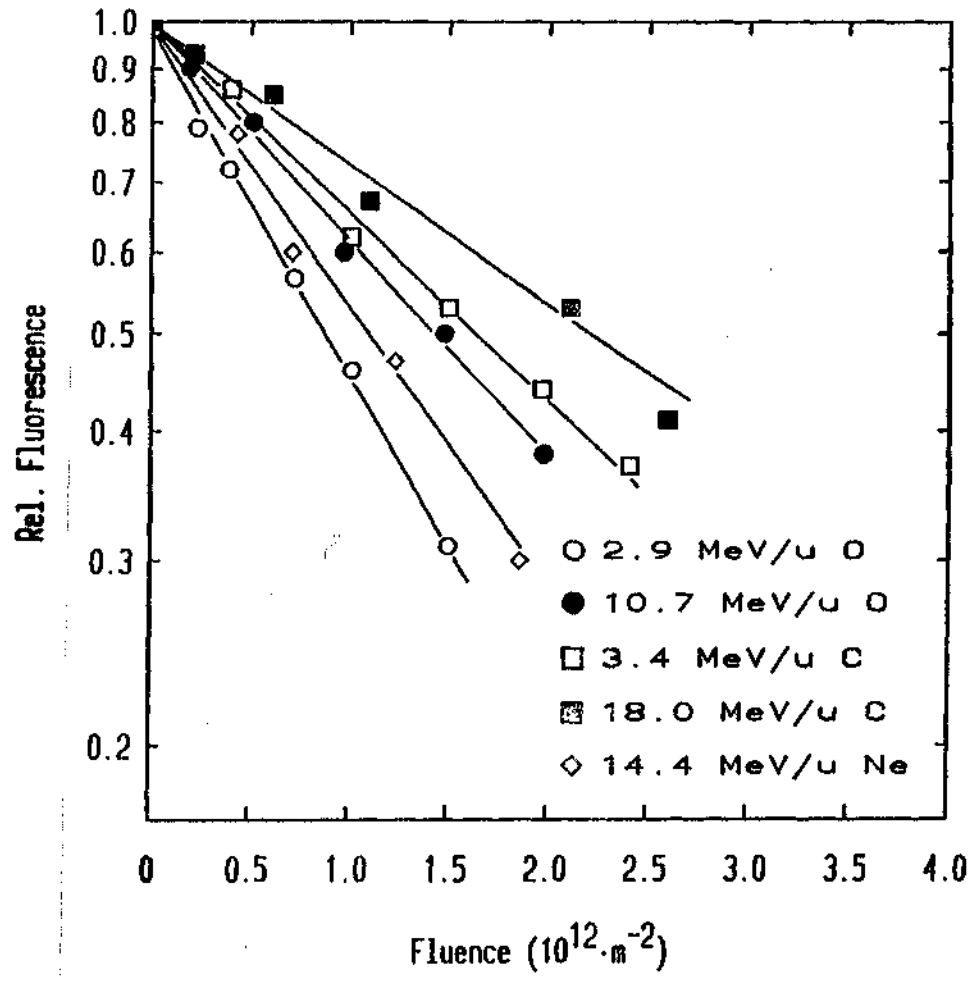


Figure 4.14: Relative fluorescence curves corresponding to the ions in figure 4.11

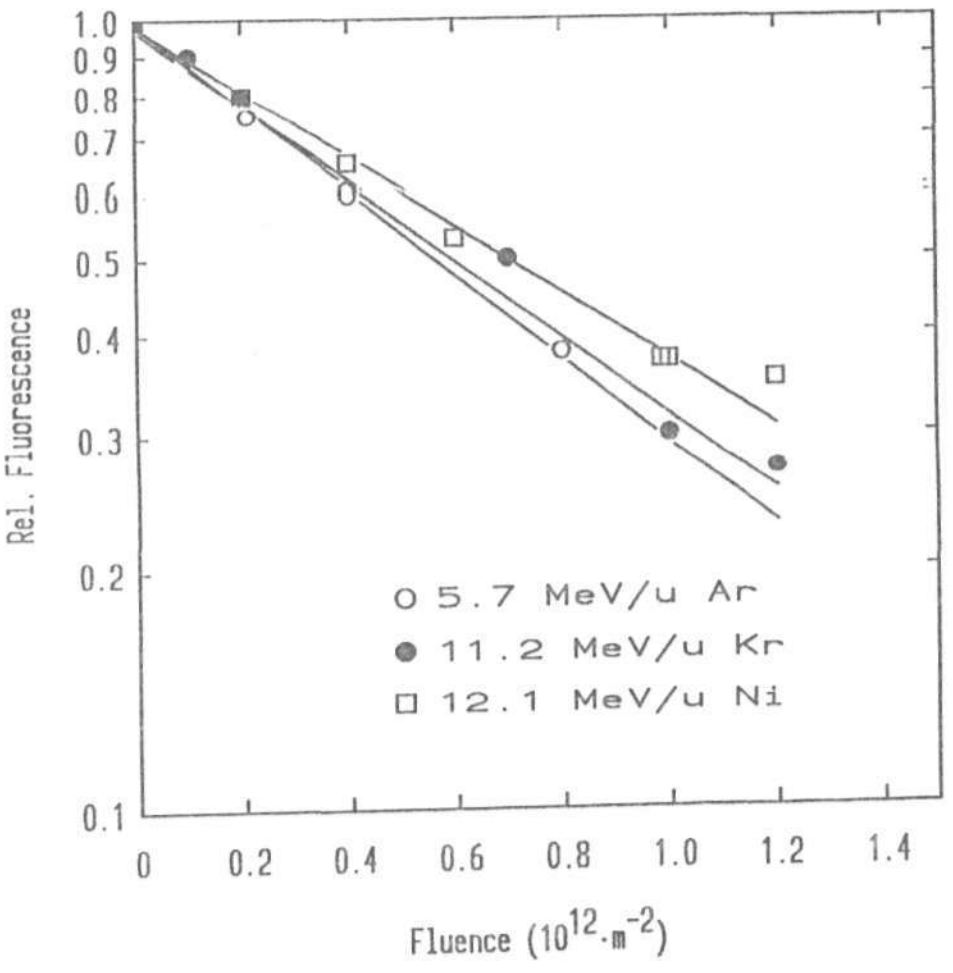


Figure 4.15: Relative fluorescence curves corresponding to the ions in figure 4.12

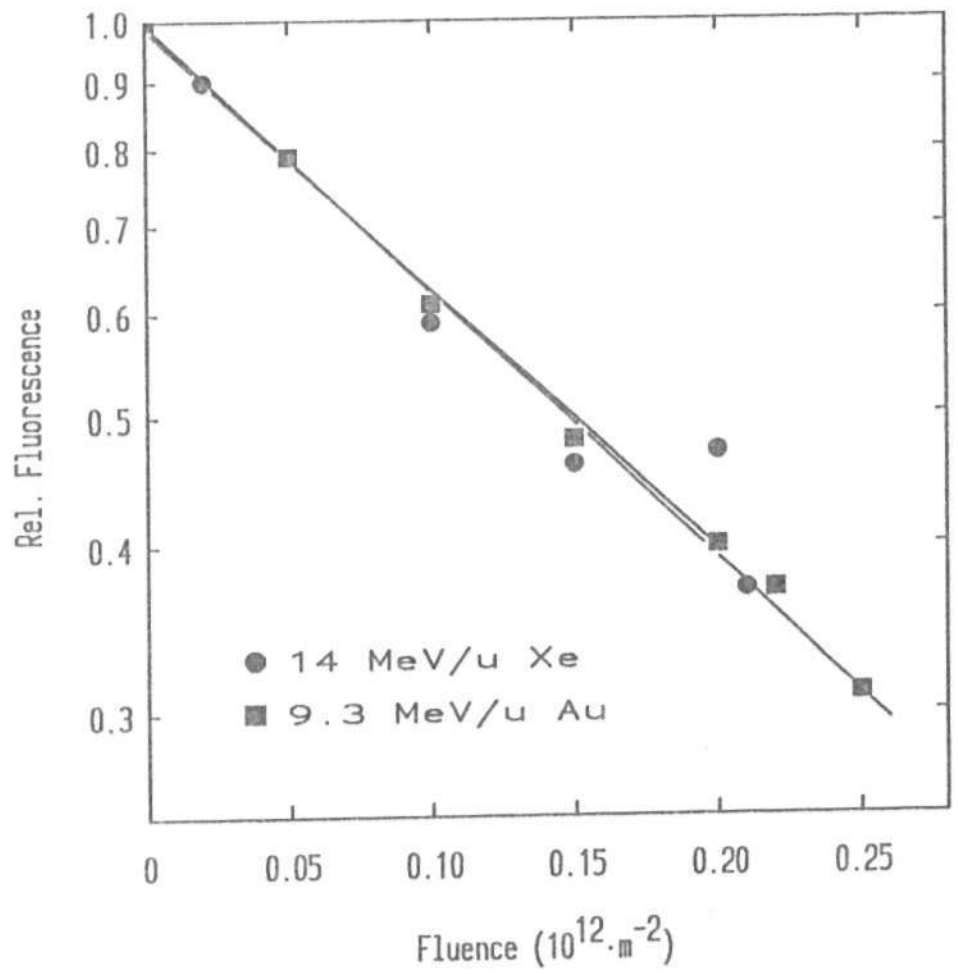


Figure 4.16: Relative fluorescence curves corresponding to the ions in figure 4.13

Figures 4.14, 4.15 and 4.16 are, respectively, the relative fluorescence curves corresponding to the LET ranges stipulated in section 4.8.1. The absolute numbers of DSB were obtained by plotting the negative logarithm of the relative fluorescence versus ion fluence. The points represents averages from two electrophoresis runs of single experiments. In all cases the DSB induction was found to increase linearly with ion fluence.

4.7.3 DSB Induction as a Function of LET

When plotted against LET values the induction cross section (figure 4.17) appears to reach a plateau value of about 1.05 $x10^{-8}$ cm^2 at LET of about $2x10^2$ - $4x10^3$ keV/μm, it then rises steeply for the higher LET values probably reflecting the importance of delta electrons in this region.

The relative biological effectiveness for DSB induction (RBE_{dsb}) (relative to unfiltered 80 kV X-rays), on the other hand, falls below unity for LET values above 10^3 keV/μm. A comparison of the derived DSB production cross-sections with the corresponding cross-section for inactivation yields shows a close relationship between the two end-points for a given ion.

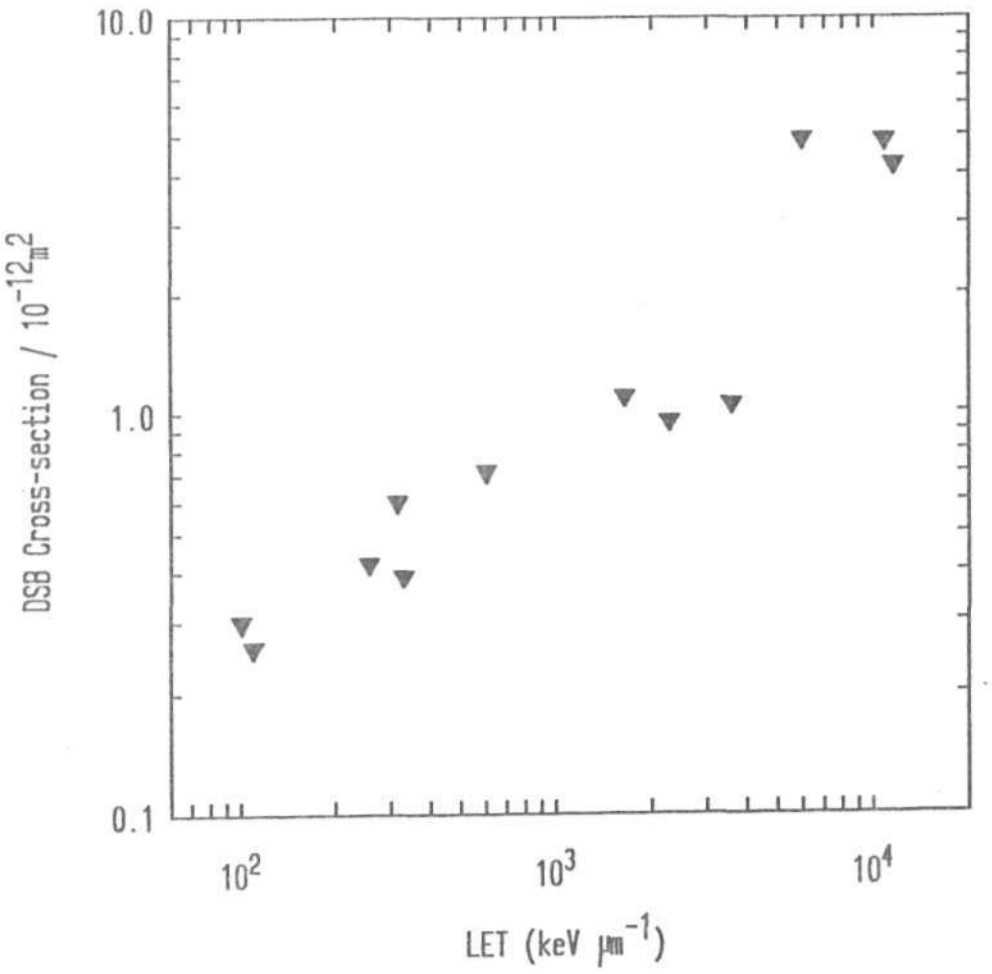


Figure 4.17: DSB production cross-section as a function of LET

CHAPTER FIVE

5.0 DISCUSSION

5.1 Separation of yeast chromosomes

The conditions used for the electrophoresis enable the separation of fifteen yeast chromosomes. Thus the described PFGE method is very applicable to yeast. Earlier problems with the system such as background fluorescence (excess fluorescence due to ethidium bromide not intercalated with the DNA) and the camera's shading effect have been eliminated. In the described method, about 70 ng of DNA was used per sample lane for the ethidium bromide fluorescence to be detectable. Preliminary experiments have demonstrated that theses are the optimal electrophoretic conditions for our technique. It has been previously reported (Löbrich *et al* 1993a) that chromosomes XII and IV are inverted with respect to their positions; consequently, chromosome IV and not XII was used for the DSB-evaluations. Therefore, a contamination of the upper band due to trapping or radiation-induced fragmentation cannot be ruled out. However, since such contamination would be expected to be dose-dependent, the exponential nature of the DSB-induction curves indicates that this is only a minor effect. Data obtained for the other bands for X-rays also supports this view since the induction rates remain virtually the same without taking account of the contamination effect.

5.2 DSB Measurement by PFGE

Other DSB assays like neutral filter elution and neutral sucrose sedimentation measure the average radiation-induced response of the constituent chromosomes in the DNA, whereas the electrophoretic method described here enables the responses of the individual chromosomes to be examined and monitored. This possibility can become very

useful since it can provide information as to whether or not the DSB induced by a given radiation follow a Poisson distribution (Löbrich *et al.* 1993b). This question was addressed by Frankenberg *et al.* (1979) by comparing yeast DNA profiles of stochastically broken controls with those of irradiated samples. More recently Friedl *et al.* (1993), who measured DSB induction in yeast exposed to γ-rays under anoxic conditions as well as Cederval and Källman (1994) also considered this problem. The doses and particle fluences considered in these reports were, however, higher (by a factor of 10) than those used in the PFGE method reported here.

The complete resolution of the chromosomes is clearly impossible with mammalian cell DNA since it is too large to enter pulsed field gels. To get round this problem, PFGE has often been used in the form of a modified elution assay (Blöcher *et al.* 1988) for DSB measurement in mammalian cells. The fraction of DNA released from the well is used as a signal to deduce DSB frequencies. Modifications exist in the literature, though, which allow for the measurement of smaller fragments of DNA after restriction enzyme digestion (Löbrich *et al.* 1994a) as well as the identification of specific pieces by hybridization to single copy genes (Löbrich *et al.* 1994b). These attempts to adapt the simplicity of the yeast technique to mammalian cells still suffer from rather low sensitivity making it necessary to apply 'supralethal' doses for the DSB measurements.

It should be pointed out, though, that the PFGE method as used here, does not measure DSB *per se*, but rather DNA fragmentation and is thus unable to resolve clusters of breaks. Whether this leads to an underestimation of the DSB induction frequencies is not clear. However the results are consistent with those published in the literature. The present work extends the measurements of DSB induced in yeast by heavy ions; previous determinations used the classical velocity sedimentation method (Frankenberg *et al.* 1981;

Akpa *et al.* 1992). The values obtained by PFGE seem to be consistent with these results although different ions and energies were used (Ikpeme *et al.* 1994). In general, one may conclude that the initial yield of DSB induced by heavy ions as determined in this work is either smaller than expected on theoretical grounds, or the breaks are present in clusters not detectable with the technique used.

5.3 DSB Repair Kinetics

DSB repair was performed by measuring the restoration of DNA of the first band after different incubation times in non-growth medium. Again the PFGE method has a clear advantage over the others, since the different chromosomes can be examined with a view to assessing 'correct' rejoining as against the neutral filter elution or sedimentation methods which 'look at' the entire DNA and hence cannot determine whether the repair is correct or not. This again demonstrates the wide applicability of the described method for studying DSB induction in yeast.

Yeast cells are particularly suitable to study DNA repair since a great variety of repair-deficient mutants are available (Haynes and Kunz 1981). Random rejoining produces a smear at higher molecular weights while correct rejoining leads to the reappearance of a band which can be measured electrophoretically or through hybridization to single copy genes . When a double strand break is formed in the DNA, the possibility exists that the two ends of the break may move apart and become enzymatically joined with the termini of a different double strand break- this constitutes incorrect rejoining or misrepair. The fact that the PFGE method detects the reappearance of a band (corresponding to a specific chromosome) means that it detects correct restitution of the original fragment.

The repair of radiation-induced DNA-DSB during postirradiation incubation in various types of cells have been reported under growth or non-growth conditions with monophasic (Bradley and Kohn 1979; Bryant and Blöcher 1980) or biphasic (Cole *et al.* 1980; Van der Schans *et al.* 1982a, 1983; Coquerelle *et al* 1987) kinetics. The repair under growth conditions in mammalian cells is exponential with time (first order reaction) and independent of dose as shown for mouse (Bradley and Kohn 1979) and Ehrlich ascites tumour cells (Blöcher and Pohlit 1982). Great variations in the half-time constants $t_{1/2}$ are observed for DSB rejoining under growth conditions, which may depend on the method of DSB measurement (Frankenberg-Schwager 1990): an initial fast component with a $t_{1/2}$-value of 3-10 minutes (Cole *et al.* 1980; Van der Schans *et al.* 1983; Weibezahn and Coquerelle 1981) is followed by a slow component, the $t_{1/2}$-value of which ranges from 40 minutes to 4 hours (Lehman and Stevens 1977; Bradley and Kohn 1979; Bryant and Blöcher 1980). On the other hand, DSB rejoining under non-growth conditions is slower with $t_{1/2}$-value of 3 hours as against $t_{1/2}$= 1.8 hours for growth conditions (Bryant and Blöcher 1980).

The results presented here (see figure 4.10) confirm the well known biphasic repair kinetics with a $t_{1/2}$-value of 2.5 hours for the fast component. It appears however, that secondary DSB are induced on incubation in a dose dependent manner. The induction of secondary DSB may be due to an interaction on incubation between non-DSB lesions. Recently, such an interaction of non-DSB lesions to form DSB has been reported for UV-induced lesions in diploid yeast *S. cerevisiae* after incubation in growth medium (Kiefer and Feige 1992). However, the issue requires further elucidation.

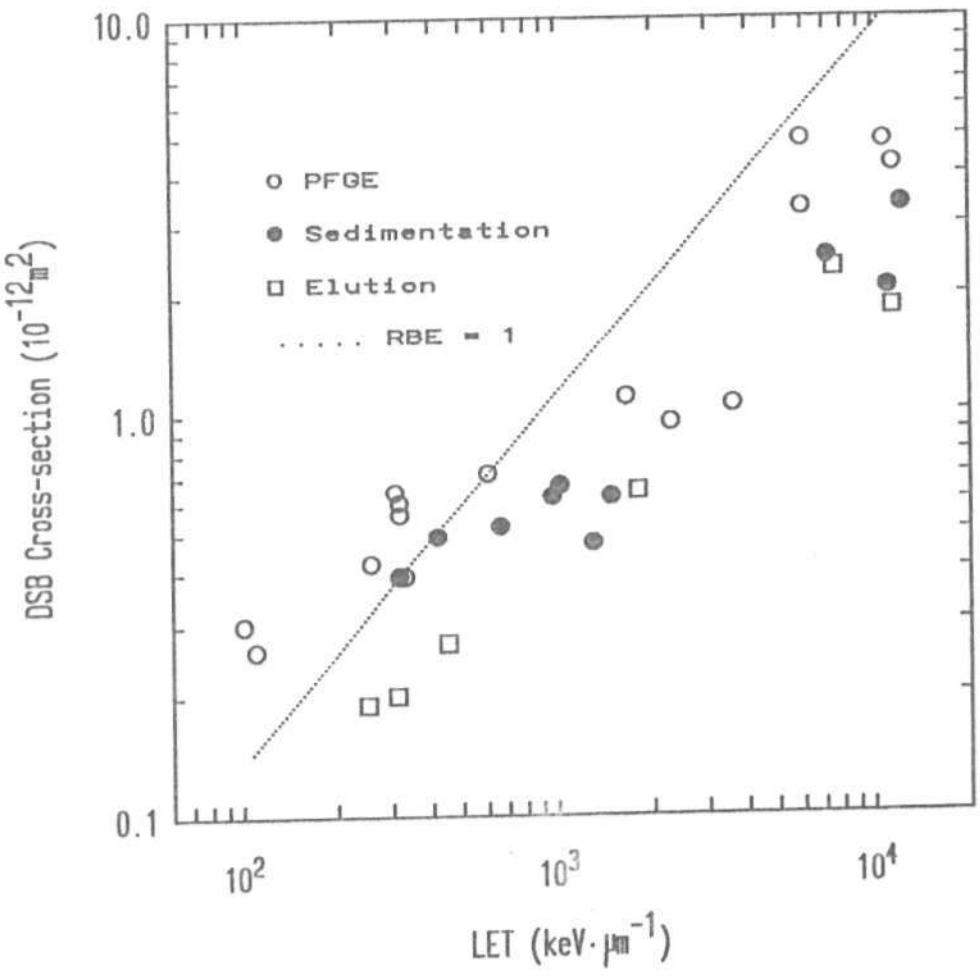


Figure 5.1: Comparison of PFGE (this work) with sedimentation (Akpa *et al.* 1993) and elution (Weber and Flentje 1993) results.

5.4 LET Dependence and RBE for DSB Induction

The results presented (see figure 4.17) show that there exists no unambiguous relationship between the LET and DSB induction cross-section. The cross-sections seem to "plateau" in the region between 200 and 1000 keV/μm. This may be interpreted as being due to a limited probability of an ion to produce DSB as long as effects by delta electrons in the so-called 'penumbra' are negligible. Inside this LET region the relative biological effectiveness (RBE) decreases from values of about 2 down to 0.5 supporting the above mentioned point. In LET regions where the number of delta electrons per particle increases so that the track structure plays a major role in the energy deposition (starting from about $2x10^3$ keV/μm), the cross-section rises above the 'plateau' region. Accordingly, the RBE does not further decrease in this region, but remains constant at a value of about 0.4. This may reflect the fact that DSB induction in the higher LET region is mainly due to interaction with the penumbra, where about 50% of the total energy is deposited (Löbrich 1994).

In the low LET region there is good agreement between the data presented in this work and those of the velocity sedimentation technique (see figure 5.1) but in the high LET region there exists some discrepancies. Such a discrepancy is, however, not without precedence; published values for low LET DSB-yields in mammalian cells have a range over a factor of four (Ward 1990). Also, it should be borne in mind that delta electrons play a more prominent role in the higher LET range and probably give rise to a high component of indirect effects that is modifiable by intracellular conditions and it is known that the sedimentation technique is less sensitive than the PFGE method. (Löbrich *et al.* (1993b) reported a higher DSB yield for 80 kV X-rays than Frankenberg *et al* (1981) did for 33 MeV electrons using the same yeast strain). Further, it is not immediately clear,

whether the two techniques actually measure the same lesions. However, for a meaningful comparison to be made between the two methods, it is necessary that not only the LETs but the ions themselves be the same because ions of the equal LETs can have different track structures depending on their mass numbers and specific energies.

As pointed out earlier, clusters of DNA breaks are not resolvable by the method presented in this work- and this applies also to the sedimentation technique. Consequently, if such clusters are present- and there is every reason to believe that they are present especially for high LET ions- approximately over distances smaller than 10-100 kilobase-pairs, they will be measured as single DSB. This leads to an underestimation of the induced breaks. Hence the overall fidelity of a given technique to detect DSB can be estimated by its sensitivity to low-ion fluence induced DSB. In this respect, the described PFGE method has a clear advantage over the velocity sedimentation technique since very low ion fluences (where the surviving fraction is very high) are used throughout in the measurements.

Cell inactivation was studied concomitantly with the DSB measurements and the inactivation cross-sections (derived from the final slope of the survival curves) seem to follow the same LET dependence (as exhibited by figure 5.2) as the DSB production cross-sections if normalized to the same DNA content. This means that a constant number of DSB are induced per lethal event. However, no such relationship between DSB induction and cell inactivation for ions with different LET values has been seen for mammalian cells (Weber and Flentje 1993). This difference in the responses of the two biological systems suggests that repair processes for heavy ion induced DSB are different in the two systems . Another aspect, however, may also play a role: the ion fluences for the same degree of inactivation are vastly different for yeast and mammalian cells (roughly

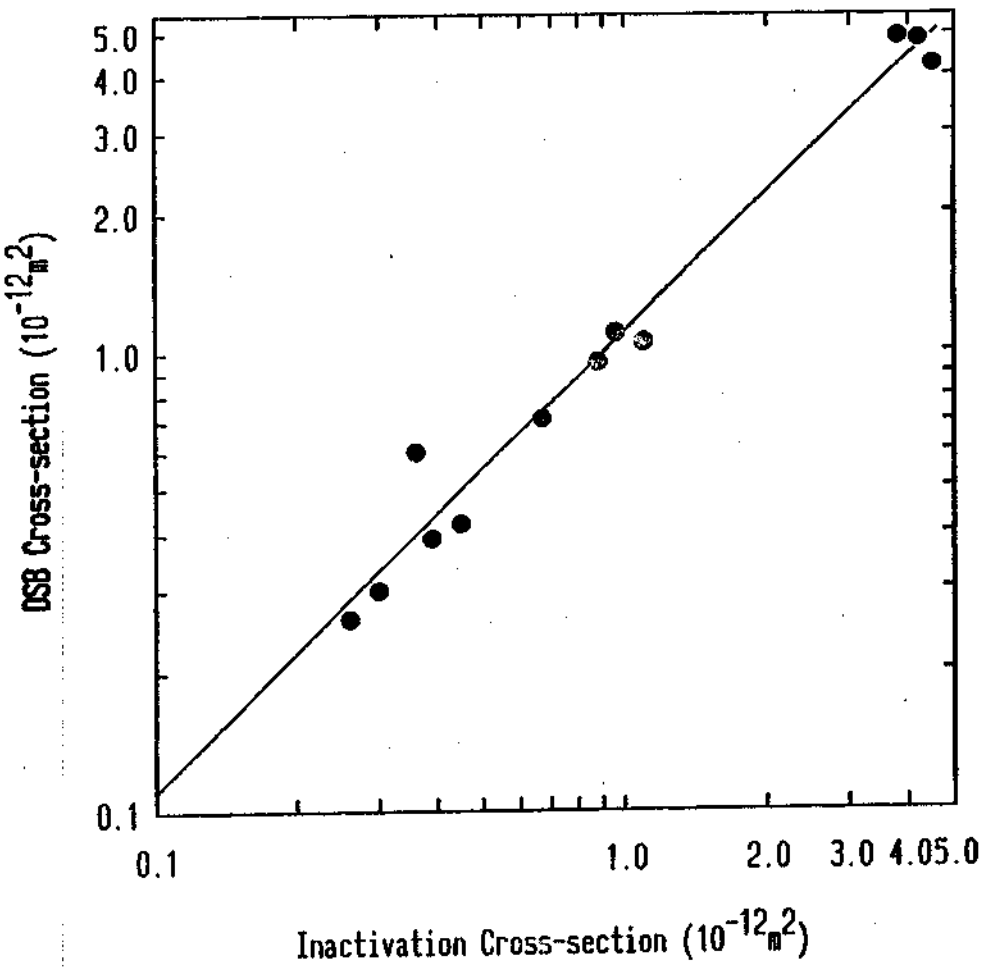


Figure 5.2: Parallelism between the production cross-section for initial DSB and that for inactivation

by a factor of hundred). This means that in mammalian cells the individual tracks are well separated while they overlap in yeast. If the repair systems act independently on the damage induced by well-separated tracks exponential survival curves are expected (Kiefer and Löbrich 1992). Indeed, it has been recently reported (Dardalhon *et al.* 1994) that the dose-rate does play a part in the induction of DSB. There is also the problem of the differences in technique - PFGE versus neutral filter elution. Therefore, it would be impossible to completely resolve these inconsistencies until studies are carried out with the two biological systems using comparative ion fluences and assays.

The close parallelism between the inactivation and cross-section for the production of initial DSB is rather surprising. If it is the unrepaired DSB that lead to cell killing (Frankenberg-Schwager *et al.* 1981) then the cross-sections for the production of such DSB should be close to the inactivation cross-sections (Löbrich 1994). This is a further argument for the supposition that the DSB cross-sections reported in this work may be lower than what they really are. It is also not beyond the realms of probability that the DSB induced by high LET ions are nearly irreparable. This would run counter to the findings of Rydberg *et a.l* (1994) who studied the repair of SV-40-transformed human fibroblasts after heavy ion irradiation and found that the residual DSB cross-sections correlated well with inactivation cross-sections, eventhough the `heavy ions they used had such high energies and consequently large penumbras that they can hardly qualify to be termed `heavy ions'.

Using track structure simulation, Brenner and Ward (1992) found that RBE values for DSB induction are low in comparison with the much higher RBE for cell reproductive death, chromosomal aberrations and other effects. They suggested that the high RBE for these effects could be due to the requirement of a very complex DSB or the production of

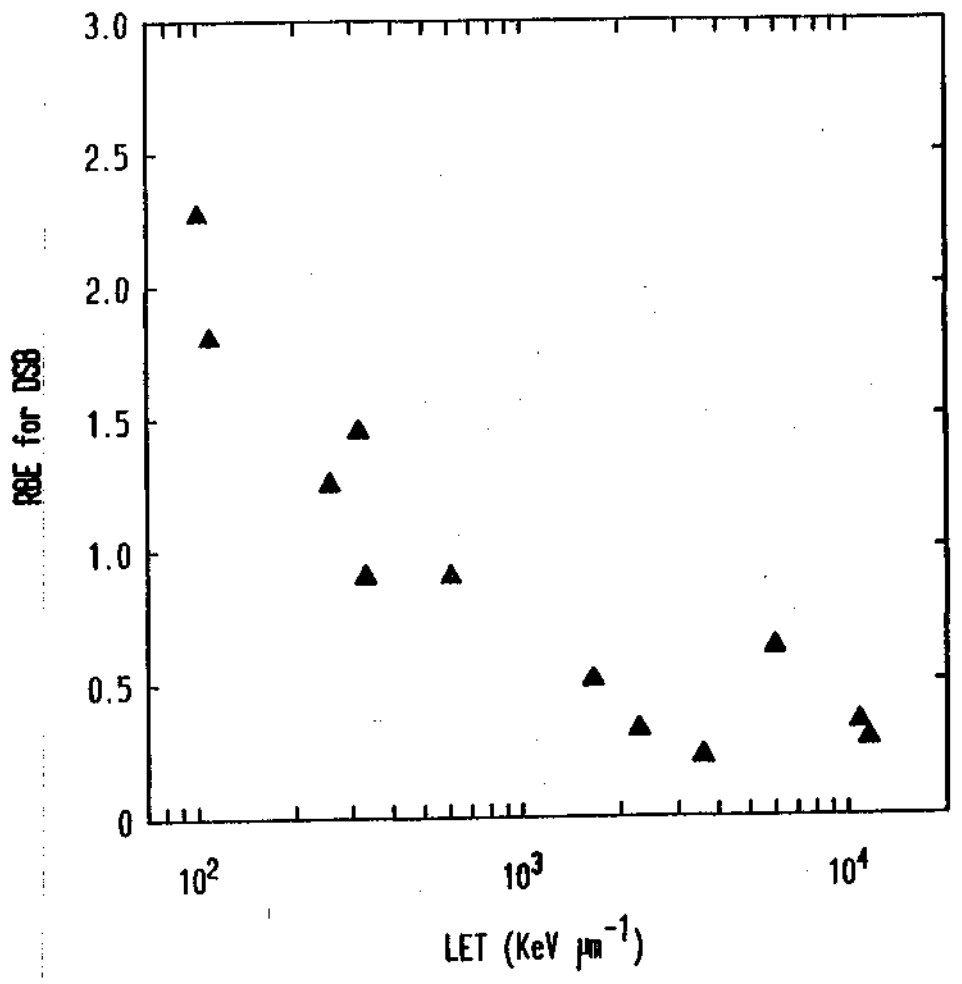


Figure 5.3: RBE for DSB production as a function of LET

two DSB in close proximity increasing the probability of an exchange type of misrepair. However, the experimental data presented here shows a more complex RBE_{dsb}-LET (see figure 5.3) relationship and requires further studies for complete elucidation. On the other hand, if heavy ion induced DSB are indeed more complex and irreparable than those induced by low LET radiation, this would mean that, for heavy ions, the initial DSB yield is not much different from the final yield.

Regarding the calculated RBE-values, it is evident that RBE values, in general, will depend on the reference radiation. This being the case, a direct comparison of RBE-values with those in the literature will always remain controversial. For instance the pioneers of heavy ion induced DSB studies reported RBE values of between 2 and 5 for α-particles of LET between 100 and 150 keV/μm, when compared with X-rays (Frankenberg *et al.* 1981, Kampf and Eichhorn 1983), more recent studies show that there is no significant difference between the two radiations (Coquerelle *et al.* 1987, Prise *et al.* 1987, Peak *et al.* 1988, Fox and Mcnally 1990).

5.5 Conclusions

A computer-based PFGE technique has been presented which has a minimum of errors and with which DSB can be rapidly and easily measured. The results confirm earlier findings that DSB are induced linearly with ion fluence. However, results do not indicate any unambiguous relationship between DSB production efficiency and either obtained the LET or ion energy.

Together with the previous measurements of Akpa *et al.* (1992), the presented set of results constitute the most complete compilation of yeast DSB induction cross-sections covering several orders of magnitude of LET. The results, in the main demonstrate, that

DSB are induced linearly with ion fluence. The conclusions which may be drawn from the foregoing are as follows: it appears that a direct correlation can be made between the induced DSB and cell lethality but how "direct" is that correlation remains to be further elucidated; at least for the "low fluences" used for the DSB analyses, it appears that the induced DSB are distributed according to Poisson statistics. More work is necessary with ions of lower LET in order to have a more complete picture regarding the LET-dependence. More studies are necessary in the following areas: to establish whether or not the so-called "LET-hooks" which have been reported for inctivation (Kiefer and Schneider 1987) also occurs for DSB induction; repair of heavy ion induced DSB; the use of higher ion fluences (and energies) probably with different electrophoretic conditions;work on the other chromosomes as well as to address the question whether or not there exists chromosome-specific effects with regard to DSB induction. Additionally, it is recommended that the smear in the electrophoretic gels as well as the amount of DNA trapped in the wells be further analysed.

REFERENCES

Adams, J. H. (JR).; M. M. Shapiro; R. Silberberg and C. H. Tsao (1981). Calculated isotopic source composition and tests for origin and propagation of cosmic rays with mass numbers 62. *Proceedings of the 17th International Cosmic Ray Conference 2*: 256-259.

Ager, D. D. and W. C. Dewey (1990) Calibration of pulsed field gel electrophoresis for measurement of DNA double-strand breaks. *Int. J. Radiat. Biol. 58*: 249-259.

Ager, D. D.; W. C. Dewey; K. Gardiner; W. Harvey; R. T. Johnson and C. A. Waldren (1990) Measurement of radiation-induced DNA double-strand breaks by pulsed-field gel electrophoresis. *Radiat. Res. 122*: 181-187.

Ahn, S. Y.; B. Nevaldine and P. J. Hahn (1991) Direct measurement by pulsed-field gel electrophoresis of induction and rejoining of X-ray-induced double-strand breaks in cultured mouse cells. *Int. J. Radiat. Biol. 59*: 661-175.

Ahnström, G. and P. E. Bryant (1982) DNA double-strand breaks generated by the repair of X-ray damage in Chinese hamster cells. *Int. J. Rad. Biol 41*: 671-676.

Akpa, T. C.; K. J. Weber; E. Schneider; J. Kiefer; M. Frankenberg-Schwager; R. Harbich and D. Frankenberg (1992) Heavy ion-induced double-strand breaks in yeast. *Int. J. Rad. Biol.* 62:279-287.

Akpa, T. C.; K. J. Weber; J. Kiefer; M. Frankenberg-Schwager; R. Harbich; and D. Frankenberg (1991) DNA double strand break induction in yeast by heavy ion irradiation. In: Fielden E. M., P. O'Neill (Eds): *The early effects of radiation on DNA*. Springer - Verlag. pp 307-308.

Alonso, J. R.; J. Howard; T. Criswell; W. Chu; F. Lothrop and C. Weber (1980) The BEVALAC biomedical facility. In: Pirruchello and C. A. Tobias (Eds.) *Biological and Medical Research with accelerated heavy ions at the Bevalac, 1977-1980* Lawrence Berkeley Laboratory, LBL-112220.

Alper, T. (1979) *Cellular Radiobiology* Cambridge University Press, Cambridge.

Angert, N. and C. Schmelzer, (1977) UNILAC, the accelerator facility for heavy ions of the GSI. *Kerntechnik 19*: 57-66

Aufderheide, E.; H. Rink; L. Hieber and G. Kraft (1987) Heavy ion effects on cellular DNA: strand break induction and repair in cultured diploid lens epithelial cells *Int. J. Radiat. Biol. 51*: 779-790.

Barendsen, G. W. (1964) Impairment of the proliferative capacity of human cells in culture by alpha-particles with differing linear energy transfer. *Int. J. Radiat. Biol. 8*: 453-466.

Barendsen, G. W. (1968) Response of cultured, tumours and normal tissues to radiation of different linear energy transfer. *Curr. Topics in Rad. Res. 4*: 293-316.

Barendsen, G. W.; H. M. D Walter; J. F. Fowler and D. K. Bewley (1963) Effects of different ionizing radiations on human cells in tissue culture III Experiments with cyclotron-accelerated alpha-particles and deuterons. *Radiat. Res. 18*: 106-119.

Barendsen, G. W.; T. L. J. Beusker; A. J. Vergroessen and L. Budke (1960) Effects of different ionizing radiations on human cells in tissue culture. *Radiat. Res. 13*: 841-854.

Barkas, M. J. and M. Berger (1963) Studies in penetration of charged particles in matter. *NAS NRC Publ. 1133 Nucl. Sci. Ser. Rep 39.*

Belli, M.; R. Cherubini; S. Finotto; G. Moschini; O. Sapora; G. Simone and M. A. Tobocchini (1986) RBE-LET relationships for the survival of V-79 cells irradiated with low energy protons. *Int. J. Radiat. Biol. 55*: 93-104.

Bertsche, U. (1977) Effekte in diploider Hefe bei bestrahlung mit verschiedenen Ionisationsdichten, *Phd Thesis,* Johann-Wolfgang Goethe Universität, Frankfurt am Main.

Bertsche, U. (1978) The response of diploid yeast to radiations of different LET I. Potentially lethal and lethal damage to reproductive capacity. *Radiat. Res. 76*: 349-367.

Bicknell, J. N. and H. C Douglas (1970) Nucleic acid homologies among species of *Saccharomyces. J. Bacteriol. 101*: 505-512.

Bimbot, R.; D. Gardes; H. Geissel; T. Kitahara; P. Armbruster; A. Fleury and F. Hubert (1983) Stopping power measurements 3-5 MeV/nucleon ^{86}Kr, ^{132}Xe, ^{208}Pb and ^{238}U in solids. *Nuclear Instrumentation Methods.*

Blakely, E. A.; C. A. Tobias; T. C. H. Yang; K. C. Smith and J. T. Lyman (1979) Inactivation of human kidney cells by high energy monoenergetic heavy-ion beam. *Radiat. Res. 80*: 122-160.

Blakely, E. A.; F. Q. H. Ngo; S. B. Curtis and C. A. Tobias (1984) Heavy-Ion Radiobiology: Cellular studies. In: Lett, J. T. (Ed.) *Advances in biology vol. II.* Academic Press, New York. pp 295-389.

Blöcher, D. (1982) DNA double-strand breaks in Ehrlich ascites tumour cells at low doses of X-rays I. Determination of induced breaks by centrifugation at low speed. *Int. J. Radiat. Biol.* 42: 317-328.

Blöcher, D. (1988) DNA double-strand break repair determines the RBE of α-particles. *Int. J. Radiat. Biol. 54*: 761-771.

Blöcher, D. (1990) In CHEF electrophoresis a linear induction of DSB corresponds to a non-linear fraction of extracted DNA with dose. *Int. J. Radiat. Biol. 57*: 7-12.

Blöcher, D. and M. Kuhni (1990) DNA double-strand break analysis by CHEF electrophoresis. *Int. J. Radiat. Biol. 58*: 23-34.

Blöcher, D. and W. Pohlit (1982) DNA double-strand breaks in Ehrlich ascites tumour cells at low doses of X-rays II. Can cell death be attributed to double-strand breaks? *Int. J. Radiat. Biol. 42:* 329-338.

Blöcher, D.; M. Einspenner and J. Zajackowski (1989) CHEF electrophoresis, a sensitive technique for the determination of DNA double strand break measurements. *Int. J. Radiat. Biol. 56*: 437-448.

Böhne, D. (1984) Heavy ion accelerators. *Interdisciplinary Science Reviews 9*:294-304.

Boniszewski, Z. A. M.; J. S. Comly, B. Hughes and C. A. Read (1990) The use of charge-coupled devices in the quantitative evaluation of images, on photographic film or membranes, obtained after electrophoretic separation of DNA fragments. *Electrophoresis 11*: 432-440.

Booz, J.; J. A. Dennis and H. Menzel (1990). Microdosimetry In: Booz, J.; J. A. Dennis and H. Menzel (Eds.) *Proc. 10th Symp. Microdosimetry in Rome, Italy. Radiation Prot. Dosimetry 31*: 1-4. Nuclear Technology Publishing, Kent, UK.

Bradley, O. and K. W. Kohn (1979) X-ray induced double strand break production and repair in mammalian cells as measured by neutral filter elution. *Nucleic Acids Res. 7*: 793-804 .

Brenner, D. J. and J.F. Ward (1992) Constraints on energy deposition and target size of multiply damaged sites associated with DNA double-strand breaks. *Int. J. Radiat. Biol. 61:* 737-748.

Bryant, P. E. and D. Blöcher (1980) Measurement of the kinetics of DNA double-strand break repair in Ehrlich ascites tumour cells using the unwinding method. *Int. J. Radiat. Biol. 38*: 335-347.

Butts, J. J. and R. Katz (1967) Theory of RBE for heavy ion bombardment of dry enzymes and viruses. *Radiat. Res. 30*: 855-871.

Carle, G. F. and M. V. Olson (1984) Separation of chromosomal DNA molecules from yeast by orthogonal-field gel electrophoresis. *Nucl. Acid Res. 12*: 5647-5664.

Carle, G. F.; M. Frank and M. V. Olson (1986) Electrophoretic separation of large DNA molecules by periodic inversion of electric field. *Science 232*: 65-68.

Cederval, B. and P. Källman (1994) Randomly distributed DNA double-strand breaks as measured by pulsed field gel electrophoresis: a series of explanatory calculations. *Radiat. Environ. Biophys.* 33: 9-21.

Chadwick, K. H.; G. Mosehini and M. Varma (1991). In: Chadwick, K. H.; G. Mosehini and M. Varma (Eds.) *Biophysical modelling of radiation effects workshop, Padua, Italy.* DOE.

Chatterjee, A. and H. J. Schaefer (1976) Microdosimetric structure of heavy ion tracks in tissue. *Radiat. Environ. Biophys. 13*: 215-126.

Chatterjee, A.; H. Maccabee and C. A. Tobias (1973) Radial cut-off LET and radial cut-off-dose calculations for heavy charged particles in water. *Radiat. Res. 54*: 479-494.

Chu, G. (1991) Pulsed-field electrophoresis of megabase-sized DNA. *Mol. Cell. Biol. 11*: 3348-3354.

Chu, G.; D. Vollrath, and R. W. Davis (1986), Separation of large DNA molecules by contour-clamped homogeneous electric field. *Science 234:* 1582-1565.

Coggle, J. E., (1983) *Biological effects of Radiation.* Taylor and Francis Ltd., London.

Coguerelle, T.; U. Hagen; W. Kohnlein and W. Crump, (1978) Radiation effects on the biological function of DNA. In: Bertinchamps, A. J. Hütterman, W. Kohnlein and R. Teole (Eds.) *Effects of Ionizing Radiation on DNA.* Springer-Verlag, Berlin/New York.

Coguerelle, T.; Weibezahn, K. F. and C. Lucke-Huhle (1987) Rejoining of double-strand breaks in normal human and *Ataxia telangiectasia* fibroblasts after exposure to ^{60}Co γ-rays, ^{241}Am α-particles or bleomycin. *Int. J. Radiat. Biol. 51*: 209-218.

Cole, A.; R. E. Meyn; R. E. Chen; P. M. Corry; W. Hittelman (1980) *Radiation biology in cancer research.* Raven Press, New York.

Contopoulou, V. Cook and R. Mortimer, (1987) Analysis of DNA double strand breakage and repair using orthogonal field alternating gel electrophoresis. *Yeast 3*: 71-76.

Cook, V. and R. K. Mortimer (1991) A quantitative model of DNA fragments generated by ionizing radiation and possible experimental applications. *Rad. Res. 125*: 102-106.

Coquerelle, T.; A. Bopp; B. Kessler and U. Hagen (1973) Strand breaks and 5' end-groups in DNA of irradiated thymocytes. *Int. J. Rad. Biol 24*: 397-404.

Coquerelle, T; K. F. Weibezahn and C. Lucke-Huhle (1987) Rejoining of double strand breaks in normal human and *Ataxia telengiectasia* fibroblasts after exposure to ^{60}Co γ-rays, ^{241}Am α-particles or bleomycin. Int. J. Radiat. Biol. 51: 209-218.

Curtis, S. B. (1974) Radiation physics and current hazards. In: Tobias, C. A. and P. Todd (Eds.) *Space Radiation Biology and Related Topics.* Academic Press, New York.

Dardalhon, M.; A. Nohturfft; V. Meniel and D. Averbeck (1994) Repair of DNA double-strand breaks in Saccharomyces cerevisiae using different γ-ray dose-rates: a pulsed field gel electrophoresis analysis. *Int. J. Rad. Biol.* 65: 307-314.

Darymple, G. V. and M. L. Baker (1973) Molecular biology. In: Darymple, G. V.; M. E. Gaulden; G. M. Kollmorgen and H. H. Vogel (Eds) *Medical Radiation Biology*. W. B. Saunders Company, Philadelphia.

Darymple, G. V.; M. E. Gaulden; G. M. Kollmorgen and H. H. Vogel (1973) *Medical Radiation Physics* W. B. Saunders Company Philadelphia, London Toronto.

Dawkins, S. J. H.; D. J. Ferrier and T. L. Spencer (1987) Field inversion gel electrophoresis (FIGE) in vertical slabs as an improved method for large DNA separation. *Nucl. Acids Res. 15*: 3634-3635.

Dunkan, W. and A. H. W. Nias (1977) *Clinical Radiobiology* Churchill Livingstone Press, Edinburgh.

Ebert, H. G. (1983) Introductory Remarks. In: Booz, J and H. G. Ebert (Eds.) *Proc. 8th Symp. Microdos.* Sept. 27- Oct. 01 Jülich, Germany EURATOM ECSC-EEC-EAEC, Brussels.

Evans, H.; M. Ricanati and M. F. Horng (1987) Deficiency in DNA repair in mouse lymphoma strain L5178Y-S. *Proc. Natl. Acad. Sci. USA 84*: 7562-7566.

Fain, J., M. Monin and M. Montret (1974) Energy density deposited by a heavy ion around its path. In: Booz, J., H. J. Ebert, R. Eickel and A. Waker, *Proceedings of the 4th Symposium onMicrodosimetry*. Luxembourg EURATOM. pp 169-188.

Fleischer, P. L.; P. B. Price and R. M. Walter (1965) Solid state track detectors: application to nuclear science and geophysics. *Annual Review of Nuclear Science 15*: 1-28.

Fowler, J. F. (1989) Applications to radiobiology and radiotherapy. *Nucl. Tracks Radiat. Meas. 16:* 89-95.

Fox, J.C. and N. J. Mcnally (1990) The rejoining of DNA doubl-strand breaks following irradiation with ^{238}Pu α-particles: evidence of a fast component of repair as measured by neutral filter elution. *Int. J. Rad. Biol. 57*: 513-519.

Frankenberg, D.; M. Frankenberg-Schwager; D. Blötcher and R. Harbich (1981). Evidence for DNA double-strand breaks as the critical lesions in yeast cells irradiated with sparsely ionizing radiation under oxic or anoxic conditions. *Radiat. Res. 88*: 524-532.

Frankenberg-Schwager, M and D. Frankenberg (1990) DNA double-strand breaks: their repair and relationship to cell killing in yeast. *Int. J. Radiat. Biol. 58*: 569-575.

Frankenberg-Schwager, M. (1990) Induction, repair and biological relevance of radiation-induced DNA lesions in eukaryotic cells. *Radiat. Environ. Biophy. 29:* 273-292.

Freeman, S. E.; L. L. Larcom and B. D. Thompson (1990) Electrophoretic separation of nucleic acid: evaluation by video and photographic densitometry. *Electrophoresis 11*: 425-431.

Fricke, H. and S. J. Hart (1968) Chemical dosimetry. In: Attix, F. H. and W. C. Roesch (Eds.) *Radiation dosimetry Vol. II.* Academic Press, New York pp 167-232.

Friedl, A. A.; W. Beisker; K. Hahn; F. Erkardt-Schupp and A. M. Kellerer (1993) Application of pulsed field gel electrophoresis to determine γ-ray induced double strand breaks in yeast chromosomal molecules. *Int. J. Radiat. Biol 63*: 173-181.

Gardiner, G. and D. Patterson, Transverse alternating electrophoresis (1988) Nature 331: 371-372 .

Gemmill, R. M. (1990) Pulsed field gel electrophoresis. In: Chrambach, A., M. J. Dunn and B. J. Radola (Eds) *Advances in electrophoresis* pp 1-44. VCH New York.

Ghiorso, A.; H. Grunder; W. Hartsough; G. Lampertson; Z. Löfgren; K. Lou; R. Main; R. Mobley; R. Morgado; W. Salsig and F. Selph (1973) The BEVALAC, an economical facility for very high energetic particle research. *IEEE Trans. Nucl. Sci.; NS-20*: 155.

Giaccia, A.; R. Weinstein; J. Hu and T. D. Stamato (1985) Cell cycle-dependent repair of double-strand breaks in a gamma-ray-sensitive Chinese hamster cell. *Somatic Cell and Molecular Genetics 11*: 485-491.

Goodhead, D. T. (1987) Relationship of microdosimetric techniques to applications in biological systems. In: Kase, K. R.; B. E. Bjärngard and F. H. Attix (Eds.) *The dosimetry of ionizing radiation Vol. II* Academic Press, New York.

Grosch, D. S. and L. A. Hopwood (1979) *Biological Effects of Radiations* Academic Press New York.

Grunder, H. A.; W. D. Hartsough and E. J. Lofgren (1971) Acceleration of heavy ions at the BEVATRON *Science 174*: 1128-1129.

Hansen, J. W. and K. J. Olsen (1984) Experimental and calculated response of a radiochromatic dye film dosimeter to high-LET radiations. *Radiat. Res. 97*: 1-5.

Haynes, R. H. and B. A. Kunz (1981) DNA repair and mutagenesis in yeast. In: Stratherm, J. N.; E. W. Jones and J. R. Broach (Eds). *The molecular biology of the yeast Saccharomyces.* Cold Spring Habor Laboratory, NY, pp 371-414.

Heinrich, W. and J. Beer (1984) The radiation situation in space and its modification by geomagnetic field and shielding. *Advances in space research 4*: 133-142.

Hubert, F.; R. Bimbot and H. Gauvin (1980) Range and stopping power tables for 2.5-500 MeV/u heavy ions in solids. *At. Nucl. Power Tables 46*: 1-215.

ICRU (1970) Linear energy Transfer *ICRU Rep. 16* ICRU, Bethesda, Maryland.

Ikpeme, S.; M. Löbrich; E. Schneider and J. Kiefer (1994) Heavy ion induced DNA double strand breaks with yeast as a model system. *Rad. Environ. Biophy.* (In Press).

Iliakis, G.; D. Blöcher; L. Mettzger and G. Pantelias (1991) Comparison of DNA double-strand break rejoining as measured by pulsed field gel electrophoresis, neutral sucrose centrifugation and non-unwinding filter elution in irradiated plateau-phase CHO-cells. *Int. J. Radiat. Biol. 59:* 927-939.

Jeggo, P. A. (1985) Genetic analysis of X-ray sensitive mutants of the CHO cell line. *Mut. Res. 146*: 265-270.

Jenner, T. J.; D. T. Goodhead; F. Ianzini; G. Simone and M. A. Tambocchini (1992) Direct comparison of biological effectiveness of protons and alpha particles of the same LET. III Initial yield of double-strand breaks in V79 cells. *Int. J. Rad. Biol 61*: 631-639.

Jung, H. and K. Kürzinger (1968) Inactivation of bacteriophage DNA and ribonuclease by thermal hydrogen atoms. *Radiat. Res. 36*: 369-383

Kampf, G. and K. Eichhorn (1983) DNA strand breakage by different radiation qualities and relations to cell killing: further results after the influence of alpha particles and carbon ions. Stud. Bioph. 93:17-26.

Katz, R. (1970) "RBE, LET and z^2/β^2" *Health Phys. 18:* 175

Katz, R.; B. Ackerson; U. Homayoonfar and S. C. Sharma (1971) Inactivation of cells by heavy ion bombardment. *Radiat. Res. 47*: 402-425.

Katz, R.; B. Ackerson; U. Homayoonfar and S. C. Sharma (1971) Inactivation of cells by heavy ion bombardment. *Radiat. Res. 47*: 402-425.

Katz, R.; D. E. Dunn and G. L. Sinclair (1985) Thin down in radiobiology. *Radiat. Proct. Dos. 13*: 281-284.

Kellerer, A. M. and H. H. Rossi (1972) The theory of dual radiation action. *Radiat. Res. Quarterly* 8: 471-488.

Kemp, D. J.; L. M. Corcoran; R. L. Coppel; H. D. Stahl; A. E. Bianco; G. V. Brown and R. F. Anders (1985) Size variation in chromosomes from independent cultured isolates of *Plasmodium falciparum. Nature 315*: 347-350.

Kemp, L. M.; S. G. Sedgwick and P. A. Jeggo (1984) X-ray sensitive mutants of Chinese hamster ovary cells defective in double-strand break rejoining. *Mut. Res. 132*: 189-196.

Kiefer, J. (1985) Energy deposition and the formation of biologically significant lesions by accelerated ions. *Radiat. Prot. Dos. 13*: 211-214.

Kiefer, J. (1985) Review: cellular and subcellular effects of very heavy ions. *Int. J. Radiat. Biol. 48*: 873-892.

Kiefer, J. (1988) Heavy ion effects on cells: An approach to theoretical understanding. In: McCormack, P. D.; C. E. Swenberg and H. Bucker (Eds.) *Terrestrial space radiation and its biological effects. Proceedings of NATO Advanced study institute on Terrestrial Space Radiation and its Biological Effects.* October 11-25, 1987 in Corfu, Greece.

Kiefer, J. (1990) *Radiation Biological Effects* Springer-Verlag Berlin Heidelberg New York.

Kiefer, J. (1991) Biological effects of electromagnetic and particle radiation. In: *Encyclopaedia of Applied Physics, Vol. 2* VCH Publishers, Inc. pp 365-401.

Kiefer, J. and E. Schneider (1987) Cellular effects of heavy ions: experimental results and theoretical approaches. Proceedings of the third European Symposium on Life Sciences Research in Space, Graz, Austria (14-18 September 1987) *ESA SP-271:* 205-208.

Kiefer, J. and H. Straaten (1986) A model of ion track structure based on classical collision dynamics. *Phys. Med. Biol. 31*: 1201-1209.

Kiefer, J. and H. Straaten (1989) Quantitative interpretation of heavy ion effects: Models for the biological effects of heavy ions. *Adv. Space Res. 10:* 21-29.

Kiefer, J. and M. Feige (1993) The significance of DNA double-strand breaks in the UV inactivation of yeast cells. *Mut. Res. 299*: 219-224.

Kiefer, J., (1987) Semi-empirical calculations of stopping power, effective charge and ranges of heavy ions (1-400 MeV/u) in water. 3rd Workshop on Heavy Charged Particles in Biology and Medicine. *GSI-Report 87*: 11.

Koval, M. and E. R. Kazmar (1988) Eluting solution composition affects DNA double-strand break analysis by filter elution. *Int. J. Radiat. Biol. 54:* 739-747.

Kozubek, S. and E. A. Krassavin (1984) Cell sensitivity to irradiation and DNA repair processes. *Neoplasma 31*: 685-695.

Kraft, G. (1987) Radiobiological effects of very heavy ions. *Nucl. Sci. Appl. 3:* 1-28.

Kraft, G. (1988) Effects of LET, fluence and Particle energy on inactivation, Chromosomal and DNA strand breaks. In: McCormack, P. C.; C. E. Swenberg and H. Bücker (Eds) *Terrestrial Space Radiation and its Biological Effects.* Plenum Press, New York.

Kraft, G.; H. W. Daues; B. Fischer; U. Kopf; H. P. Liebold; D. Quis; H. Stelzer; J. Kiefer; F. Schöpfer; E. Schneider; K. Weber; H. Wulf and H. Dertinger (1980) Irradiation chamber and sample changer for biological samples. *Nucl. Instr. and methods 168:* 175-179.

Kraft, G.; Krämer, and M. Scholz (1992) LET, track structure and models. *Radiat. Environ. Bio. 31*: 161-180.

Krämer, M. and G. Kraft (1987) Radiobiological effects of very heavy ions. *Nucl. Sci. Appl. 3*: 1-28.

Lehman, A. R. and M. G. Ormerod (1970) Double strand breaks in the DNA of a mammalian cell after X-irradiation. *Biochimica et Biophysica Acta* 217: 268-277.

Lehmann, A. R. and S. Stevens (1977) The production and repair of double strand breaks in cells from normal humans and from patients with ataxia telangiectasia. *Biochimica et Biophysica Acta* 474:49-70.

Lett, J. T. (1992) Damage to cellular DNA from particulate radiations, the efficacy of its processing and the radiosensitivity of mammalian cells. Emphasis on DNA double-strand breaks and chromatin breaks. *Radiat and Environ. Biophy. 31*: 257-277.

Levene, S. D. (1992) Theories of Pulsed Field Gel Electrophoresis. In: Burmeister, M. and L. Ulanovsky (Eds.) *Methods in Molecular Biology Vol. 12: Pulsed Field Gel Electrophoresis* pp 347-366. The Humana Press Inc., Totowa, NJ.

Löbrich, M. (1994) *Mechanismen der DNA-Doppelstrangbruch Induktion und Reparatur nach Exposition mit ionisierender Strahlung untersucht an menschlichen Zellen. Doctoral thesis. Justus Liebig Universität, Gießen, Germany.*

Löbrich, M., Ikpeme, S. and Kiefer, J. (1994b): DNA double strand break measurement in mammalian cells: An approach using restriction enzymes and gene probing. *Int. J. Radiat. Biol.* (In Press).

Löbrich, M; S. Ikpeme and J. Kiefer (1993a) Analysis of the inversion effect by a two-dimensional contour clamped electric field system. *Analytical Biochemistry 208*:65-73.

Löbrich, M; S. Ikpeme and J. Kiefer (1994a) Measurement of DNA double-strand breaks in mammalian cells by pulsed-field gel electrophoresis: A new approach using rarely cutting enzymes. *Rad. Res.138:* 186-192.

Löbrich, M; S. Ikpeme; P. Haub; K. J. Weber and J. Kiefer (1993b) Double strand break induction in yeast by X-rays and α-particles measured by pulsed field gel electrophoresis system. *Int. J. Rad. Biol. .64:* 539-546.

Maizel, J. V. Jr., (1971) Polyacrylamide gel electrophoresis if viral proteins. In: Maramorosch, K. and H. Koprowski (Eds.) *Methods in Virology* Academic Press, London.

Manney, T. R.; T. Brustad and C. A. Tobias (1963) Effects of glycerol and anoxia on the radiosensitivity of haploid yeast to densely ionizing particles. *Radiat. Res. 18*: 374-388.

Manney, T. R.; T. Brustad and C. A. Tobias (1963) Effects of glycerol and anoxia on the radiosensitivity of haploid yeast to densely ionizing particles. *Rad. Res. 18:* 374-388.

Metting, N. F.; H. H. Rossi; L. A. Braby; P. J. Kliauga.; J. Howard; M. Zaider; W. Schimmerling; M. Wong and M. Rapkin (1988) Microdosimetry near the trajectory of heavy ions. *Radiat. Res. 116*: 183-195.

Mortimer, R. K. and D. Schild (1985) Genetic map of *Saccharomyces cerevisiae*. *Microbiological Rev. 49*: 181-212.

Mozunder, A and J. L. Magee (1975) The early events of radiation chemistry. *Int. J. Radiat. Phys. Chem. 7:* 83.

Northcliffe, L. C. and R. F. Schilling (1970) Range and stopping power tables for heavy ions. Nucl. *Data Tables A7*: 233-437.

O'Farrell, P. H. (1975) High Resolution, two-dimensional electrophoresis of Proteins. *J. Biol. Chem. 250*: 4007-4021.

Obaturov, G. M. (1979) Biophysical model of ionizing radiation action on DNA. *Radiobiologica 19*: 163-171.

Okayasu, R.; D. Blöcher and G. Illiakis (1988) Variation through the cell cycle of DNA filter elution dose response in X-irradiated synchronous CHO-cells. *Int. J. Rad. Biol. 53*: 729-747.

Oleinick, N. L.; S. Chiu; L. Xue; N. Ramakishnan and L. R. Friedman (1990) Properties of DNA crosslinks (DPCs) induced by ionizing radiation. *J Cell Biochem*, [Suppl] 14A (abstr) UCLA Symposium: 80.

Peak, J. G.; E. R. Blazer; C. K. Hill and M. J. Peak (1988) Measurement of double strand breaks in Chinese hamster cell DNA by neutral filter elution: Calibration by ^{125}I decay. *Rad. Res. 115*: 624-629.

Perris, A.; P. Pialoglou; A. A. Katsanlos and E. G. Sideris (1986) Biological effectiveness of low energy protons. Survival of Chinese hamster cells. *Int. J. Radiat. Biol. 50*: 1093-1101.

Pizzarello, D. J. (1981) Radiation Biology CRC Press Florida.

Prise, K. M.; S. Davies and B. D. Michael (1987) Therelationship between radiation-induced DNA double-strand breaks and cell killing in hamster V79 fibroblasts irradiated with 250 kVp X-rays, 2.3 MeV neutrons or ^{238}Pu α-particles. *Int. J. Rad. Biol. 52*: 892-902.

Prunell, A.; F. Strauss and B. Leblanc (1977) Photographic quantitation of DNA in gel electrophoresis. *Analyt. Biochem. 78*: 57-65.

Radford, I. R. and G. S. Hodgson (1985) ^{125}I-induced DNA double strand breaks: use in calibration of the neutral filter elution technique and comparison with X-ray induced breaks *Int. J. Rad. Biol 48*: 555-566.

Radford, I. R. and G. S. Hodgson (1987) Effect of ploidy in the response V79 cells to ionizing radiation. *Int. J. Rad. Biol 51*: 765-778.

Raju, M. R.; E. Blakely; J. Howard; J. Lyman; D. P. Kalofonos; B. Martins and C. H. Yong (1976) Human cell survival as a function of depth for a high energy ion beam. *Radiat. Res. 65*: 191-194.

Ramakishnan, N.; S. Chiu and N. L. Oleinick (1987) Yield of DNA-protein cross-links in gamma-irradiated Chinese hamster cells. Cancer Res. 47: 2032-2035.

Resnick, M. A. (1976) The Repair of double-strand breaks in DNA: model involving recombination. *J. Theor. Biol. 59*: 97-106.

Ribeiro, E. A.; L. L. Larcom and D. P. Miller (1989) Quantitative fluorescence of DNA-intercalated ethidium bromide on agarose gels. *Analyt. Biochem. 181*: 197-208.

Rickwood, D. and B. D. Hames (1982) *Gel electrophoresis of Nucleic Acids*. IRL Press Ltd., London.

Roots, R., W. Holley; A. Chatterjee; M. Irizarry and G. Kraft (1990) The formation of strand breaks in DNA after high-LET irradiation: a comparison of data from *in vivo* and cellular systems. *Int. J. Rad. Biol 58*: 55-69.

Roots, R.; W. Holley; A. Chatterjee; M. Irizarry and G. Kraft (1990) The formation of strand breaks in DNA after high-LET irradiation: a comparison of data from *in vivo* and cellular systems. *Int. J. Rad. Biol 58*: 55-69.

Rydberg, B.; M. Löbrich and P. Cooper (1994) DNA double-strand breaks induction by high energy Ne and Fe ions in human fibroblasts. I. Pulsed field gel electrophoresis method. Rad. Res. (In the Press).

Sawada, S. and S. Okada (1970) Rejoining of single-strand breaks of Dna in cultured mammalian cells. *Radiat. Res. 41*: 145-162.

Schäfer, M.; H. Bücker; R Facius; G. Hörneck; G. Reitz and G. Kraft (1978) High LET irradiation of *Bacillus subtilis* spores. In: Booz, J. and H. G. Ebert. *Proceedings of the 6th Symposium on microdosimetry*. London: Harwood Publishers.

Schiott, H. E. (1966) Range energy relations for low energy ions. *Mat Fys Dan Vid Selsk 35*: 9.

Schmidt, S.; C. Kelbch; H. Schmidt-Böcking and G. Kraft (1988) Delta electron emission in heavy ion collisions. In: McCormak, P. D.; ChE Swenberg and H. Bücker. *Terrestrial Space_Radiation and its biological effects.* Plenum Press, New York, pp 205-212.

Schneider, E.; M. Kost and Schäfer, M., (1990) Inactivation cross section of yeast and bacteria exposed to heavy ions of low energy. *Radiat. Protect. Dos. 31:* 291-295.

Schöpfer, F. (1980) Die Inaktivierung von Hefezellen durch ionisierende Strahlung unterschiedlicher Energie-depositionmuster in Abhängigkeit von Sauerstoff- und Wassergehalt. *Inaugural disertation der Naturwissenschaften der Justus-Leibig-Universität Giessen.*

Schöpfer, F.; E. Schneider and G. Kraft (1978) The inactivation of cells by accelerated heavy ions of very high LET. In: Booz, J. and H. G. Ebert. *Proceedings of the 6th Symposium on_microdosimetry.*_London: Harwood Publishers.

Schöpfer, F.; E. Schneider; S. Rase and J. Kiefer (1982) Heavy ion effects in yeast: survival and recovery in vegetative cells of different sensitivity. *Radiat. Res. 92:* 30-46.

Schwartz, J. L. and C. R. Cantor (1984) Separation of yeast chromosome-sized DNAs by pulsed-field gradient gel electrophoresis. *Cell 37*: 67-75.

Stamato, T. D. and N. Denko (1990) Asymmetric field inversion gel electrophoresis: a new method for detecting DNA double-strand breaks in mammalian cells. *Radiat. Res. 121:* 196-205.

Stewart, G; A. Furst and N. Avdalovic, Transverse alternating gel electrophoresis (TAFE). *Bio_Techniques 6*: 68-73.

Sutherland, J. C.; B. Lin; D. C. Monteleone; J. Mugavero; B. M. Sutherland and J. Trunk (1987) Electronic imaging system for direct and rapid quatitation of fluorescenc from electrophoretic gels : application to ethidium bromide stained DNA. *Analyt. Biochem. 163*: 446-457.

Sutherland, J. C.; B. Lin; D. C. Monteleone; J. Trunk and G. Ciarrochhi (1984) Two-dimensional computer-controlled film scanner: quantitation of fluorescence from ethidium bromide-stained DNA gels. *Analyt. Biochem. 139*: 390-399.

Sweigert, A.; A. Rowley; R. Warters and L. Dethlefsen (1988) Cell cycle effect on the induction of DNA double strand breaks by X-rays. *Radiat. Res. 116*: 228-244.

Sweigert, S. E; R. Rowley; R. L. Warters and L. A. Dethlefsen (1988) Cell cycle effect on the induction of DNA double-strand breaks by X-rays. *Radiat. Res. 116*: 228-244.

Todd, P. W. and C. A. Tobias (1974) Cellular radiation biology. In: Tobias, C. A. and P. W. Todd (Eds.) *Space Radiation Biology and Related Topics* Academic Press, New York.

Van der Schans, G. P.; M. C. Paterson and W. G. Cross (1983) DNA strand-break and rejoining in cultured human fibroblasts exposed to fast neutrons or gamma rays. *Int. J. Radiat. Biol. 44*: 75-85.

Van der Schans, G. P.; S. B. Centen and P. H. M. Lohman (1982) *Progress in mutation research*, vol. 4. Elsevier, Amsterdam pp 17 - 30.

Van der Ploeg, H. T.; D. C. Schwartz; R. C. Cantor and P. Borst (1985) Antigenic variation in Trypanosoma brucei analysed by electrophoretic separation of chromosome-sized DNA molecules. *Cell 37:* 77-84.

von Sonntag, C.; U. Hagen; A. Schön-Bopp and D. Schulte-Frohlinde (1981) Radiation-induced strand breaks in DNA: Chemical and enzymatic analysis of end groups and mechanistic aspects. In: Lett, J. T. and H. Adler (Eds.) *Advances in radiation biology 9* Academic Press New York.

Walden, T. L. and N. K. Farzaneh (1990) *Biochemistry of ionizing radiation.* Raven Press, New York.

Wang, C. H. and D. L. Willis (1965) *Radiation Methodology in Biological Sciences.* Prentice Hall Inc., London.

Ward, J. F. (1988) DNA damage produced by ionizing radiation in mammalian cells: Identities, mechanisms of formation and reparability. *Prog. in Nucl. Acid Res. and Mol. Biol. 35*: 95-125.

Ward, J. F. (1990) DNA damage and repair. In: Glass, W. A. and M. N. Varma (Eds.) *Physical and chemical mechanisms in molecular radiation biology.* Plenum Press, New York and London.

Weber, K. J. and M. Flentje (1993) Lethality of heavy ion-induced double strand breaks in mammalian cells. *Int. J. Radiat. Biol. 46*: 169-178.

Weibezahn, K. F. and T. Coguerelle (1981) Radiation-induced DNA double-strand breaks are rejoined by ligation and recombinational processes. *Nucl. Acids Res.* 9: 3139-3150.

Whitaker, S. J. and T. J. Mcmillan (1992) Pulsed-field gel electrophoresis in the measurement of DNA double strand break repair in xrs-6 and CHO cell lines: DNA degradation under some conditions interferes with the assessment of double-strand rejoining. *Rad. Res. 130:* 389-392.

Whitaker, S. J.; S. N. Powell and T. J. McMillan (1991) Molecular assays of radiation-induced DNA damage. *Eur. J. Cancer 27*: 922-928.

White, M. G.; M. Isaila; K. Prelec and H. L. Allen (1971) Acceleration of nitrogen ions up to 7.4 GeV in the Princeton particle accelerator. *Science 174*: 1121-1123.

Wlodek, D. and P. L. Olive (1990) Physical basis for detection of DNA double-strand breaks using neutral filter elution. *Rad. Res. 124*: 326-333.

Wulf, H.; W. Kraft-Weyrather; H. G. Miltenburger; E. A. Blakely; C. A. Tobias and G. Kraft (1985) Heavy ion effects on mammalian cells: Inactivation measurements with different cell lines. *Radiat. Res. 104*: 122-143.

Zaider, M. and H. H. Rossi (1986) Microdosimetry and its application to biological processes. In: Orton, C. G. (Ed.) *Radiation dosimetry*. Plenum Press, New York.

Ziegler, J. F. (1980) *Handbook of Stopping Cross-Sections for Energetic Ions in all Elements*. Pergamon Press New York.

Zirkle, R. E. and C. A. Tobias (1953) Effects of ploidy and LET on radiobiological survival curves. *Arch. Biochem. Biophys.* 47: 282-306.

APPENDIX

Appendix A: A summary of DSB measurements in yeast and mammalian cells for sparsely ionizing radiation

Cell line	Radiation	Method	Y_{dsb} (μm^{-2})	References
V79 Hamster	250kVp X-rays	Elution	$15\pm1x10^{-12}$	Radford and Hodgson (1987)
Hamster cells (V79-cells)	X-rays	Elution	$6.1x10^{-12}$	Radford and Hodgson (1985)
(V79, L)	X-rays	Elution	$8.6x10^{-12}$	Radford and Hodgson (1985)
CHO cells	250 kVp X-rays	PFGE	$8.2x10^{-12}$	Ager et al. (1990)
CHO cells	X-rays	PFGE	$6\text{-}10x10^{-12}$	Iliakis et al. (1991)
Hamster cells	X-rays	sedimentation	$4.3x10^{-12}$	Jenner et al. (1992)
Caski cells	X-rays	PFGE	$8.3x10^{-12}$	Weber and Flentje (1993)
Caski cells	X-rays	Elution	$9.1x10^{-12}$	Weber and Flentje (1993)
Hamster cells	X-rays	PFGE	$9.3x10^{-12}$	Ager and Dewey (1990)
Mouse cells	X-rays	PFGE (weight average)	$22.5x10^{-12}$	Ahn et al.(1991)
Mouse cells	X-rays	mode method	$33x10^{-12}$	Ahn et al.(1991)
Human cells (Oxic)	$^{60}Co\ \gamma$	PFGE	$4.04x10^{-12}$	Whitaker and Macmillan (1992)
Human cells (Hypoxic)	$^{60}Co\ \gamma$	PFGE	$1.6x10^{-12}$	Whitaker and Macmillan (1992)
Diploid yeast	γ-rays	PFGE	$1.6x10^{-12}$	Friedl et al.(1993)
Diploid yeast (oxic)	30 MeV e^-	sedimentation	$5.8x10^{-12}$	Frankenberg-Schwager et al. (1981)
Diploid yeast (anoxic)	30 MeV e^-	sedimentation	$2.1x10^{-12}$	Frankenberg-Schwager et al. (1981)
Mammalian (Caski) cells	$^{60}Co\ \gamma$	electrophoretic elution	$10.5x10^{-12}$	Weber and Flentje (1993)
V79 Hamster cells	$^{60}Co\ \gamma$	Filter elution	$9.0x10^{-12}$	Weber and Flentje (1993)
Mammalian (Caski) cells	50 kV X-rays	Filter elution	$9.1x10^{-12}$	Weber and Flentje (1993)

Appendix A Contd.

Cell line	Irradiation	Method	DSB Yield (DSB/Dalton/Gy)	References
Mouse L5178Y	220kVp X-rays	Sedimentation	$4\pm1 \times 10^{-12}$	Lehmann and Ormerod (1970)
Mouse L5178Y	1MeVp X-rays	Sedimentation	$16\pm1\times10^{-12}$	Sawada and Okada (1970)
Rat thymocytes	10 MeV e^-	Sedimentation	5.0×10^{-12}	Coquerelle et al. (1973)
Human fibroblasts	$^{60}Co\ \gamma$	Sedimentation	8.0×10^{-12}	Lehmann and Stevens (1977)
V79 Hamster	150kVp X-rays	Sedimentation	12.0×10^{-12}	Ahnström and Bryant (1980)
Mouse EAT	140kVp X-rays	Sedimentation	$12\pm2\times10^{-12}$	Blöcher (1982)
Human (SP3) cells	X-rays	PFGE	8.7×10^{-12}	Löbrich et al. (1994a)
V79 Hamster cells	X-rays	Sedimentation	4.3×10^{-12}	Jenner et al. (1992)

Appendix B: Summary of DSB measurements for Heavy ions

Cell line	Ion Energy (MeV/u)	Method	σ_{dsb} 10^9 (μm^{-2})	References
Mammalian (Caski)) cells	O (10.8)	Filter elution	0.19	Weber and Flentje (1993)
V79 Hamster cells	Ne (14.0)	Filter elution	0.20	Weber and Flentje (1993)
Mammalian (Caski)) cells	Ne (10.0)	Filter elution	0.27	Weber and Flentje (1993)
Hamster cells	Neutrons	Filter elution	$7.2x10^{-12}$	Weber and Flentje (1993)
Mammalian (Caski)) cells	Ar (5.9)	Filter elution	0.64	Weber and Flentje (1993)
Mammalian (Caski)) cells	Xe (11.4)	Electrophoretic elution	2.04	Weber and Flentje (1993)
V79 Hamster cells	Au (9.8)	Filter elution	1.85	Weber and Flentje (1993)
Diploid yeast	Ne (4.9)	Sedimentation	0.64	Akpa et al. (1992)
Diploid yeast	Ne (9.8)	Sedimentation	0.58	Akpa et al. (1992)
Diploid yeast	Ne (14.4)	Sedimentation	0.41	Akpa et al. (1992)
Diploid yeast	Ar (14.0)	Sedimentation	0.71	Akpa et al. (1992)
Diploid yeast	Ar (13.4)	Sedimentation	0.71	Akpa et al. (1992)
Diploid yeast	Ar (12.9)	Sedimentation	0.57	Akpa et al. (1992)
Diploid yeast	Xe (11.8)	Sedimentation	2.57	Akpa et al. (1992)
Diploid yeast	Au (9.1)	Sedimentation	5.37	Akpa et al. (1992)
Diploid yeast	Pb (12.7)	Sedimentation	2.85	Akpa et al. (1992)
Human cells	Ne (21.25)	PFGE	0.034	Löbrich (1994)
Human cells	Fe (600.0)	PFGE	0.13	Löbrich (1994)
Human cells	Fe (400.0)	PFGE	0.16	Löbrich (1994)

Appendix B Contd.

Cell line	Ion Sp. Energy (MeV/u)	Method	σ_{dsb} (μm^{-2})	References
Human cells	Fe (250.0)	PFGE	0.24	Löbrich (1994)
Bovine epithelial cells	U (4.1)	Filter elution	**1.7**	Aufderheide et al. (1987)
Bovine epithelial cells	U (1.5)	Filter elution	**0.7**	Aufderheide et al. (1987)
Bovine epithelial cells	Xe (16.5)	Filter elution	**3.97**	Aufderheide et al. (1987)
Bovine epithelial cells	Xe (10.1)	Filter elution	**2.33**	Aufderheide et al. (1987)
Bovine epithelial cells	Xe (5.4)	Filter elution	**1.30**	Aufderheide et al. (1987)
Bovine epithelial cells	Kr (18.0)	Filter elution	**2.23**	Aufderheide et al. (1987)
Bovine epithelial cells	Ar (19.3)	Filter elution	**1.0**	Aufderheide et al. (1987)
Bovine epithelial cells	O (3.5)	Filter elution	0.13	Aufderheide et al. (1987)
Bovine epithelial cells	O (8.7)	Filter elution	0.20	Aufderheide et al. (1987)

Appendix C: Survival Data for Yeast (Rad 53-4) after X-Ray Irradiation and Incubation in Phosphate Buffer (the data is plotted in figure 4.9).

Incubation period: None

X-ray Dose (Gray)	Surviving Fraction
0	1.0
21.67	0.8235
43.33	0.7407
43.33	0.756
65.00	0.732
65.00	0.6122
108.33	0.5475
216.66	0.2092
216.66	0.1368
325.00	0.0359
325.00	0.0301
433.33	0.0236
433.33	0.0272

Incubation period: 7 hours

X-ray Dose (Gray)	Surviving Fraction
0	1.0
21.67	1.0086
43.33	0.9183
43.33	0.7227
65.00	0.592
65.00	0.7055
108.33	0.5388
216.66	0.1221
216.66	0.1871
325.00	0.0675
325.00	0.0911
433.33	0.0236
433.33	0.0227

Incubation period:24 hours

X-ray Dose (Gray)	Surviving Fraction
0	1.0
21.67	0.9692
43.33	0.8899
43.33	0.8899
65.00	0.9339
65.00	0.8884
108.33	0.5272
216.66	0.1762
216.66	0.2176
325.00	0.0852
325.00	0.1157
433.33	0.0357
433.33	0.0335

Incubation period: 48 hours

X-ray Dose (Gray)	Surviving Fraction
0	1.0
21.67	0.9330
43.33	0.6720
43.33	0.7440
65.00	0.6790
65.00	0.7000
108.33	0.6260
216.66	0.2350
216.66	0.2690
325.00	0.0920
325.00	0.1330
433.33	0.0330
433.33	0.0340

APPENDIX C Contd.

Incubation period: 72 hours

X-ray Dose (Gray)	Surviving Fraction
0	1.0
21.67	1.2000
43.33	1.0400
43.33	1.1316
65.00	0.8290
65.00	1.0240
108.33	0.7670
216.66	0.2350
216.66	0.4080
325.00	0.2374
325.00	0.2372
433.33	0.0640
433.33	0.0690